

**CONCEPTION D'UN RÉSEAU
D'ANTENNES ADAPTIF EN UTILISANT
LES MÉTAMATÉRIAUX**

**Thèse de Ph.D. de
BETTY SAVITRI**

UNIVERSITE DU QUEBEC EN OUTAOUAIS

Prof. LARBI TALBI, DIRECTEUR



Conception d'un réseau d'antennes adaptatif en utilisant les métamatériaux

Par

BETTY SAVITRI

Thèse présentée au
Département d'informatique et d'ingénierie
pour l'obtention du grade de

Philosophiae Doctor (Ph.D.)

en Science et technologies de l'information

Membres du jury:

Président

Examineur interne

Examineurs externes

Directeur de thèse

Co-directeur

Prof. Luigi Logrippo, UQO

Prof. Jules Lebel, UQO

*Prof. Jafar Shaker, Collège militaire royal
du Canada*

Prof. Rony E. Amaya, Université Carleton

Prof. Larbi Talbi, PhD., UQO

Dr. Khelifa Hettak, CRC-Ottawa



Design of a Beamforming Antenna Array Using Metamaterials

By

BETTY SAVITRI

A thesis submitted to the
Departement of Computer Science & Engineering
in partial fulfillment of the requirements for the degree of

**Philosophiae Doctor (Ph.D)
en Science et technologies de l'information**

Members of jury :

*Chairman
Examiners*

*Prof. Luigi Logrippo, UQO
Prof. Jules Lebel, UQO
Prof. Jafar Shaker, Royal Military College
of Canada
Prof. Rony E. Amaya, Carleton University
Prof. Larbi Talbi, UQO
Dr. Khelifa Hettak, CRC-Ottawa*

*Thesis Supervisor
Co-Supervisor*

*In the Name of God, most merciful and most compassionate,
With His blessings of another breath, another moment of life, and that
we may walk on a path of truth and understanding.*

Author's Declaration

I hereby declare that I am the sole author of this thesis.

This is a true copy of the thesis, including any required final revisions, as accepted by my examiners.

I understand that my thesis may be made electronically available to the public.

Gatineau, December 2017

Betty Savitri

ABSTRACT

Design of a beamforming antenna array using metamaterials

By

Betty Savitri

Metamaterials are attracting more and more interest among researchers in the fields of microwave, radio frequency and antenna. These revolutionary materials artificially made from metallic and dielectric patterns very smaller than the wavelength used to obtain unique properties, fascinating, extraordinary and impossible to achieve with natural materials. Some of these properties opened up promising pathways to surprising applications in the field of radio frequencies to improve the performance of components such as filters, couplers and antennas while offering the potential to miniaturize, minimize energy losses, expanding the frequency band and extend the range. The objective of this thesis project is to apply the metamaterial in the design of a network of adaptive antennas, multibeam and multi-band, in order to miniaturize. The study and modeling are based on electromagnetic analysis and the theory of transmission lines. The design process and the geometric constraints formulation phase will be carried out based on the following steps. The first step is studying the feasibility of designing artificial materials unit cells and testing the new formulation to address the fundamental constraints. In the following steps, the various components of the antenna array will be designed separately, namely, phase shifters, cross-overs, Butler matrix and antennas. Finally, the crucial step is to combine all these components in a single device and validate its functionality while achieving the desired miniaturization sub bands required frequencies.

Résumé

Conception d'un réseau d'antennes adaptatif en utilisant les métamatériaux

Les métamatériaux suscitent de plus en plus l'intérêt des chercheurs dans les domaines des micro-ondes, d'antennes et radiofréquences. Ces matériaux révolutionnaires réalisés artificiellement à partir de motifs métalliques et diélectriques de dimensions très inférieures à la longueur d'onde permettent d'obtenir des propriétés uniques, fascinantes, et extraordinaires impossibles à obtenir avec des matériaux naturels. Certaines de ces propriétés ont ouvert des voies prometteuses à des applications surprenantes dans le domaine des radiofréquences afin de perfectionner les performances des composants tels que les filtres, les coupleurs et les antennes tout en offrant la potentialité de les miniaturiser, minimiser les pertes d'énergie, élargir la bande de fréquences et étendre la portée. L'objectif de cette thèse consiste à appliquer les métamatériaux dans la conception d'un réseau d'antennes adaptatif, multifaisceaux et multibandes, afin de le miniaturiser. L'étude et la modélisation se basent sur l'analyse électromagnétique et sur la théorie des lignes de transmission. Le processus de conception ainsi que la phase de formulation des contraintes géométriques sont effectués en se basant sur les étapes suivantes. La première étape étudie la faisabilité de conception des cellules unitaires des matériaux artificiels et teste la nouvelle formulation pour répondre aux contraintes fondamentales. Dans la deuxième étape, les différents composants du réseau d'antennes sont conçus séparément, à savoir, les déphaseurs, les chemins de croisements, la matrice de Butler et les antennes. Finalement, l'étape cruciale est de combiner tous ces composants dans un seul dispositif et de valider sa fonctionnalité tout en réalisant la miniaturisation souhaitée sous les bandes de fréquences exigées.

Acknowledgement

I wish to express sincere appreciation and gratefulness to my supervisor Professor Larbi Talbi for his knowledge, insight, valuable guidance and contagious enthusiasm throughout this research, and I would like to record my gratitude to my co-supervisor Dr. Khelifa Hettak as well for his supervision, suggestions and guidance since the very early stage of my research. Indeed, my gratitude to them could not be expressed in a few words and it was an honor to be their student. I have gained a life-long role model to which I look up to and hope to follow their footsteps. I am also grateful to Dr. Ali Kabiri for sharing his expertise and knowledge in Metamaterial and electromagnetic theory. His truly scientific intuition, professional and passions in science inspire and enrich my growth as a researcher and as a future scientist. In first year of my PhD period, he was my advisor for one of my course who gave me support and encourage in every step of my research. It was a great honour to learn and work with him. I would like also to thank Dr. Babak Alivia. I feel greatly fortunate when I had opportunity to work and publish some articles with him. Their contribution is greatly appreciated.

The Most of all, I would like to thank Directorate general of higher education ministry of national education of republic Indonesia for giving me a scholarship for my doctoral program at Universite du Quebec en Outaouais (UQO), Canada and Gunadarma University as my intuition. I would like to thank Professor Sarifuddin Madenda for introducing me with UQO and as my advisor during my PhD period in Canada.

I would like to recognize my officemate Moustapha Mbaye. We had good conversation and discussion in electromagnetic field and all subjects in life. He looked like as a mentor at our office. Thank to my officemate and friend Vincent A. Fono. I will forever remember the many great conversations we've had about all subjects. We passed many times in bitter and sweet as a classmate, laugh and argue for everything in life. I wish you success in your PhD and next career as well. I would like to thank my officemate Dr. Tahar Haddad for his wise advises in everything related to my study or life. Also, thank to Dr. Ousama Abu Safia, as my officemate and friend. We had good time in conversation about electromagnetic field and for sharing about experience

in life. I am sure, He will make an excellent professor and supervisor one day. Thanks to Yassine Zouaoui and Khaled Kedjar as my officemate, for their constant support and guidance, and for giving me those laughs when I needed them the most.

Last but certainly not least I have to express my everlasting gratitude to my family. I thank to my parents, my late beloved father (alm) Kosasih Adireja who passed away at a week before my thesis defense and my beloved mother Sugiah Herawati, who gave me an inspiration to be the best that I can be, and my lovely husband, Damien Imberdis, who always supports me in bad and good times with his love, and all my children Natasha, Raphael and Rachel who have been sacrificed with my time which I had to share between them and my study. They gave me all the tools in life to be able to succeed, and taught me never to stop achieving, and to never settle for less than best. I derive my strength from the strength they exuded through all their battles in life. Thanks to my parents in law, Jean-Rene and Maryse Imberdis and my sister in law, Aude Imberdis. Thank you to my sisters Alice and Irma for supporting me, my nieces Sonia, Yoan and Muthia which is I hope I will one day inspire to be the best that I can be. I would like to thank my friends Wiwin Budiyaniti, Emmy Aishah, and Irma Leblond , and all of Indonesian friends in Canada and Indonesia who always support me and beside me in good and bad time throughout this PhD period.

Gatineau, December 7th, 2017

Betty Savitri

This thesis is dedicated to

My exotic and proud homeland, Indonesia

My late father Kosasih Adireja and my mother S. Herawati, for their infinite love and support.

Table of Contents

Chapter 1 : Preface	1
1.1 Background	1
1.2 Research Question	3
1.3 Methodology	4
1.4 Literature Review of Previous Work	4
1.5 Thesis Outline	6
Chapter 2 : Fundamental Theory of Metamaterial	8
2.1 Definition of Metamaterial and Left Handed Media	8
2.2 Fundamental Formula of Artificial Magnetic Material	11
2.3 Determination of Negative Permeability From Reflection and Transmission Coefficient	16
2.4 Rose Curve Characteristic	18
2.5 Microwave Application of Metamaterial Concept with Microstrip line Based on Complementary Rose Curve Resonators (CRCRs)	23
Chapter 3 : Metamaterial Power Divider for Beamforming System Based on Butler Matrix	32
3.1 Theory and Circuit Model of Compact 90 ⁰ Microwave Directional Coupler	33
3.2 Analysis and Design of Power Divider Conventional	35
3.3 Analysis and Design of Metamaterial Power Divider	38
3.4 Experimental and Measurement	43
Chapter 4 : Metamaterial Antenna for Beamforming System Based on Butler Matrix	46
4.1 Analysis and Design of Patch Antenna Conventional	47
4.2 Analysis and Design of Metamaterial Patch Antenna	49
4.2.1 Patch Antenna Based on Complementary Split Ring	

Resonators (CSSRs)	51
4.2.2 Patch Antenna Based on Complementary Rose Curve	
Resonators (CRCRs)	53
Chapter 5 : Beamforming System Based on Butler Matrix	59
5.1 Analysis and Design of a 4x4 Butler Matrix	62
5.2 Future Work	67
5.2.1 A 4x4 Butler Matrix Based on Complementary Split Ring	
Resonators (CSSRs)	67
5.2.2 A 4x4 Butler Matrix Based on Complementary Rose Curve	
Resonators (CRCRs)	68
Conclusion	70
References	72
Publications	81
Résumé	82

List of Abbreviations

AMM	Artificial Magnetic Material
ENG	ϵ -Negative Material
LHM	Left-Handed Material
DNG	Double Negative
SNG	Single Negative
MNG	μ -Negative Material
CRLH-TL	Composite Right/Left Handed Transmission Line
SRR	Split Ring Resonator
SR-R	Swiss Roll Resonator
MSRR	Modified SRR
n-RCR	nth order Rose Curve Resonator
CSRR	Complementary Split Ring Resonator
RCR	Rose Curve Resonator
CRCR	Complementary Rose Curve Resonator
CS-RR	Complimentary Spiral Ring Resonator
<i>M</i> -factor	Miniaturization Factor

List of Symbols

c	speed of electromagnetic waves in vacuum
λ_0	wavelength of electromagnetic waves in vacuum
λ_g	guided wavelength
ω	angular frequency of an electromagnetic wave
ϵ_{eff}	effective permittivity
μ_{eff}	effective permeability
n_{eff}	effective refractive index
k	wave vector
E	electric field
H	magnetic field
ϵ_r	relative permittivity of a material
μ_r	relative permeability of a material
χ_m	magnetic susceptibility
M	magnetization vector
V_{emf}	electromotive force
$\delta x, \delta y, \delta z$ x, y and z	dimensions of a unit cell of an AMM
A	area of cell
V	volume of cell
σ	conductivity
$R_0 \sqrt{\omega}$	resistance per unit length of an inclusion
C₀	capacitance per unit length of an inclusion
L₀	inductance per unit area of an inclusion
F	geometrical factor of an inclusion
P	physical factor of an inclusion
l	perimeter of an inclusion
s	area of an inclusion
ϵ_0	permittivity of the free space

μ_0	permeability of the free space
<i>Mfactor</i>	Miniaturization Factor
ω_0	resonance frequency of an inclusion
Ω	normalized frequency with respect to the resonance frequency
BW	frequency bandwidth
Re	real part of a complex function
Im	imaginary part of a complex function
fo	operational frequency
(s,l) (area, perimeter)	pair of geometrically reliable curves
Pr Pr[.]	perimeter function of a curve
Ar Ar[.]	area function of a curve
Rn(r,a)	nth order Rose curve of radius r and amplitude
Z₀	impedance of free space
IL	insertion loss
I	isolation
CF	coupling factor
RL	return loss
D	directivity
Γ	reflection coefficient
r	radius of the ring
d	length between 2 rings
c	width of the ring

LIST OF FIGURES

Figure 1.1 Rose curve model	2
Figure 2.1 Effective material parameters represented on a set of Permittivity- permeability ($\epsilon - \mu$)	10
Figure 2.2 SRRs configuration	11
Figure 2.3 The configuration of a unit cell of an magnetic material with arbitrary of the inclusion	12
Figure 2.4 Permeability versus frequency of n^{th} Rose Curve for order $n=0$, $n=13$ and $n=23$	19
Figure 2.5 Variation of the resonant frequency with different value of n	20
Figure 2.6 Variation of the resonant frequency with $n=7$ versus radius (r)	22
Figure 2.7 Variation of the resonant frequency with $n=7$ versus different value of amplitude of RCR	23
Figure 2.8 Microstrip line stopband with CRCRs	24
Figure 2.9 Comparing the permeability versus frequency of n^{th} Rose Curve for n -th order	25
Figure 2.10 Permeability vs Frequency for some orders	26
Figure 2.11 S_{11} parameter in microstrip lines stopband with n^{th} order of CRCRs	26
Figure 2.12 S_{21} parameter in microstrip lines stopband with n^{th} order of CRCR	27
Figure 2.13 Fabrication of Microstrip lines Stop-band Filter based on CRCRs with $n=0$, $n=13$, $n=23$ orders and without CRCRs	29
Figure 2.14 S_{11} parameter in microstrip lines stopband with n^{th} order of CRCRs	29
Figure 2.15 S_{11} parameter in microstrip lines stopband with n^{th} order of CRCRs	30
Figure 3.1 Geometry of the Quadrature Hybrid coupler	33
Figure 3.2 Directional 90° microstrip conventional coupler	36

Figure 3.3 Phase Difference of 90° Microstrip Conventional Coupler	37
Figure 3.4 Simulation results of the <i>S</i> parameters for the Conventional Coupler	37
Figure 3.5 Parameters of Split ring resonator and Rose curve resonator with n=13	39
Figure 3.6 Directional 90° microstrip coupler	40
Figure 3.7 Different Phase of 90° Microstrip Coupler	41
Figure 3.8 Simulation result of the <i>S</i> parameters for the structure	42
Figure 3.9 Fabrication design of 90° Microstrip Coupler	43
Figure 3.10 Experimental results of the <i>S</i> parameters in the frequency range 0 GHz to 20 GHz	44
Figure 3.11 Experimental results of the <i>S</i> parameters in the frequency range 0 GHz to 5 GHz	44
Figure 3.12 Experimental phase shifting between port 2 and 3 in the frequency range 0 GHz to 5 GHz	45
Figure 4.1 Configuration of Patch antenna	47
Figure 4.2 Configuration of Patch antenna conventional	47
Figure 4.3 <i>S</i> ₁₁ parameter result for conventional Patch antenna	48
Figure 4.4 Radiation pattern of the designed conventional patch antenna	49
Figure 4.5 (a) Split Ring Resonator (SRR), and (b) Rose Curve Resonator with order=13.....	50
Figure 4.6 Configuration of Patch antenna based on Complementary Split Ring Resonators (CSSRs)	51
Figure 4.7 <i>S</i> ₁₁ parameter of Patch antenna based on Complementary Split Ring Resonators (CSSRs)	52
Figure 4.8 Radiation pattern of Patch antenna based on Complementary Rose Curve Resonators (CRCRs)	53
Figure 4.9 Configuration of Patch antenna based on Complementary Rose Curve Resonators (CSSRs)	54
Figure 4.10 <i>S</i> ₁₁ Parameter of patch antenna based on CRCRs	55
Figure 4.11 Simulation result of the Radiation pattern of Patch antenna	

based on CRCRs	55
Figure 4.12 Measurement result of S_{11} Parameter of patch antenna based on conventional and metamaterial model	56
Figure 5.1 Butler Matrix diagram system	60
Figure 5.2 A 2x2 Butler Matrix diagram	60
Figure 5.3 General block diagram of a 4x4 Butler Matrix	61
Figure 5.4 General block diagram of a 8x8 Butler Matrix	62
Figure 5.5 General block diagram of a 4x4 Butler Matrix without crossover	63
Figure 5.6 4x4 Butler Matrix design on HFSS at 2.4 GHz	64
Figure 5.7 S-Parameters of the 4x4 Butler Matrix conventional	65
Figure 5.8 S-Parameters of a coupler on the 4x4 Butler Matrix conventional	66
Figure 5.9 Butler matrix with CSRRs design on HFSS at 2.4 GHz	68
Figure 5.10 4x4 Butler Matrix with CRCRs design on HFSS at 2.4 GHz	69

LIST OF TABLES

Table 2.1 Parameters of the simulated n th rose curve	19
Table 2.2 Effect of n^{th} order of RCR with similar shape in radius, amplitude and are.....	20
Table 2.3 Effect of the radius of RCR with similar shape in amplitude and order (n)	21
Table 2.4 Effect of the amplitude of RCR with similar shape in radius and order (n)	22
Table 2.5 Value of negative permeability for n th order of CRCRs on the microstrip lines stop-band	25
Table 2.6 Relative bandwidth and rejection depth of microstrip band-stop filter based on CRCRs	28
Table 2.7 Comparison table of the different miniaturized Size of CRCRs	30
Table 3.1 Comparison table of compact 90° Microstrip Coupler based on CSRRs and CRCRs	43
Table 4.1 Parameters of the conventional Patch antenna	48
Table 4.2 Comparison table of Patch Antenna based on CSRRs and CRCRs	57
Table 5.1 Phase difference between input port with the antenna port on the 4x4 conventional butler matrix	66

Chapter 1

Preface

1.1 Background and Motivation

In electromagnetic wave, electric permittivity and magnetic permeability control the propagation through to the materials. Metamaterial belong to the natural sciences categories of physic and material sciences which are positive in nature. Metamaterial generates negative permittivity with sub wavelength thin wires and negative permeability with split ring resonators. The electric and magnetic dipoles are generated in the wire and rings when an electric field is parallel to the wires and a magnetic field (H) is perpendicular to the plane of rings. Artificial Magnetic Material (AMM) consists of metallic broken-loop inclusion which aligned in parallel planes perpendicular to the direction of incident magnetic field. Metamaterials are commonly used for Split-Ring Resonators (SRRs) and Swiss Roll-Resonator (SR-Rs), as originally proposed by Pendry et al[1]. Split-ring Resonators (SRRs) consist of two rings which are separated by a gap and having splits on the opposite sides. The open metal loop of rings forms induce current resonance and behaves as an LC resonator. Magnetic resonance is induced by the gap between two rings and the splits at the rings [2] and it was demonstrated that the effective permeability can reach reasonably high values over a wide frequency range when using such inclusions [3]. SRRs configurations are shown in Fig. 1. In recent work, many researchers propose a Rose Curve inclusion geometry with the primary feature being the perimeter and the area where they can be arranged[3-6]. The shape of area is similar to the original circle and the perimeter can be tuned to the amplitude and the function of sinusoidal frequency. The main purpose to generate the magnetic properties is the electric current and then the current circulation occurs contour to have magnetic flux. To generate capacitive properties, the first contour is positioned adjacent with another to generate a coupling between the two contours. An example of the Rose Curve model is shown in Fig. 1.1:

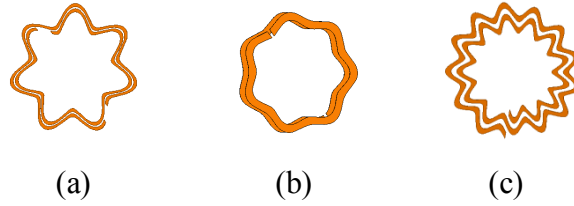


Fig. 1.1 (a) A broad-side coupled inclusion with order $(n)=7^{\text{th}}$ order Rose curve, (b) An edge-coupled inclusion with order $(n)=7^{\text{th}}$ order Rose curve, (c) a spiral inclusion

Effective permittivity is obtained from the coupling between two contours which creates capacitance between them. After getting the capacitance and inductance properties, they create the potential for resonance at a certain frequency which is known as the resonance frequency [4][5][6]. In recent works, a new approach was proposed to develop of metamaterial structures. Split-ring resonators (SRRs) and complementary split-ring resonators (CSRRs) coupled to planar transmission lines, as well as the electromagnetic behavior of these elements were investigated. Analytical equivalent-circuit models were proposed for the isolated and coupled SRRs/CSRRs [7]. A new methodology was developed for the design of compact planar filters using microstrip technology, with microstrip bandpass or highpass filter based on Complementary Split-Ring Resonators (CSRRs) [8, 9]. Another paper showing the complementary spiral resonators (CSRs) etched in the ground plane of a microstrip line proves useful for the implementation of band pass filters with very small dimensions and wide stop bands [10]. The concept of complementary ring resonators is used for the ground plane of microstrip lines. Originally proposed by Falcone, the concept of complementary SRRs (CSRRs) introduces a microstrip stopband structure design based on the introduction of an effective negative- ϵ along the line [11]. This approach is widely addressed in literature[6, 12, 13].

Complementary Split Ring Resonators (CSRRs) have been studied in great detail over the last decade as metamaterial structure. The promise of SRRs is achieved in the design of miniaturized microwave circuits in microstrips line design configuration. The major challenge in metamaterial is to incorporate active elements to achieve electronic tunability. Furthermore, this requires the circuit to be patterned on the ground plane to allow isolation between multi-level circuits. Microstrip metamaterial circuits need to be designed to operate at high frequencies or

X-band frequency range. The high frequencies, rather than lower frequencies, are used in communication for higher data density. In this study, we propose to select X-band frequency for microwave circuit design. In wireless communication we choose a frequency band of 2.4 GHz.

Moreover, our metamaterial circuit design will be implemented in antenna application. The purpose of this research to first develop and analyze a novel design of metamaterial antenna application with a 4x4 Butler Matrix systems with a 2.4 GHz frequency, and secondely to design and compare between the simulations analysis results using HFSS 15.

1.2 Research Contribution

In this research, design of a 4x4 Butler Matrix is introduced. The proposed metamaterial unit cells allow the miniaturization of circuit design as well as achieving new functionalities are achieved. The following works have been completed:

- A 90⁰ Hybrid coupler based on complementary rose curve resonators (CRCRs).

A novel compact 90⁰ power divider based on complementary rose curve resonators (CRCRs) is proposed. We designed a conventional coupler size reduction, based on CSRRs and CRCRs which behave as left hand material in a narrow band for a specific resonating frequency of 2.4 GHz. As a result, it is shown that CRCRs extend the possibility of design with higher miniaturization factor and relative bandwidth in comparison with using complementary split ring resonators (CSRRs). The device compactness increases proportionally to the order of CRCRs.

- A Patch Antenna based on complementary rose curve resonators (CRCRs).

A novel metamaterial Patch antenna is proposed. It demonstrates the comparison between the Patch antenna conventional with Patch antenna based on Complementary split ring resonators (CSRRs) and Patch antenna based on Complementary rose curve resonators (CRCRs). CRCRs have the potential to extend the possibility of design with an higher miniaturization factor in comparison with using complementary split ring resonators (CSRRs). The device compactness increases proportional to the order of CRCRs.

- A compact beamforming system based on Butler Matrix design

A novel compact 4x4 Butler Matrix system without crossover circuit is proposed.

These circuits extend the possibility of design with higher miniaturization factor. A major contribution is a size reduction. The device compactness of the microstrip line increases proportional to the order of CRCRs. An increase from n to $n+1$ of the CRCRs order will result in 2.67% miniaturization. From the conventional model to the CRCRs of the following designs are able to reduce the size in 62% miniaturization of microstrip line, 53% miniaturization of 90° microstrip coupler, and 92% miniaturization of patch antenna. Other contribution is a realization of the difference blocks for array antenna.

1.3 Methodology

Nowadays, a broadband wireless point-to multipoints communication system is required to provide digital, data, voice, internet and video services at high frequencies. These systems require a good antenna performance and low-cost beamforming. We chose the Butler matrix as the key components in beamforming antenna systems. In this system, to increase the carrier-to-interference ratio (CIR), the interference signals are rejected and the desired signal is enhanced. Furthermore, enhancing CIR improves both system's capacity and performance. [a compact 24-26 GHz].

The Butler matrix device is a passive multi beam with multiple input and output ports to generate the phase distributions of equal amplitudes at the output ports. Therefore, depending of which input port of the N ports is accessed, the antenna beam can be directed to a specific direction.

Traditionally, Butler matrix were developed by microstrip lines with a large area because of the use of the quarter-wavelength transmission lines in the couplers. We will initially develop components to design a Butler matrix system, namely: a directional 90° Couplers, Phase Shifter and Crossover. In this work, we designed a compact 4x4 Butler matrix for beam forming antenna system without crossover.

Therefore, the goal of this research is to look at the feasibility of a compact integrated Butler matrix of four beams. The size of a Butler Matrix is the main contributor for the cost of a beamforming system. Hence, miniaturization of a Butler matrix is essential to reduce the cost of

beamforming systems. Finally, the novelty of the proposed techniques and designs will be presented with a metamaterial Butler matrix based on complementary rose curve resonators (CRCRs).

1.4 Literature Review

Classical electromagnetics is one of the best established theories of science and technology in physics such as telecommunications, biomedical imaging, chemical spectroscopy and sub-wavelength sensing applications. In microwave frequencies, natural materials are limited to certain levels of polarization and magnetization. Although in certain level, magnetization and polarization is achieved, the material presents high magnetic electric and magnetic losses. For example, ferrite composites are strongly magnetized but suffer from sizable magnetic loss and high resistivity in the microwave frequencies range [11, 14]. Due to these limitations, artificially materials were designed to provide a specific permeability and permittivity in microwave frequencies range.

In recent years, a new expression appeared in the universe of classical electromagnetic theory: metamaterials. From 2000 to 2007, the number of researches related to metamaterials has grown exponentially. Electromagnetic metamaterials, as artificial material, are defined as electromagnetic structure with unusual properties that are not readily available in nature [15]. The theoretical aspects of electromagnetic metamaterial were first introduced by Viktor Veselago in 1967 [16]. He proposed the concept of the existence of substances with simultaneously negative permittivity (ϵ) and permeability (μ) on metamaterial or Left-Handed Media (LHM).

An ensemble of metallic broken loop resonators aligned in parallel planes normal to their surface and in a host dielectric is defined as an AMM. The effective permeability can reach reasonably high values over a wide frequency range when using such inclusions. The Metasolenoid has introduced a new magnetic particle for a new artificial magnetic inclusion. Circular split ring resonators (SRRs) and Swiss Roll resonators (SRRs) are common forms where the two rings are very strong capacitive coupling. Capacitive coupling may be even more increased in so-called modified split-ring resonators (MSRR) [1, 17]. The open metallic loop behaving as a LC resonators has been demonstrated by Kabiri et al and then proposed as a generic inclusion's

geometry called n^{th} order rose curve resonator (n-RCR) which provides a full control on the design of a desired magnetic response achievable by AMMs [6, 12]. The parametric study of the behavior of n^{th} order rose curve resonator (n-RCR) has been investigated based for its geometrical and physical characteristic of n-RCR [18].

The implementation of some model inclusions has been introduced for many applications. An electromagnetic dual of SRRs called complementary split ring resonators (CSRRs) was proposed by the etching of SRRs off a conducting sheet [19, 20]. A microstrip line stop-band filter was designed based on complementary rose curve resonators (CRCRs). The stop-band microstrip lines based on the complementary rose curve resonator (CRCRs) was developed by patterning the ground plane of the microstrip under the conductor trace [21]. Another application was developed in designing simple planar filter [22, 23]. There is a number of resonator types that can be useful in RF, microwave filters as well as size reduction applications [24, 25]. In many references such as: [26-29], branch line has been studied and presented as a combiner. The application of CSRRs properties with selective frequency in microstrip lines, where miniaturization was a key aspect has been developed [30]. Then Complementary Rose Curve Resonators (CRCRs) used in the design of microstrip coupler were achieved by using CRCR for better size reduction [31]. Some design applications in microwave properties were developed for compact antennas [32, 33], circularly polarized antenna [34, 35] and dual band antennas [36, 37]. A novel design of dual band antenna with Complementary Split Ring Resonators (CSRRs) and Complementary Rose Curve Resonators (CRCRs) has also been proposed [37, 38].

Application of multibeam antennas is used when antenna with high capacities of low-cost beamforming is required. These are the various type of RF beamforming [39]: Blass matrices, Rotman lenses, and the Butler matrix [40, 41]. Its use was appropriate in Butler Matrix design with some united circuit consisting of coupler, phase shifter, crossover and antenna. The design of a novel ultra-wideband compact 4x4 Butler Matrix has been developed to provide compact size [42, 43]. Another design of a 4x4 Butler Matrix with millimeter microstrip technology at 40 GHz is shown without any crossover circuit [44].

1.5 Thesis Outline

This thesis focuses on the design and analysis of a novel metamaterial consisting of a 4x4 Butler Matrix system. It will be developed under the following properties and actions: 1) Frequency operation at 2.4 GHz. 2) Parametric studies. 3) Simulations results. 4) Miniaturization compact design. Basic theory of composite right/left handed transmission line (CRLH TL) is described in order to realize the characteristic of the unit cell. Microwave circuits describe the high potential of the proposed unit cell. Miniaturizing a Butler Matrix system is proposed and designed for microwave circuits and applications. This thesis contains five chapters including preface.

Chapter 2 provides a review of the state of the art of metamaterial. Chapter 2, provides of the definition of Metamaterial and Left handed media, the composite right/left handed (CRLH) metamaterial and the fundamental formula of artificial magnetic material.

Chapter 3 covers Metamaterial Power Divider for beamforming system based on Butler Matrix. This chapter describes theory and circuit model of compact 90° microwave directional coupler, analysis and design of conventional Power divider, analysis and design of Metamaterial Power divider, and concludes on the comparison between the simulation and experimental results.

Chapter 4 addresses metamaterial antenna for beamforming system based on Butler Matrix. This chapter describes theory and circuit model of Patch antenna, analysis and design of Patch antenna conventional, analysis and design of Metamaterial Patch antenna, and concludes on the comparison between the simulation and experimental results.

Chapter 5 is about the Beamforming system based on Butler Matrix. This chapter describes the theory of Butler Matrix system, analysis and design of a 4x4 Butler Matrix conventional and future work for another design of Metamaterial a 4x4 Butler matrix.

Chapter 2

Fundamental Theory of Metamaterials

The propagation of electromagnetic wave through a medium is controlled by the medium's electric permittivity and magnetic permeability (μ). At microwave frequencies, the permittivity and permeability are positive in natural materials. Metamaterials are artificial material whose electromagnetic properties can be engineered to be effectively negative.

Electromagnetic metamaterials as artificial material are defined as electromagnetic structure with unusual properties that are not readily available in nature [2, 15]. The theory of electromagnetic metamaterial was first introduced by Viktor Veselago in 1967 [16]. He suggested the existence of substances with simultaneously negative permittivity (ϵ) and permeability (μ) on metamaterial or Left-Handed Media (LHM).

2.1 Definition of Metamaterials and Left Handed Media

In electromagnetic wave, electric permittivity and magnetic permeability control the propagation through to the materials. Metamaterial belongs to the natural sciences category of physics, to natural materials, which are positive in nature. Metamaterial generates negative permittivity with sub wavelength thin wires and negative permeability with split ring resonators. The electric and magnetic dipoles are generated n the wire and rings when the electric field is parallel to the wires and the magnetic field (H) is perpendicular to the plane of rings. The metamaterial is a material medium which is aggregated electrically with small inclusion.

The metamaterial is required to have a cellular size or structure cell size p much smaller than the guided wavelength λ_g for an effective homogeneous structure, at least less than a quarter wavelength ($p < \lambda_g/4$). In effective condition, limit $p = \lambda_g/4$ is used to recognize each component where p is the size of component that is considered. The components are classified, for example as lumped components ($p > \lambda_g/4$), quasi-lumped

components ($\lambda_g/4 < p < \lambda_g/2$) and distributed regime components ($p < \lambda_g/4$) [15]. In electromagnetics, the heterogenous artificial structure can be featured as a homogenous medium from an *effective* material parameters as an effective permittivity ϵ_{eff} and as an effective permeability μ_{eff} . The following equation provides an effective description of length scale d with an electromagnetic radiation wavelength λ ,

$$d \ll \lambda = 2\pi c / \omega \quad (2.1)$$

where ω is the angular frequency of the electromagnetic radiation.

Inequality (2.1) defines the effective medium limit [45, 46]. The source-free Maxwell's equation described the electromagnetic properties of the artificial medium with a set of constitutive relation of $\epsilon_{\text{eff}}(\omega)$ and $\mu_{\text{eff}}(\omega)$. Design of an artificial electromagnetic material with ϵ_{eff} and μ_{eff} can achieve the effective functions value which are not found in natural materials.

The constitutive parameters of the propagation of an electromagnetic wave in medium which are imparted to the refractive index $n(\omega)$ and the wave vector k , are defined as:

$$n = \sqrt{\epsilon_{\text{eff}}(\omega)\mu_{\text{eff}}(\omega)} \quad (2.2)$$

$$k = \frac{\omega}{c} n(\omega) \quad (2.3)$$

Fig. 2.1 shows the various four possibilities combination of $\epsilon_{\text{eff}}(\omega)$ and $\mu_{\text{eff}}(\omega)$.

The first three quadrants are well-known as conventional material, with the combination (+,+), (+,-), and (-,+). The last quadrant is the combination (-,-) that correspond to a new class of materials known as LHM. This class has simultaneously double negative sign of $\epsilon_{\text{eff}}(\omega)$ and $\mu_{\text{eff}}(\omega)$. In the first quadrant, $\epsilon_{\text{eff}}(\omega)$ and $\mu_{\text{eff}} > 0$, and hence, the wave vector is real number. The second quadrant is the epsilon negative materials (ENGs), and provides an imaginary k where the electromagnetic wave is evanescent. Noble metal at high frequencies has negative permittivity.

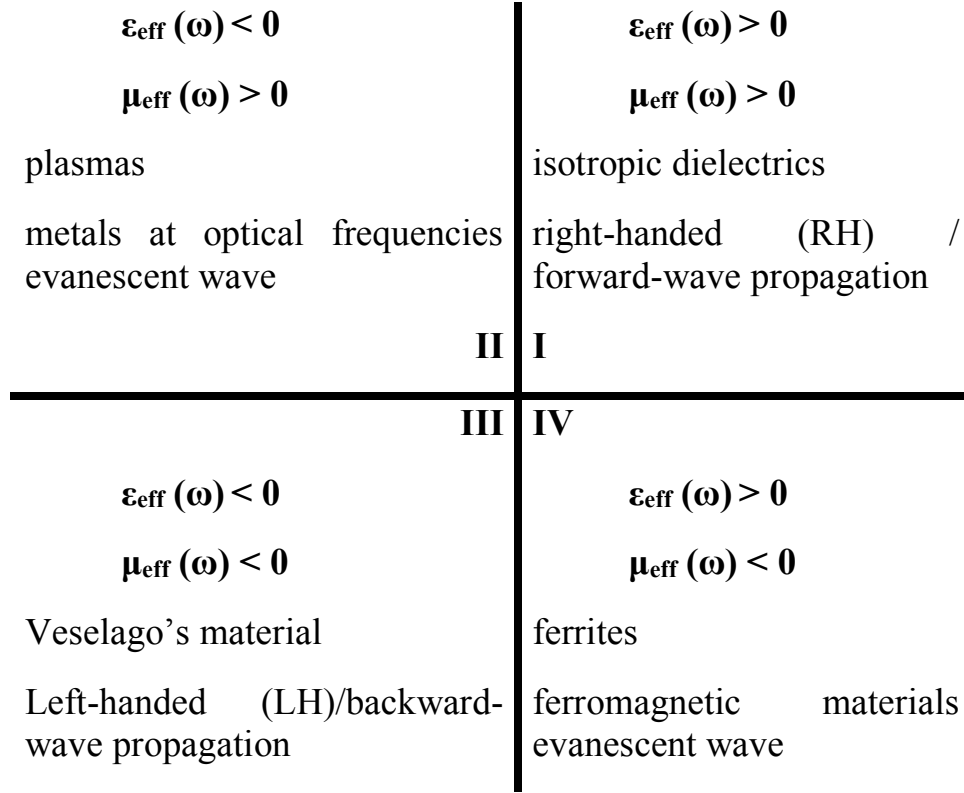


Fig. 2.1 Effective material parameters represented on a set of Permittivity-permeability ($\epsilon - \mu$)

In the third quadrant, the permittivity and permeability are simultaneously negative [47]. This material is a left-handed materials (LHMs) with a triad (E,H, k) forms [16], where E corresponds to the electric field and H corresponds to the magnetic field, respectively. Due to Maxwell's equation, the left-handed system can be written for harmonic electromagnetic field defines as:

$$kx E = \frac{\omega}{c} \mu_0 \mu_{\text{eff}}(\omega) H \quad (2.4)$$

$$kx H = -\frac{\omega}{c} \epsilon_0 \epsilon_{\text{eff}}(\omega) E \quad (2.5)$$

As a consequence, the group velocity and phase velocity are in opposite direction or in backward propagation of electromagnetic waves in double negative (DNG) media. The quadrant four represents the materials with positive permittivity and negative permeability. Referring to a μ -negative material (MNGs), this quadrant has a single negative (SNG) region. The consequence of negative medium parameter is the amplification of evanescent wave in the SNG and leads to a perfect lensing and sub-wavelength imaging, a high-resolution imaging beyond the diffraction limit [48-53].

2.2 Fundamental Formula of Artificial Magnetic Material

Metamaterials have some class in different types based on their heterogeneities. Metamaterials which are designed to enhance the magnetic properties of a medium are known as artificial magnetic materials (AMMs). Artificial Magnetic Material (AMM) consists of metallic broken-loop inclusion which aligned in parallel planes perpendicular to the direction of incident magnetic field. Metamaterials are commonly used to split-ring resonators (SRRs) and swiss roll resonator (SR-Rs), as originally proposed by Pendry et al [1].

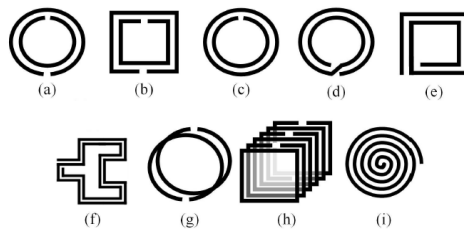


Fig. 2.2 (a) Double Split Ring Resonators, (b) Double Split Square Resonators, (c) Singly Split Resonator, (d) Two-turn (circular) Spiral Resonator, (e) Two-turn (rectangular) Spiral Resonator, (f) Hilbert Fractal Resonator, (g) Modified Ring Resonators, (h) Metasolenoid, (i) Cross section of a Swiss Roll

Split-ring resonators (SRRs) consist of two rings which are separated by a gap and have splits on the opposite sides. The open metal loop of rings form induces current resonance and behaves like an LC resonator. Magnetic resonance in the SRR is induced as the result of encircling electric current within the loop [2] and it has been demonstrated that the effective permeability can reach reasonably high values over a wide frequency range when using such inclusions [16]. Typical SRRs configuration is shown in Fig. 2.2

Furthermore, the implementation of SRR-based left-handed metamaterial in one dimension is results in microstrip lines. SRRs provide a negative effective permeability, but, to achieve backward-wave propagation, microstructuring is needed in order to obtain the required negative effective permittivity. Microstrip lines can be designed by photolithography processes and can be integrated easily with passive and active microwave devices [4]. The Complementary split ring resonators (CSRRs) can be derived from a SRR structure, specifically with a negative- μ behavior arising in a SRRs system, which can achieve negative- ϵ effective permittivity in CSRR system. The concept of complementary split ring resonators (CSRRs) is introduced as an alternative to the design of metamaterials based on resonant elements, providing an effective negative permittivity, rather than permeability [5, 6].

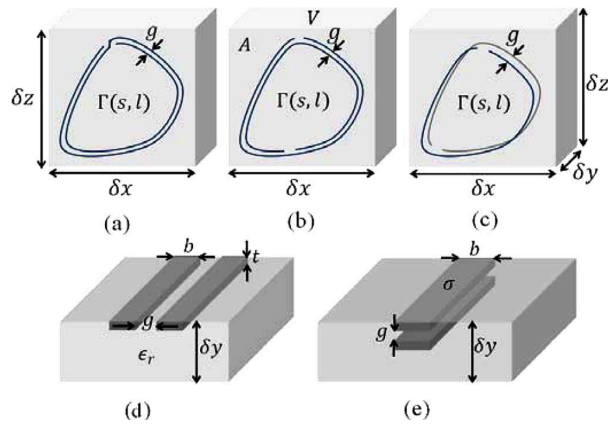


Fig. 2.3 (a) Two-turn spiral inclusion, (b) Edge-coupled double split ring resonator, (c) Broadside-coupled double modified split ring resonator, (d) Coupled lines as edge-coupled double split ring resonator , (e) Coupled lines as broadside-coupled double modified split ring resonator

The usefulness of CSRRs to implement super-compact stopband microstrip lines due to the presence of a frequency band with effective negative permittivity has been demonstrated by Falcone. The complementary resonators were introduced as complementary split ring resonator (CSRRs) or complementary spiral ring resonator (CSRRs) [6, 7]. Fig. 2.3 shows the configuration of a unit cell of magnetic material with an arbitrary inclusion. The inclusion's contour, area and perimeter are denoted by Γ , s , and l , respectively. Fig. 2.3 (a-c) show a two-turn spiral ring resonator; a split ring resonators that are edge-coupled and a split ring resonators that are broadside-coupled. Finally, Fig. 2.3 (d) and (e) show respectively a cross section of an edge-coupled and a broadside-coupled ring resonator.

The unit samples have an height of δz , width of δx and depth of δy . The area of the cell is $A = \delta x \delta z$ and its volume is $V = A \delta y = \delta x \delta y \delta z$. The area and circumference of the contour are denoted by s and l , respectively. The conductor material used in the printed inclusion is assumed to have electric conductivity of σ , a width of b , and height of t . In Fig. 2.3 (e), we assume that the other conductor is positioned either to the inside and follow the shape of the outer conductor with the uniform gap g , or in parallel to the former and separated by a distance of g .

To derive an explicit relationship for the magnetic susceptibility based on the physical and geometrical characteristic of the inclusion-filled medium, we conceive a circuit model for the inclusions. The induced V_{emf} dropped over any inclusion and can be expressed by the impedance of the rings and the induced current on the inclusions. Where the effective impedance of the loops has been modeled with a resistor, R , in series and with a capacitor C .

$$V_{emf} = I \left(R + \frac{1}{j\omega C} \right) \quad (2.6)$$

The skin depth of the conductor determines the relationship between the resistance and the frequency.

Therefore, R is given by:

$$R = \frac{1}{\delta\sigma} \left(\frac{n'l}{b} \right) = \frac{n'l}{b} \left(\sqrt{\frac{\mu_0\omega}{2\sigma}} \right) = R_0 l \sqrt{\omega} \quad (2.7)$$

$$R_0 = \frac{n'}{b} \left(\sqrt{\frac{\mu_0}{2\sigma}} \right) \quad (2.8)$$

$$C = C_0 l \quad (2.9)$$

Where n' is the number of wire turns which contribute to ohmic losses. $R_0 \sqrt{\omega}$ and C_0 are defined as the per-unit-length resistance and the per-unit-length capacitance of the inclusion.

The per-unit-length capacitance, for the edge-coupled inclusion can be expressed as (2.10):

$$C_0 = \varepsilon_0 \varepsilon_r \frac{F(\sqrt{1-u^2}, \frac{\pi}{2})}{F(u, \frac{\pi}{2})}, \quad u = \frac{g}{2b+g} \quad (2.10)$$

And for the broadside-coupled inclusion as (2.11):

$$C_0 = \frac{1}{4} \varepsilon_0 \varepsilon_r \frac{F(u, \frac{\pi}{2})}{F(\sqrt{1-u^2}, \frac{\pi}{2})}, \quad u = \tanh\left(\frac{\pi b}{2g}\right) \quad (2.11)$$

The effective magnetic susceptibility can be expressed as:

$$\chi_m = -\frac{S}{A} \left(\frac{j\omega L}{R+j\omega L+\frac{1}{j\omega C}} \right) = \frac{S}{A} \left(\frac{\omega^2 LC}{1-\omega^2 LC+j\omega RC} \right) \quad (2.12)$$

The inductance L , is defined as:

$$L = \left(\frac{n^2 \mu_0}{\delta y} \right) s = L_0 S \quad (2.13)$$

Where L_0 is the per-unit-area inductance of the inclusion.

From equation (2.7), (2.9) and (2.12) and 2.13 with substituting the resistance, inductance and capacitance will result an expression for the net magnetic susceptibility as function of geometrical and physical properties of the contour Γ :

$$\chi_m(\omega) = -\frac{1}{A} \left(\frac{L_0 C_0 \omega^2 S^2 l}{1 - L_0 C_0 \omega^2 S l + j R_0 C_0 \omega \sqrt{\omega l^2}} \right) \quad (2.14)$$

The susceptibility is related to the perimeter l and area s of the contour. Thus, inclusions with different topologies but having the same perimeter and area.

The same values for the magnetic susceptibility and permeability can be expressed as equation (2.12) can be rewritten as:

$$X_m(\omega; s; l) = \frac{\left(\frac{\omega}{\omega'_0} \right)^2 \left(\frac{s}{A} \right) s l}{1 - \left(\frac{\omega}{\omega'_0} \right)^2 s l + j \left(\frac{\omega}{\omega''_0} \right)^{3/2} l^2} \quad (2.15)$$

$$\omega_0'^2 = \frac{1}{L_0 C_0}, \quad \omega_0''^3 = \frac{1}{(R_0 C_0)^2} \quad (2.16)$$

$$\omega_0 = \frac{1}{\sqrt{LC}} = \frac{1}{\sqrt{L_0 C_0 s l}}, \quad s l = \left(\frac{\omega_0'}{\omega_0} \right)^2 \quad (2.17)$$

Where the frequency ω_0 is considered as the resonance frequency of the artificial magnetic medium. The formula $\Omega = \frac{\omega}{\omega_0}$ represents the normalized frequency (with respect to the resonance frequency ω_0) and F is the fractional area of the cell occupied by the interior of the inclusion and P is the grouping of all the physical parameters into one parameter.

$$F = \frac{S}{\delta x \delta z} = \frac{S}{A} \quad (2.18)$$

$$P = \frac{1}{A^2} \frac{\omega_0^4}{\sqrt{\omega_0^5 \omega_0^3}} \quad (2.19)$$

$$x_m(\Omega; F, P) = \frac{F\Omega^2}{1 - \Omega^2 + jPF^{-2}\sqrt{\Omega^3}} \quad (2.20)$$

Then, the effective permeability can be written as:

$$\mu(\Omega; F, P) = 1 + x_m(\Omega; F, P) = 1 + \frac{F\Omega^2}{1 - \Omega^2 + jPF^{-2}\sqrt{\Omega^3}} \quad (2.21)$$

2.3 Determination of Negative Permeability from Reflection and Transmission Coefficient

In our simulation on HFSS, it has been demonstrated that the reflection and transmission coefficient calculated from transfer matrix simulations on finite lengths of electromagnetic materials, allows us to determine the effective permittivity (ϵ) and permeability (μ). Our approach is shown by the S-parameter, we invert the scattering data to determine n and z to obtain the value of ϵ and μ [54].

$$z = \pm \sqrt{\frac{(1+r)^2 - t^2}{(1-r)^2 - t^2}} \quad (2.22)$$

We can resolve these ambiguities by making use of additional knowledge about the material. For example, if the material is passive, the requirement that $\text{Re}(z) > 0$ fixes the choice of sign in equation (2.22). Likewise, $\text{Im}(n) > 0$ leads to an unambiguous result for $\text{Im}(n)$:

$$\text{Im}(n) = \pm \text{Im} \left(\frac{\cos^{-1} \left(\frac{1}{2t} \left[1 - (r^2 - t^2) \right] \right)}{kd} \right) \quad (2.23)$$

When we solve for the right-hand side of equation (2.24), we select whichever of the two roots yields a positive solution for $\text{Im}(n)$. $\text{Re}(n)$, however, is complicated by the branches of the arccosine function, or,

$$\text{Re}(n) = \pm \text{Re} \left(\frac{\cos^{-1} \left(\frac{1}{2t} \left[1 - (r^2 - t^2) \right] \right)}{kd} \right) + \frac{2\pi m}{kd} \quad (2.24)$$

where m is an integer.

To determine the value of permittivity and permeability, they are defined from n and z . Then, the permittivity and permeability can be written as:

$$\epsilon = \frac{n}{z} \quad (2.25)$$

$$\mu = nz \quad (2.26)$$

2.4 Rose Curve Characteristic

In this section, we propose the n th order Rose Curve. This new innovative inclusion geometry will be analysed and discussed. In fact, the rose curve can minimize the dependency the value of the inductive and capacitive response of the inclusions. These curves have a principal characteristic, namely the area and the perimeter of these rose curves can be adjusted independently. The parameterization of rose curve can be described in polar coordinates by this equation:

$$R_n(r_0, a): r(\theta) = r_0 + a \cdot \cos(n\theta) \quad (2.27)$$

Where $r(\theta)$ represents the position of an inclusion's contour in the polar coordinate, and θ is the polar angle which sweeps the contour aside the slit. The parameters r_0 and a are constants and n is an integer representing the order of the curve. Note that, due to its formulation, the area and the perimeter of the Rose curve can independently and controllably be selected to achieve enhanced properties of the resonator. To study the characteristics of this inclusion, we have simulated the Rose curve at different orders but within the same area and perimeter.

The new complementary resonators, introducing the rose curve resonators (RCRs), are then used to enhance the miniaturization factor (M -factor). The miniaturization is defined as the ratio of the wavelength to which the complementary inclusions resonate to the length of the microstrip line in the filter device. Henceforth, we design the CRCRs with different order, so as to be able to compare them in terms of frequency bandwidth and M -factor for the CRCRs region. The miniaturization is defined as the ratio of the wavelength at which the complementary inclusions resonate at the length of the microstrip line in the filter device. Table 2.1 summarizes the parameters used to simulate the structure.

Table 2.1 Parameters of the simulated n th rose curve

metal thickness: $t= 35 \mu\text{m}$
traces: copper ($\sigma = 59.6 \text{ s}/\mu\text{m}$)
trace width: $b= 200 \mu\text{m}$
trace gap: $g = 700 \mu\text{m}$
slit width: $d=1 \text{ mm}$

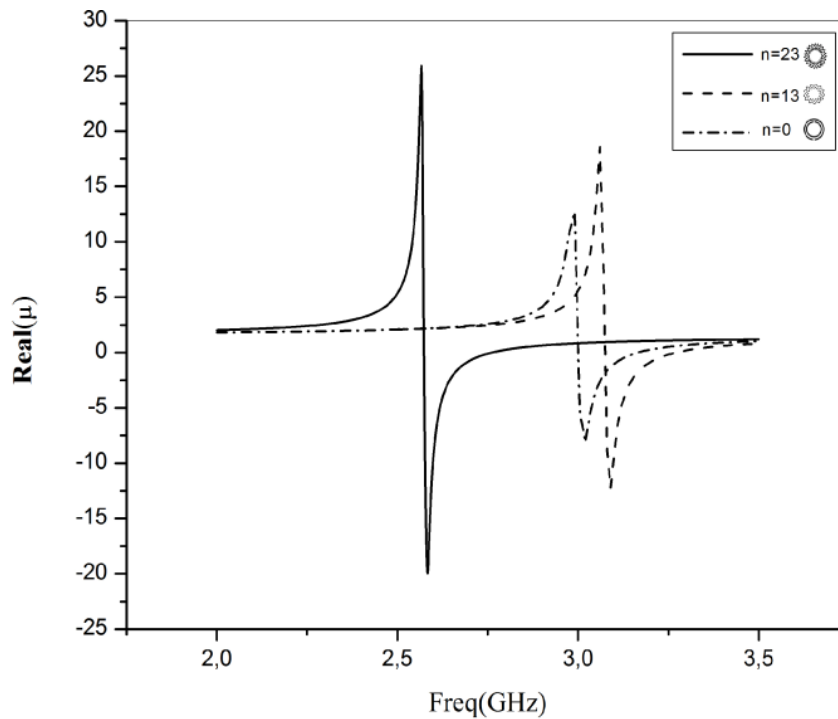


Fig. 2.4 The permeability versus frequency of n^{th} Rose Curve for order $n=0$, $n=13$ and $n=23$.

Then, using Matlab application, the Ansoft HFSS results as S-parameters have been converted to desired parameters based on extraction equation (2.26). Fig. 2.4 shows the variation of the permeability function for the three structures of n -RCR by frequency levels. It shows rose curve of different order while the area is kept constant. For the same geometrical and physical parameter, the frequency resonates at 2.6 GHz, 3 GHz and

3.1GHz. It shows rose curve of different orders while the area are kept constant. Note that the amplitude of the permeability decreases while the order n increases. Moreover, the resonance frequency decreases when the order of the rose curve increases. In fact, higher order rose curve resonators introduce the higher coupling factor.

Table 2.2 shows the effect of the order n of RCR. From order 0 to 23th with radius (r)=0.003mm, amplitude (a)=0.0002 and Area (A)=28.33 μ m.

Table 2.2 Effect of n^{th} order of RCR with similar shape in radius, amplitude and area

n	r	a	A	P	f_r (GHz)	BW (GHz)
0	0.003	0.0002	2.8337.e-005	0.022	3.14	0.76
3	0.003	0.0002	2.8337.e-005	0.019034	3.05	0.72
4	0.003	0.0002	2.8337.e-005	0.019177	3.12	0.73
5	0.003	0.0002	2.8337.e-005	0.01936	3.05	0.69
6	0.003	0.0002	2.8337.e-005	0.01958	3	0.7
7	0.003	0.0002	2.8337.e-005	0.019835	2.96	0.69
13	0.003	0.0002	2.8337.e-005	0.02202	2.85	0.62
18	0.003	0.0002	2.8337.e-005	0.024439	2.69	0.59
23	0.003	0.0002	2.8337.e-005	0.027257	2.61	0.56

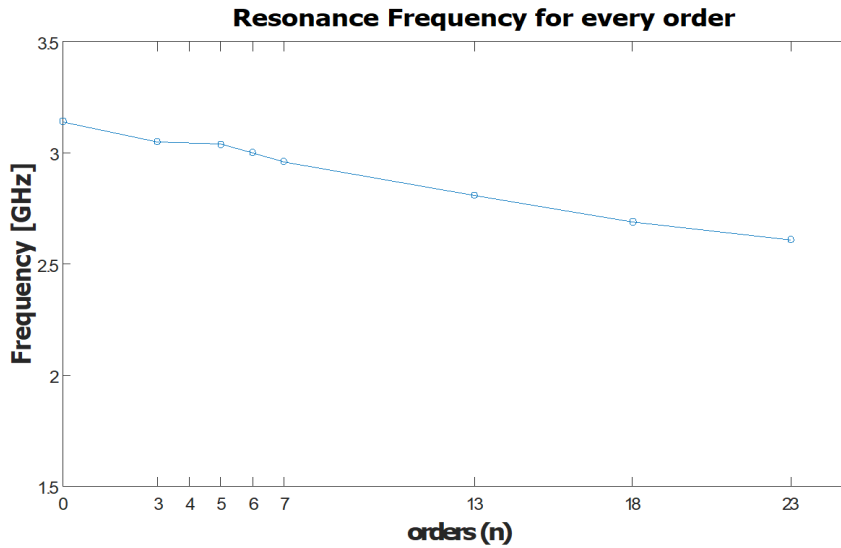


Fig. 2.5 Variation of the resonant frequency with different value of n

Fig. 2.5 demonstrates the resonant frequency of n-RCR versus the order of inclusions when the value of order is changed and radius, amplitude and area are constant. Moreover, the resonant frequency decreases while the n-order of the rose curve increases.

Table 2.3 shows the effect of the radius of an RCR. When order (n)=7 amplitude (a)=0.002 mm then the value of Area (A) and Perimeter (P) are not constant. Fig. 2.6 demonstrates the resonant frequency of n-RCR versus the radius (r) of RCR with some value of radius when order and amplitude are constant. Moreover, the resonant frequency decreases while the value of radius of RCR increases.

Table 2.3 Effect of the radius of RCR with similar shape in amplitude and n=7

n	r	a	A	P	fr (GHz)	BW (GHz)
7	0.002	0.002	1.2629.e-005	0.013988	4.07	0.45
7	0.0025	0.002	1.9698.e-005	0.016874	3.67	0.68
7	0.003	0.002	2.8337.e-005	0.19835	2.96	0.69
7	0.0035	0.002	3.8547.e-005	0.022843	2.51	0.65
7	0.004	0.002	5.0328.e-005	0.025882	2.14	0.58
7	0.0045	0.002	6.368.e-005	0.028942	1.92	0.47
7	0.005	0.002	7.8603.e-005	0.032018	1.86	0.56

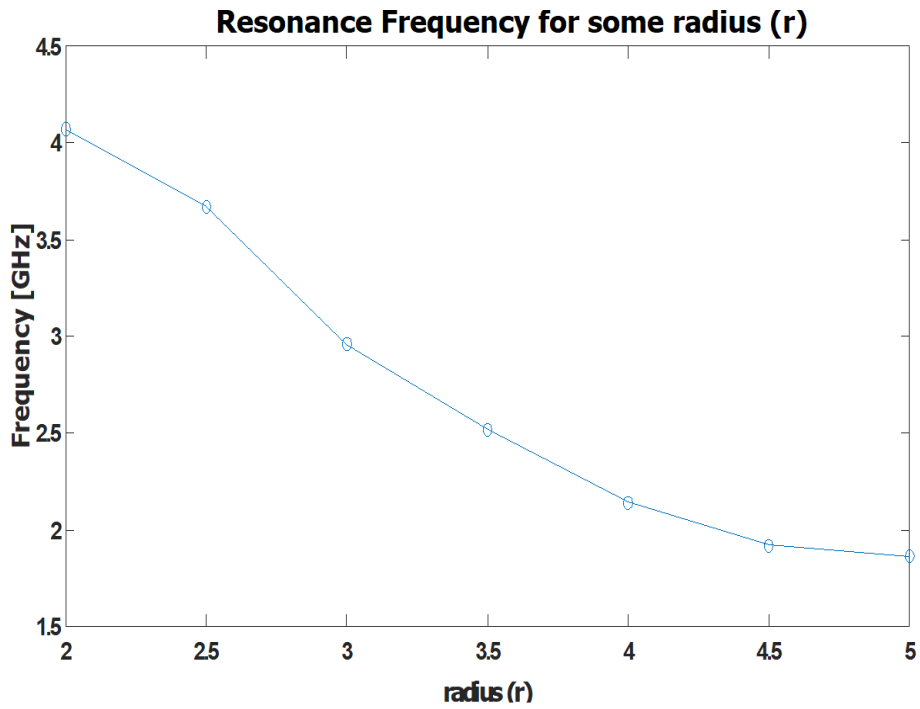


Fig. 2.6 Variation of the resonant frequency with $n=7$ versus radius (r)

Table 2.4 shows the effect on the amplitude of an RCR, when order (n)=7 radius (r)=0.003 mm and value of Area (A) and Perimeter (P) are not constant.

Table 2.4 Effect of the amplitude of RCR with similar shape in radius and $n=7$

n	r	a	A	P	fr (GHz)	BW (GHz)
7	0.003	0.0001	0.00002829	0.019101	3.13	2.67
7	0.003	0.00015	0.00002831	0.019411	3.07	0.65
7	0.003	0.0002	0.000028337	0.019835	2.99	0.63
7	0.003	0.00025	0.000028373	0.020362	3.02	0.79
7	0.003	0.0003	0.000028416	0.020982	3.07	0.76
7	0.003	0.00035	0.000028467	0.021684	2.77	1.09
7	0.003	0.0004	0.000028526	0.022459	2.71	0.5
7	0.003	0.00045	0.000028592	0.023299	2.63	0.51
7	0.003	0.0005	0.000028667	0.024194	2.48	0.4

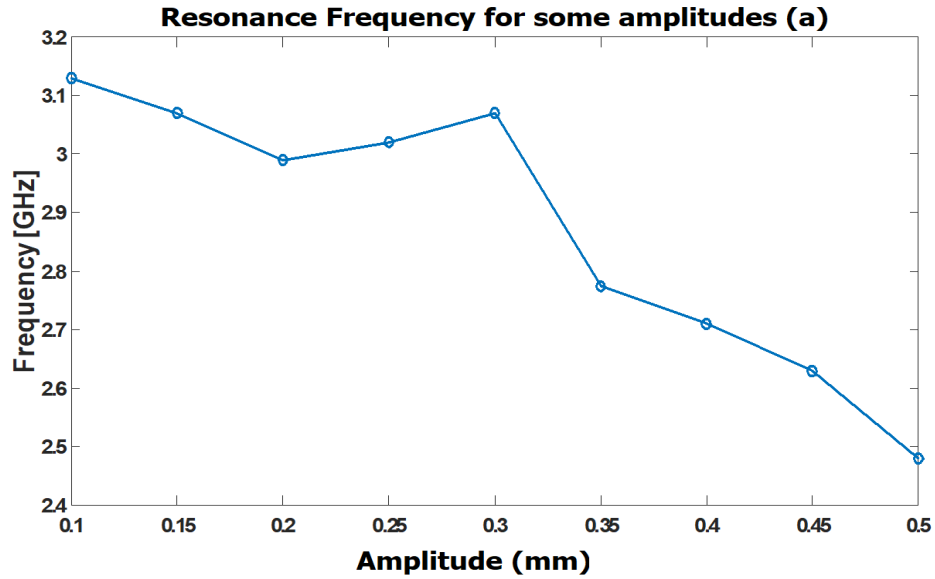


Fig. 2.7 Variation of the resonant frequency with $n=7$ and different value of amplitude of RCR

Fig. 2.7 demonstrates the resonant frequency of n -RCR versus the amplitude of inclusions when the value of order and radius are constant, under different values of amplitude of RCR. Moreover, the resonant frequency decreases while the amplitude of the rose curve increases.

2.5 Microwave Application of Metamaterial Concept with Microstrip Line Based on Complementary Rose Curve Resonators (CRCRs)

This work discusses the complementary rose curve resonators (CRCRs) etched on ground plate under the microstrip transmission line. The CRCRs are applied to increase the miniaturizing factor. Using the basic topology of SRRs, the RCRs behave as an LC resonator that can be excited by an external magnetic flux, exhibiting a strong

diamagnetism above their first resonance [21, 55]. Design of the microstrip line stop-band is shown in Fig. 2.8.

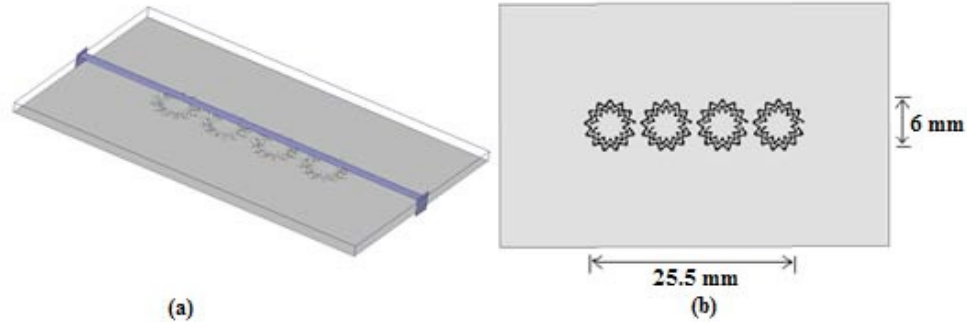


Fig. 2.8 The Microstrip line stopband with CRCRs

The miniaturization is defined as the ratio of the wavelength for which the complementary inclusions resonate to the length of the microstrip line in the filter device. Fig. 2.8 illustrates a schematic representation of the stop-band microstrip filter based on the complementary edge-coupled rose curve resonators. The substrate of microstrip line stop-band set under the following parameters is Rogers RO3010 with length and width of = 45 mm and 25 mm, respectively, and thickness $h =$ of 1.27 mm. The designed microstrip line stop-band consists of 4 CRCRs with a shape that looks like roses. The width of CRCRs trace (etched traces) and the distance between traces are 0.3 mm. The resonant frequency of CSRRs in each design has to be similar to achieve identical and accumulative frequency response for inclusions. The width of the slit at each ring is 0.3 mm, the upper plane conductor strip has a width $w = 1.2$ mm corresponding to an impedance of 50Ω characteristic.

Fig. 2.9 shows the permeability versus frequency of Rose curve n^{th} order with the same area and perimeter. In fact, we can notice that the responses of the inclusions are very similar. Comparing this variation, we observe that the amplitude of the permeability decreases when the order n increases. Moreover, the resonance frequency decreases when the order of the rose curve increases (Table 2.5).

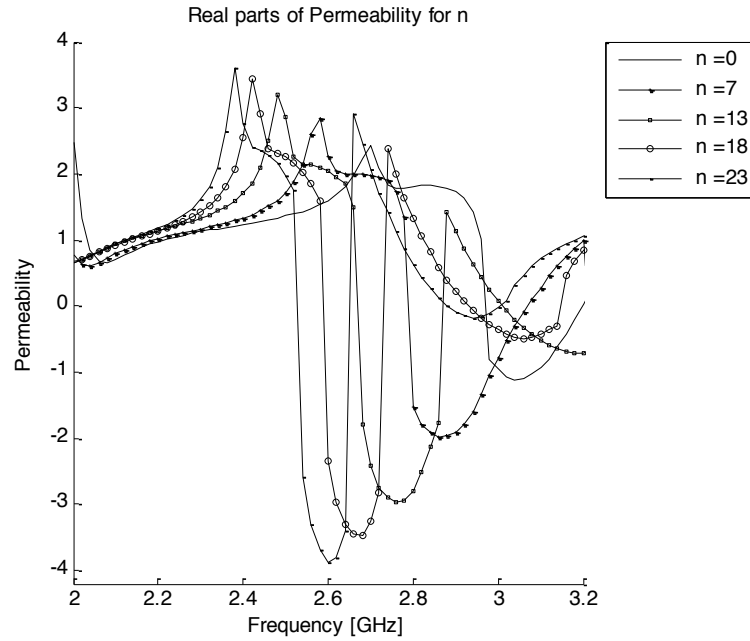


Fig. 2.9 Comparing the permeability versus frequency of nth Rose Curve for n-th order

Table 2.5. Value of negative permeability for nth order of CRCRs on the microstrip lines stop-band

Order (n)	Permeability (u) in dB	Frequency (f) in GHz
0	-1.11	3.04
7	-1.97	2.87
13	-2.96	2.76
18	-3.5	2.68
23	-3.9	2.61

In fact, higher order rose curve introduce the higher coupling factor. Consequently, the resonance frequency and the permeability decrease. In addition, this higher order allows the reduction of the largest dimension inclusions to fit in the unit cell. The resonance frequency could be increased using the rose curve. This enhancement is due to the new coupling scheme between the adjacent segments of the Rose curve. So,

widening the frequency band is an attractive feature of the proposed n^{th} rose curve compare to the circle

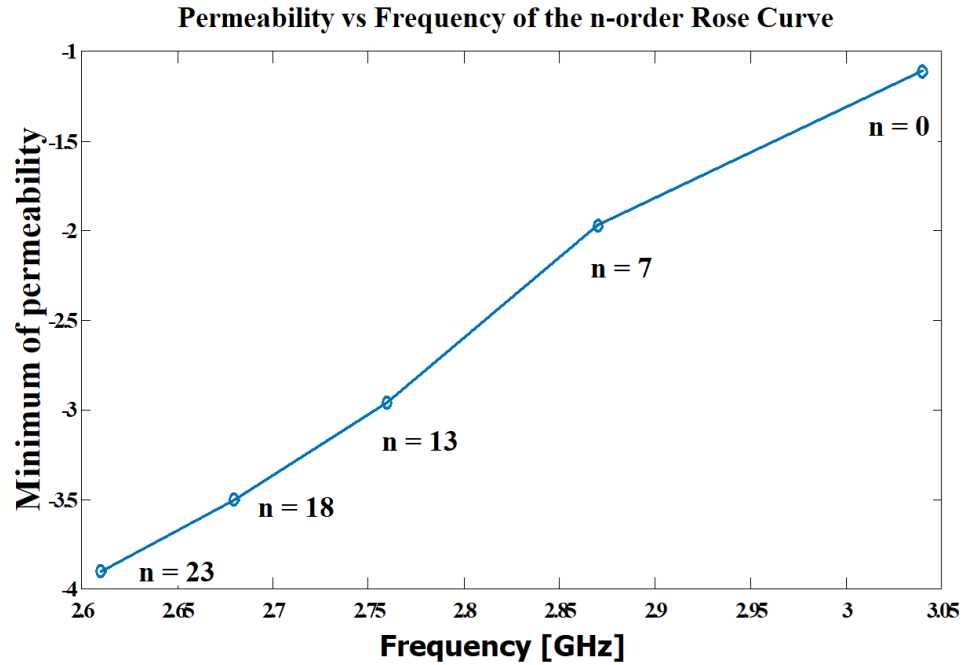


Fig. 2.10 The Permeability vs Frequency for some orders

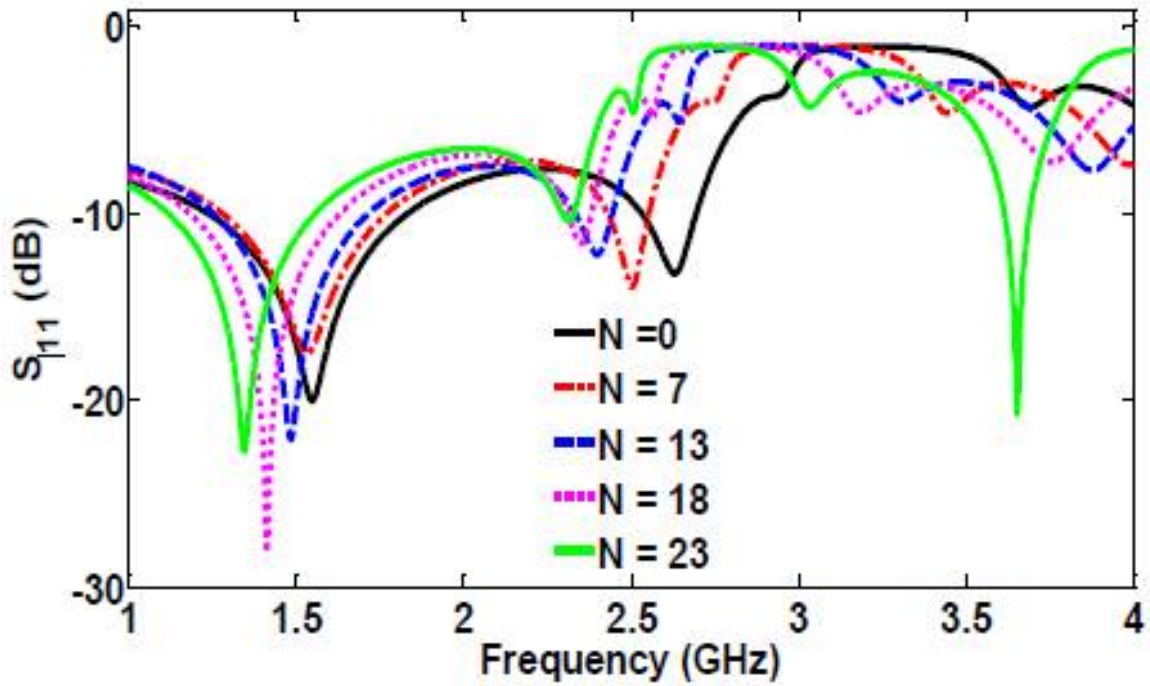


Fig. 2.11 The S_{11} parameter in microstrip lines stopband with n^{th} order of CRCRs

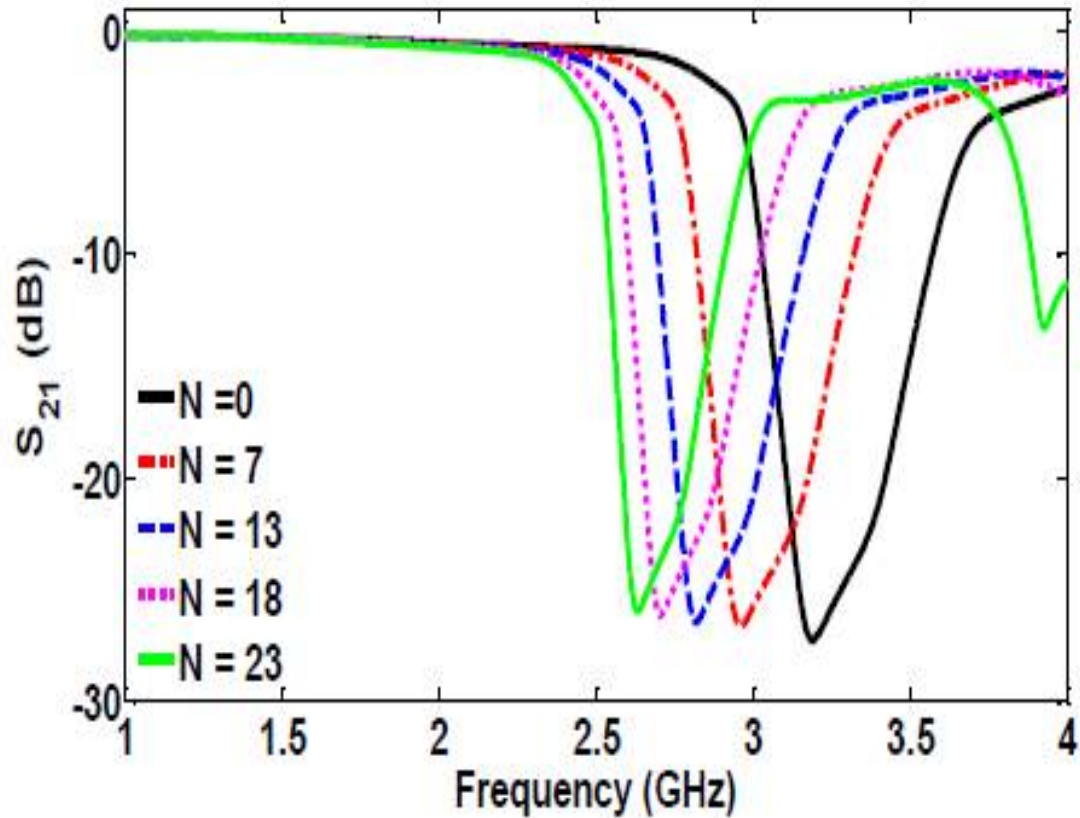


Fig. 2.12 The S_{21} parameter in microstrip lines stopband with n^{th} order CRCR

Fig. 2.10 illustrates the deep rejection of the n^{th} order of CRCRs on the microstrip line stop-band. The resonant frequency increases while the value of n order decreases. However, the minimum amplitude of the permeability function decreases while the resonant frequency increases.

The results of this microstrip line design are shown in Fig. 2.11 and Fig. 2.12 using the HFSS. Fig. 2.11 shows the S_{11} parameter in input source and Fig. 2.12 shows the S_{21} parameters in microstrip lines stopband using the rose curve resonator CRCRs. The results show the impact of increasing of the rose curve resonators order is the frequency resonant of RCR is decreased. It should be emphasized that rose curve resonators increases the miniaturization of the filter. In fact, higher order provides more miniaturization of the bandwidth of the rejection depth.

Table 2.6 Relative bandwidth and rejection depth of microstrip band-stop filter based CRCRs

Order (n)	Bandwidth rejection (%)	Deep rejection (dB)
0	21	54.6
7	20	53.3
13	19	53.1
18	18	52.3
23	17	52

Moreover, Table 2.6 summarizes the resonance frequency of the microstrip lines stopband filter for different n^{th} order and the deep rejection bandwidth. According to fig. 2.9 and table 3, as an example, a good result of simulation has been obtained with a deep rejection band for design frequency for microstrip lines stopband in 23^{th} order. The rejection frequency with sharp cutoffs is obtained at the maximum of 52 dB at a frequency 2.7 GHz. It should be emphasized that using rose curve resonator improves the miniaturization of the filter. In fact, higher order provides more miniaturization of the bandwidth of the rejection wide.

Fig. 2.13 illustrates the fabrication of the microstrip lines stop-band filter based on CRCRs with n^{th} order with microstrip lines without CRCRs.

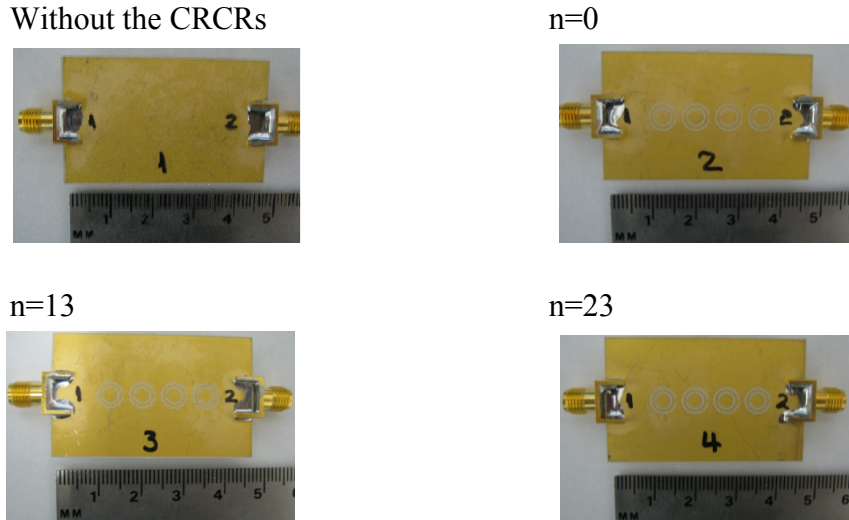


Fig. 2.13 Fabrication of Microstrip lines Stop-band Filter based on CRCRs with $n=0$, $n=13$, $n=23$ orders and without CRCRs

The measurement results of this project are shown in Fig. 2.14 and Fig. 2.15. Fig. 2.14 illustrates the use of the S_{11} parameter and Fig. 2.15 shows the S_{21} parameters in microstrip lines stopband using the rose curve resonator CRCRs. This measurement result shows the resonance frequency of the microstrip line decreases to the number of order of RCRs.

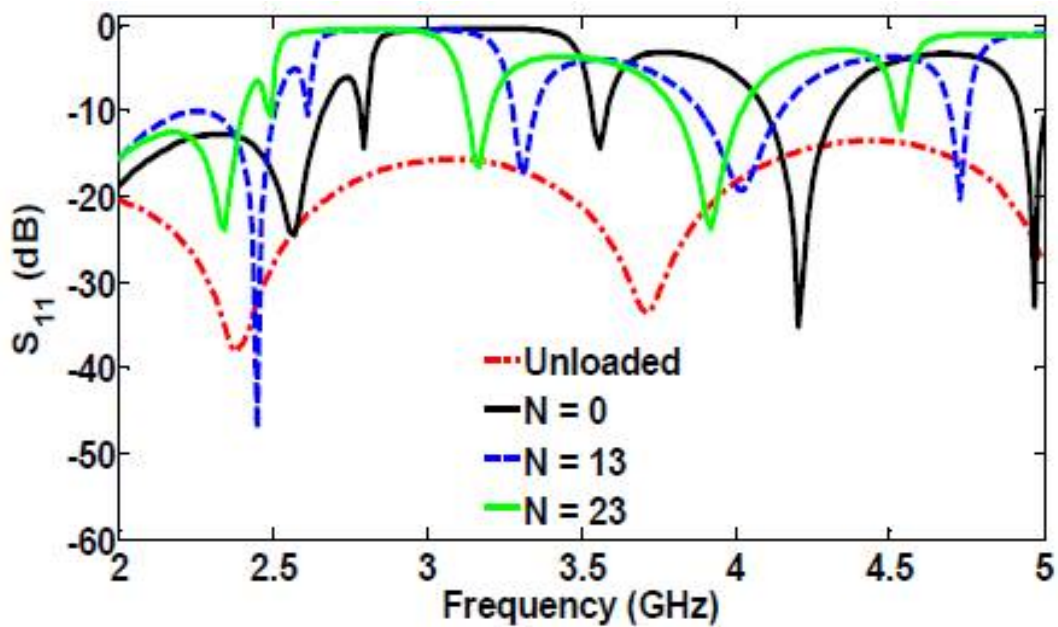


Fig. 2.14 S_{11} parameter in microstrip lines stopband with n^{th} order CRCRs

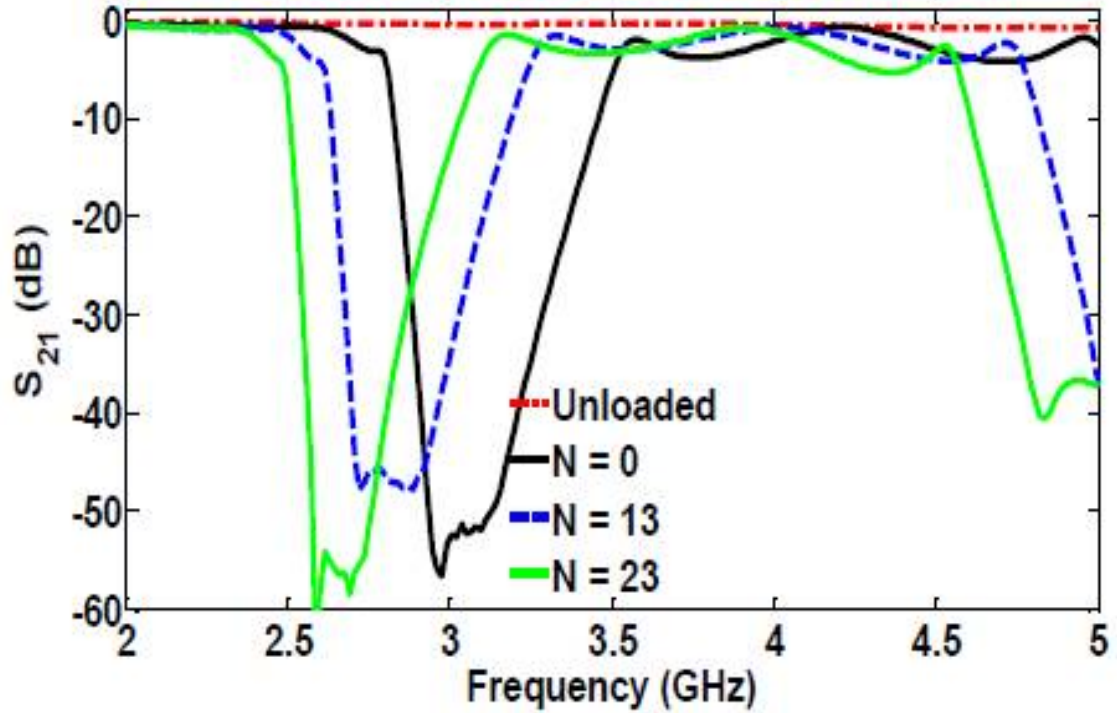


Fig. 2.15 S_{21} parameter in microstrip lines stopband with n^{th} order CRCRs

To examine numerically the miniaturization effect of the CRCR-loaded ground plate, the microstrip stop-band filter is designed to operate at 2.4 GHz. For this purpose, proper inclusions are designed so that the stop-band frequency remains approximately identical.

Table 2.7. Comparison table of the different miniaturized Size of CRCRs

Order (n)	Radius (r) mm	Length (l) mm	Wide (l*2r) mm ²	Miniaturized Size (%)	Frequency (f) Ghz
0	3	51	306	0	2.43
13	2.8	35.6	199	35	2.31
23	2.3	25.6	118	62	2.47

Table 2.7 summarizes the design values for different CRCRs. It is noticeable that the miniaturization is increased by a factor of about 2 when the order changes from 13 to 23. The technique in design can be used for integration of the microstrip line filters in any size packages while maintaining the device performance.

Chapter 3

Metamaterial Power Divider for Beamforming System Based on Butler Matrix

Directional coupler is a four-port circuit with one of ports is isolated from the input ports. Passive reciprocal networks with four ports are ideally matched and lossless [26]. It can be realized in microstrip, stripline, coax and waveguide. They are used for sampling a signal, sometimes for sampling both incidents and reflected waves (this specific application is called a reflectometer, which is an important part of a network analyzer). Assuming that the 4 ports have the following assignments: Port1 is the Input port and its functionality is to direct the input power P_1 , Port2 is the through port, on which one part of input power is directed while Port3 is a coupled port, and port4 is a isolated one.

The Hybrid coupler (3-dB) is a special directional coupler with four ports that is designed for a 3-dB equal power split. This kind of coupler comes in two types: 90° (or quadrature) hybrid and 180° hybrids. In many references papers such as: [26-29, 56], branch line has been studied and presented as a combiner , where the input signal are the vectors of magnitude A and phase B, and the outputs are splitting identically the input power. In [27] a reduction method about 45% and 90% coupler size was proposed. It consists at combining a short high-impedance transmission line to a shunt lumped capacitor. Based on the same idea, the efficient plan approached to reduce circuit size without increasing complexity of the fabrication process [29]. This allows considerable size reduction of 3-dB coupler in the range about 62%. It has been proved that metamaterials with resonators on the transmissions lines can be applied for size reduction in microwave applications, such as transmission lines, filters and antennas. There are number of resonator types that can be useful in the development of RF and microwave filters and size reduction applications [22, 25, 57]. Many researches for 3-dB conventional coupler with miniaturization size indicates that they behave as left hand materials close to the narrow band around their resonating frequency [12, 30, 56, 58-60].

It is important to mention that the frequency selectivity properties of CSRR allows to use them in applications where miniaturization is a key development aspect [30]. Common branch line coupler is design on microstrip line. Fig. 3.1 shows the geometry of the Quadrature Hybrid coupler

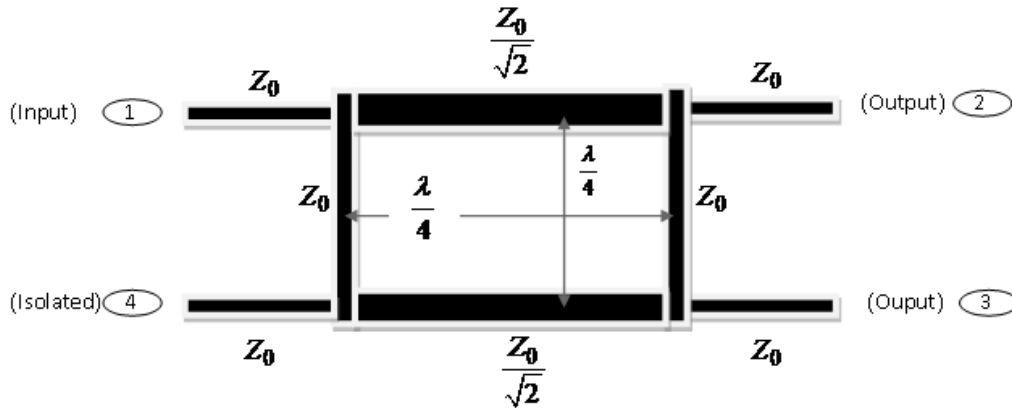


Fig. 3.1 Geometry of the Quadrature Hybrid coupler

In addition, CSRRs and CRCRs are also used in the design of 90° microstrip coupler. The configurability of the footprint and performance of the design can be compared with a coupler loaded with or without circular shape CSRRs. The focus of our study is to shrink the size of 90° microstrip coupler using CSRRs and CRCRs while maintaining good performance from a conventional coupler. It is important to mention that the frequency selectivity properties of CSRR allow to use them in applications where miniaturization is a key development aspect [28, 29, 61].

3.1 Theory and Circuit Model of Compact 90° Microwave Directional Coupler

Fig.1 is shown a single 3-dB-branch line hybrid coupler. In general, the 3-dB directional coupler is characterized by four important parameters: Insertion Loss(IL), Isolation(I), Coupling Factor (CF), Return Loss(RL) and Directivity(D), as defined bellow:

$$IL = 10 \log \left(\frac{P_1}{P_2} \right) = -20 \log(S_{21}) \quad (3.1)$$

$$I = 10 \log \left(\frac{P_1}{P_4} \right) = -20 \log(S_{41}) \quad (3.2)$$

$$CF = 10 \log \left(\frac{P_1}{P_3} \right) = -20 \log(S_{31}) \quad (3.3)$$

$$RL = -20 \log(S_{11}) \quad (3.4)$$

$$D = 10 \log \left(\frac{P_4}{P_3} \right) = -20 \log \left(\frac{S_{31}}{S_{41}} \right) \quad (3.5)$$

In fact, the operational frequency of the 3-dB coupler outputs must be matched, so we will choose the line parameters in the following relations:

$$S_{12} = S_{21} = -\frac{j}{\sqrt{2}} \quad (3.6)$$

$$S_{13} = S_{31} = -\frac{1}{\sqrt{2}} \quad (3.7)$$

$$S_{11} = S_{22} = S_{33} = S_{44} = 0 \quad (3.8)$$

The S-parameters are obtained for 3-dB Branch line Hybrid coupler with electrical length of 90° by applying the even-odd mode decomposition techniques [26, 58]. In even mode, the approach consists at determining equivalent electric circuit of coupler and deriving the open stub in two distinct pairs of ports. Each open circuit is replaced by an admittance $Y = j \tan(\beta l) = j$ when $l = \frac{\lambda}{8}$ and $\beta = \frac{2\pi}{\lambda}$. Then, the circuit is subdivided in three transmission matrices such as: the transmission line (T_1), the shunt stub circuit (T_2) and the upper part (T_e).

$$T_1 = \begin{pmatrix} A & B \\ C & D \end{pmatrix} = \begin{pmatrix} \cos \beta l & \frac{1}{2} j \sin \beta l \\ j\sqrt{2} \sin \beta l & \cos \beta l \end{pmatrix} \quad (3.9)$$

$$T_2 = \begin{pmatrix} A & B \\ C & D \end{pmatrix} = \begin{pmatrix} 1 & 0 \\ j & 1 \end{pmatrix} \quad (3.10)$$

The global matrix T_e is given as:

$$T_e = T_2 T_1 T_2 = \frac{1}{\sqrt{2}} \begin{pmatrix} -1 & j \\ j & -1 \end{pmatrix} \quad (3.11)$$

According to equation (3.11) we derive the values of the reflexion and transmission coefficients given by $\Gamma_e=0$ and $T_e=-\frac{1+j}{\sqrt{2}}$. More details about how to derive these relations are provided in [26, 58]. An analog explanation leads to obtain the same coefficients for odd mode analysis: $\Gamma_o=0$ and $T_o=\frac{1-j}{\sqrt{2}}$.

Derivation of reflection and transmission coefficients in even and odd mode is undertaken to obtain the S-matrix:

$$S = \begin{pmatrix} S_{11} & S_{12} & S_{13} & S_{14} \\ S_{21} & S_{22} & S_{23} & S_{24} \\ S_{31} & S_{32} & S_{33} & S_{34} \\ S_{41} & S_{42} & S_{43} & S_{44} \end{pmatrix} = -\frac{1}{\sqrt{2}} \begin{pmatrix} 0 & j & 1 & 0 \\ j & 0 & 0 & 1 \\ 1 & 0 & 0 & j \\ 0 & 1 & j & 0 \end{pmatrix} \quad (3.13)$$

The value of S-parameters relate to the line length and frequency of the 3-dB 90° Hybrid branch line coupler. One fundamental principle of wave propagation in lossy media by using the following equations:

$$f = \frac{c}{4l\sqrt{\epsilon_r}} \quad (3.14)$$

Eq. (3.14) is a typical relation between the electrical length and fix length of a coupler to quarter of wave length. Where c is the light velocity in free space, l is the transmission line length and ϵ_r is the relative permittivity of the transmission line material. The frequency of the directional coupler sees its matched output decreases while the line length increases. The symmetry of S matrix in eq. (13) can be used for any port of coupler as the input port S.

3.2 Analysis and Design of Conventional Power Divider

A 90° coupler is a special case of four ports directional coupler that is designed for an equal power split. In a number of references such as: [29] and [27], branch line coupler has been studied and presented as a combiner, where the input signals are vectors of magnitude A and B , then the outputs are as shown. In [27], a technique to reduce the size of the coupler by 45% was presented. The technique is based on the combination

between the short high-impedance transmission lines and shunt lumped capacitor. The same idea is proposed in [27], this is an efficient approach to reduce the design size without increasing the complexity of the fabrication process with a 62% size reduction of the 90° microstrip coupler. The method used lumped element and distributed element to reduce the size of the device. In this research, we propose a conventional coupler size reduction, which behave as left hand material in a narrow band for a specific resonating frequency. The coupler is designed at the operational frequency $f_0 = 2.5GHz$.

Simulation and Discussion

In fig. 3.1, represents the top of conventional coupler. The structure consists of two pairs of transmission lines on the substrate to create identical power divider between the two output ports (Port 2 and Port3). Due to the fact that the expecting functional frequency is $f = 2.5$ GHz and electrical length of the transmission line corresponding to $\Theta = 90^\circ$ the phase shifting between port 2 and port 3 represented on figure 1 is $l = \frac{\lambda}{4}$,

for the Duroid Rogers TM substrate with the thickness $h = 0.25mm$ and relative permittivity $\epsilon_r = 2.2$. The 3-dB coupler transmission line working at $f = 2.5$ GHz. Fig. 3.2 is the HFSS model of a conventional coupler with an area of 32.94 millimeters x 32.94 milimeters in a Duroid Roger TR substrate. It is possible to decrease its size by loading CSRR or CRCR on its ground plane.

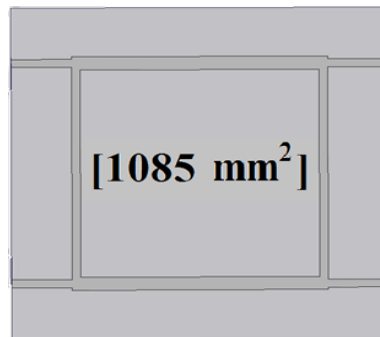


Fig. 3.2 Directional 90° microstrip conventional coupler

In [25, 57] it has been proved that negative left hand material combined with the strip line, allows the shifting of its functional frequency. The issue to recover the identical

frequency on which the transmission line worked without resonator consists at shrinking its length. This important property leads to the size reduction of many RF components.

Fig. 3.3 and Fig 3.4 show the HFSS simulation result for S parameters conventional coupler. The frequency range is from 2.4 GHz to 2.6 GHz. Fig 3.3 shows the coupler having the -3dB power divided at port 1 and port 2, and the attenuation at port 1 and port 4. It shows no power reflection at the ports. The different phase between S_{21} and S_{31} has a 90° phase shifting. Fig. 3.4 shows the 90° microstrip coupler frequency response S_{11} , S_{21} , S_{31} and S_{41} of the device without any ring.

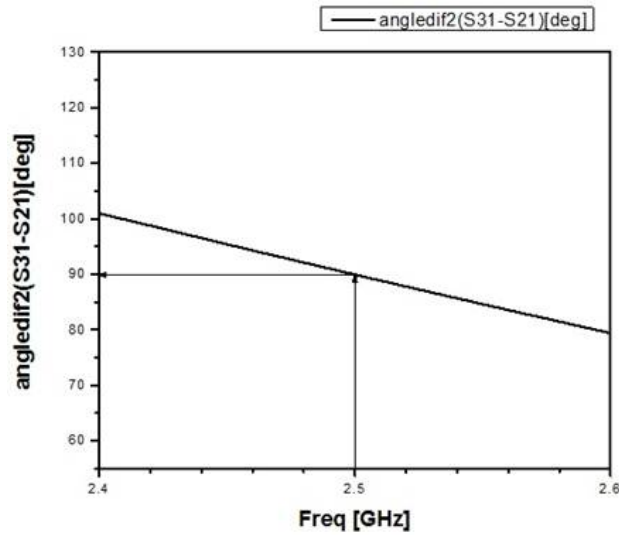


Fig. 3.3 Phase Difference of 90° Microstrip Conventional Coupler

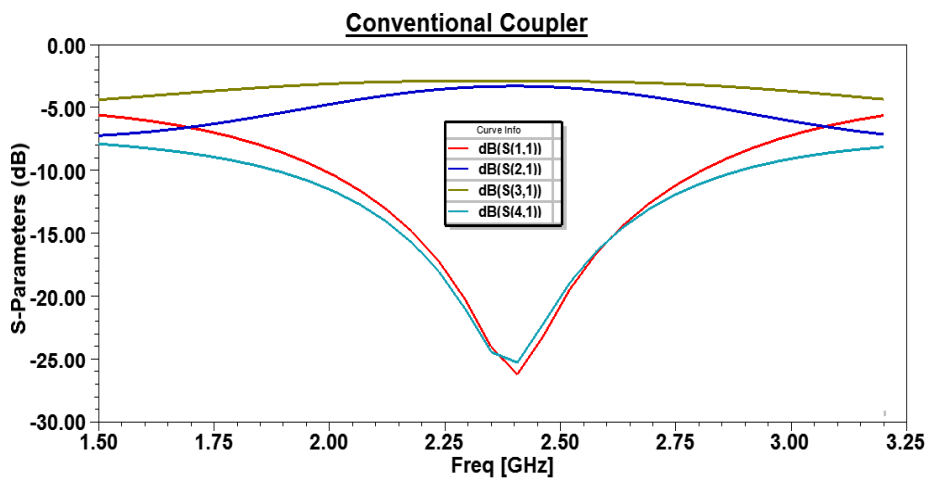


Fig. 3.4 Simulation results of the S parameters for the Conventional Couple

This coupler design results in value of s_{21} and s_{31} close to -3 dB while those of s_{11} and s_{41} are smaller than -20 dB which means that there are not return loss and all the input power are distributed to ports 2 and 3. At $f = 2.5$ GHz the device behaves like a good 3-dB Quadrature Branch line coupler.

3.3 Analysis and Design of Metamaterial Power Divider

In this section, we make comparison between the conventional 90° microstrip coupler (without ring), 90° microstrip coupler with CSRRs and 90° microstrip coupler with CRCRs. By combining CSRRs with the strip lines in series, then a compact bandpass filter can be obtained. With the left-hand property of CSRRs due to its negative electromagnetic properties, it acquires a frequency shifting property when added to a simple transmission lines. Our approach is to load the ground plane effect of the CSRRs on the microstrip transmission line. We introduce an efficient way to shift the resonance frequency of CSRRs by transforming circular circumference to Rose curve form. We propose a conventional coupler size reduction, based on CSRRs and CRCRs which behave as left hand material in a narrow band for a specific resonating frequency.

The coupler is designed at the operational frequency $f_0 = 2.5$ GHz. Fig. 3.5 shows the parameters of Split ring resonator and Rose curve resonator with $n = 13$. The parameters of the SRR are: the external radius of outer ring $r_1 = 2.35$ mm, the external radius of inner ring $r_2 = 1.85$ mm, the width of the ring $c = 0.3$ mm, and the length between ring $d = 0.2$ mm.

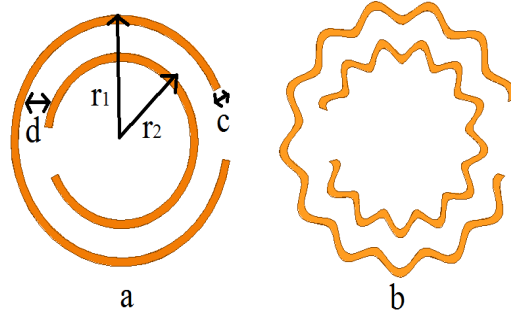


Fig. 3.5. (a) Split Ring Resonator (SRR), and (b) Rose Curve Resonator with order=13

The substrate material is a Duroid Rogers *tm* with: a relative permittivity $\epsilon_r = 2.2$, and a thickness $t = 0.25\text{mm}$. The area of the coupler with no inclusion is 1085 mm^2 . Several complementary resonators topologies such as complementary split ring resonators (CSRRs) and complementary rose curve resonators (CRCRs) have been used to design compact directional microstrip couplers. The complementary split ring resonators (CSRRs) and the complementary Rose Curve resonators (CRCRs) are etched from the ground plate, under the microstrip lines of the coupler. M -factor is defined as the miniaturization factor (*Original Coupler Area*)/(*Compact Coupler Area*). The area for a 90° microstrip coupler based on CSRRs with the M -factor = 8.85 is 508 mm^2 and the area of a patch antenna based on CRCRs with M -factor = 2.15 is 501.3 mm^2 . Fig. 3.6(a) shows a 90° microstrip coupler based on complementary split ring resonators (CSRRs) and Fig. 3.6(b) shows a 90° microstrip coupler based on a complementary edge-coupled rose curve resonators (CRCRs). Ansoft HFSS version 15.0, a commercial 3D full-wave simulator, is used to calculate the S parameters to optimize and to investigate the coupler over the center frequency f_0 . Next, CSRR and CRCR are patterned on the ground plane and the design optimized for the compact size.

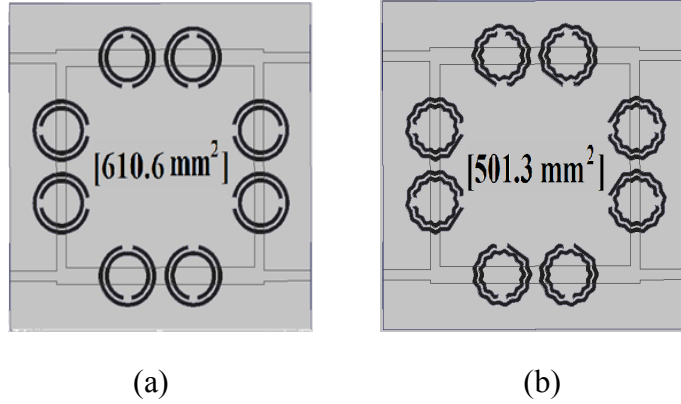
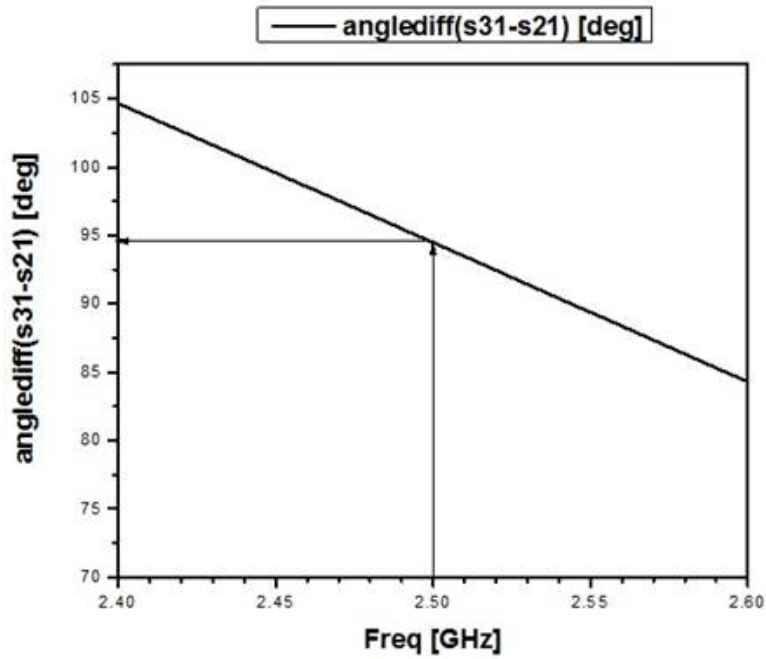


Fig. 3.6 Directional 90° microstrip coupler (a) Compact coupler design based on CSRRs, and (b) Compact coupler design based on CRCRs

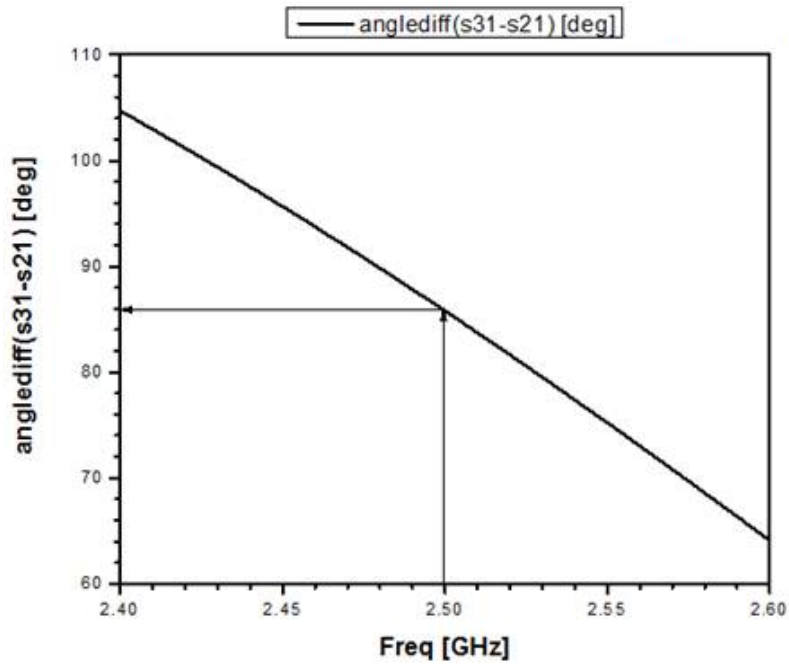
Simulation Results

In this work, we make comparison between the conventional 90° microstrip coupler (without ring), 90° microstrip coupler with CSRRs and 90° microstrip coupler with CRCRs. By combining CSRRs with the strip lines in series, compact bandpass filter can be obtained. With the left hand property of CSRRs due to its negative electromagnetic properties, it behaves as frequency shifting when added to a simple transmission lines. Our approach is to load the ground plane effect of the CSRRs on the microstrip transmission line. We were able to demonstrate an efficient way to shift the resonance frequency of CSRRs by transforming circular circumference to a Rose curve form.

The sizes of conventional coupler of fig. 3.6 have been reduced by 25% for the miniaturized hybrid according to CSRR and by 32% when using CRCR. Fig. 3.7 shows the HFSS simulation result of the different phase of the microstrip coupler with CSRR and with CRCRs and Fig 3.8 shows the HFSS simulation result for S parameters of the microstrip coupler with CSRR and with CRCRs. The frequency range is from 2.4 GHz to 2.6 GHz.



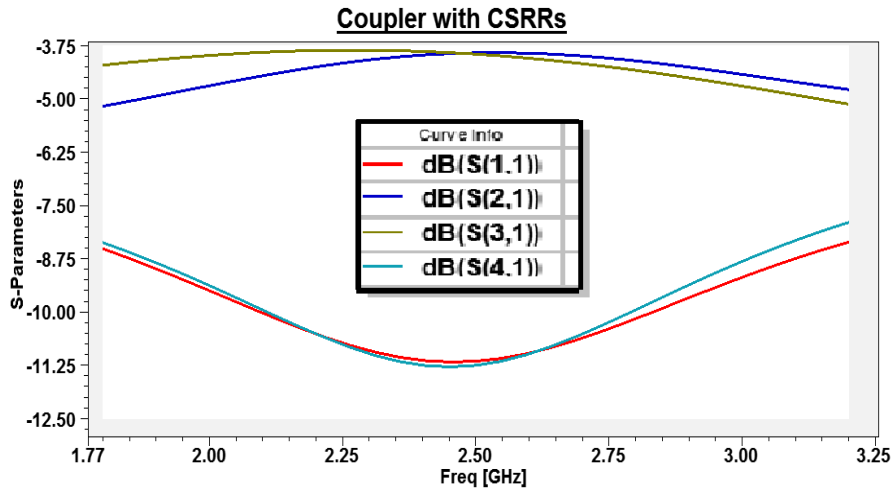
(a)



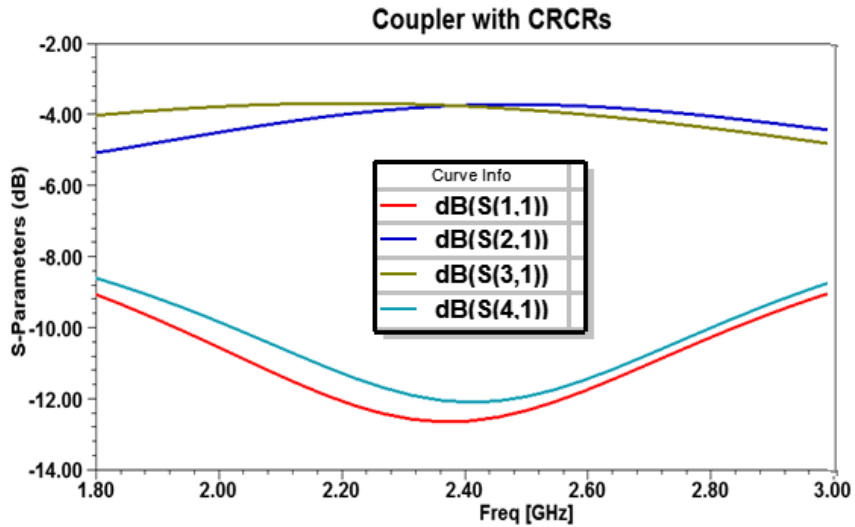
(b)

Fig. 3.7 Different Phase of 90° Microstrip Coupler (a) Compact coupler design based on CSRRs and (b) Compact coupler design based on CRCRs

Fig 3.7 (a) shows the microstrip coupler with CSRRs has an attenuation of around -12dB with a phase difference of about 94° , which is acceptable for a phase shifting of 90° . In the same way, we can obtain the identical power split using the microstrip coupler based on CRCRs. Fig 3.7(b) shows that the phase difference between S_{21} and S_{31} of the microstrip coupler with CRCRs is around 90° . Fig 8(a) shows the 90° microstrip coupler frequency response S_{11} , S_{21} , S_{31} and S_{41} of the device with CSRRs and Fig. 3.8(b) with CRCRs.



(a)



(b)

Fig. 3.8 Simulation result of the S parameters for the structure (a) based on CSRRs, and (b) based on CRCRs

Moreover, Table 3.1 summarizes the design values for different CRCRs. Based on the standard of a 90° microstrip coupler (without inclusion), we can observe that CSRRs ($n=0$) reduce the size by almost 44%, whereas the CRCRs ($n=13$) reduce the size by about 53%. The same value of phase difference of microstrip coupler without ring, with CSRRs and with CRCRs is obtained. The CRCRs are applied to increase the miniaturizing factor.

Table 3.1 Comparison table of compact 90° Microstrip Coupler based on CSRRs and CRCRs

Order (n)	90° Microstrip Metamaterial Coupler	
	Size (mm ²)	Size Reduction (%)
0 (CSRRs)	610.6	44
13 (CRCRs)	501.3	53

3.4 Experimental

In Fig. 3.9, we illustrate the measured couplers. It is clear that for the coupler loaded with CRCR, the reduction size is greater than the one using CSRR.

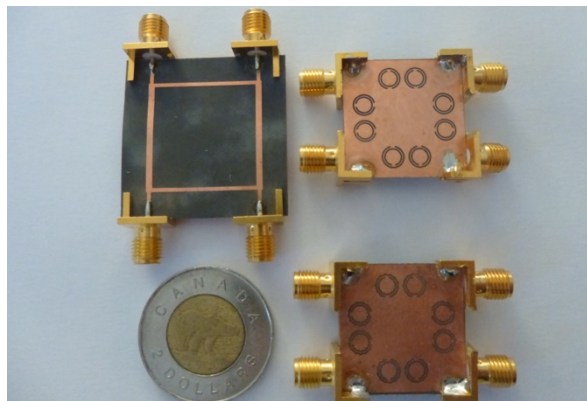


Fig. 3.9 Fabrication design of 90° Microstrip Coupler

Fig. 3.10 illustrates a good agreement of experimental and numerical study. We use an Agilent Vectorial Network Analyser to derive the amplitude and phase shifting of S parameter of a microstrip coupler with CSRR and CRCR. We found that in the narrow band between 2.4 GHz and 2.6 GHz, the models of couplers behave as a power divider.

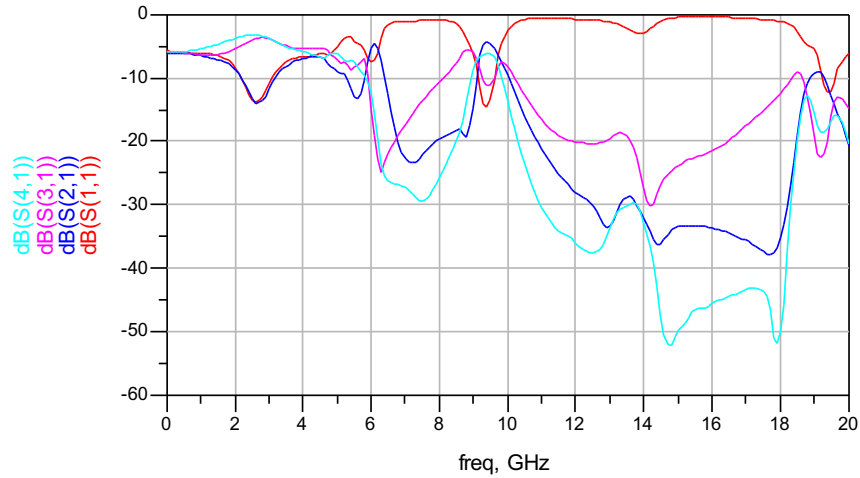


Fig. 3.10 Experimental results of the S parameters in the frequency range 0 GHz to 20 GHz.

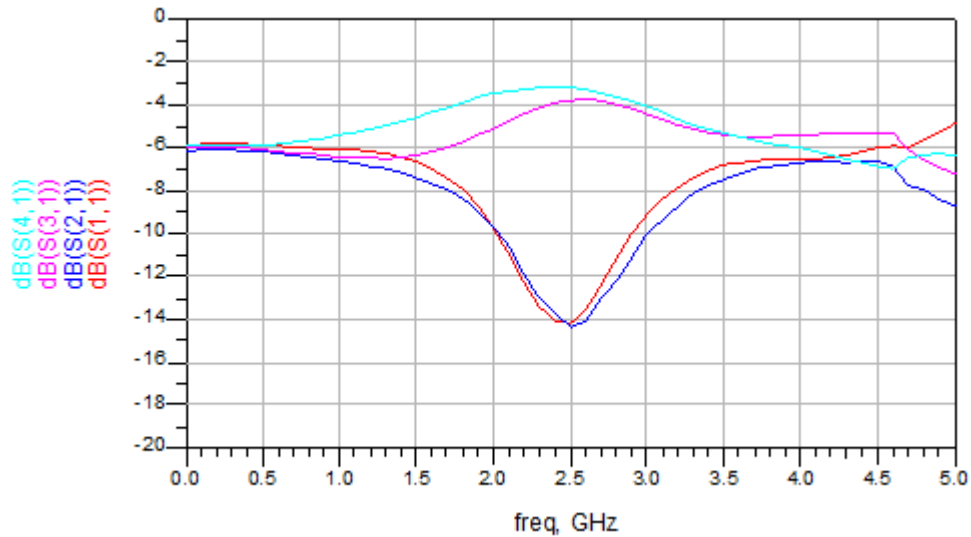


Fig. 3.11 Experimental results of the S parameters in the frequency range 0 GHz to 5 GHz.

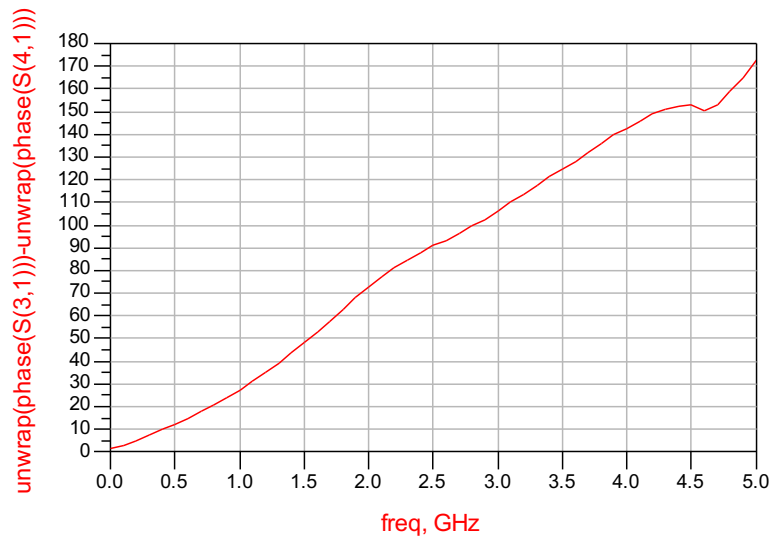


Fig. 3.12 Experimental phase shifting between port 2 and 3 in the frequency range of 0 GHz to 5 GHz

Chapter 4

Metamaterial Antenna for Beamforming System Based on Butler Matrix

In this section, we introduce the properties of arrays antenna for Butler matrix system. Array antennas consist of multiple stationary elements, which are fed by signal of amplitude and phase to have an appropriate beam at different angle in space. They can give the ability to scan in both vertical and horizontal direction. Each antenna of an array radiates a vector directional pattern which has both radial and angle depending on the distance of each antenna. However, when the distance is very far from the element, then the *far field* dominates over the *near field* [62]. It shows that the required distance (R) formula using the far field approximation depends on the degree of the fine structure of the antenna pattern.

$$R = 10L^2 / \lambda \quad [4.1]$$

Which, R is the required distance, L is the largest array dimension of the antenna and λ is the actual wavelength.

The distance commonly used for many pattern measurements is

$$R = 2L^2 / \lambda \quad [4.2]$$

We design four patch antennas for the Butler matrix system. According to the Babinet principle, the apertures with metal plates have its metal parts replaced with the complementary of planar metallic structure. Hence, due to the duality theorem, these two structures have approximately the same resonant frequency. The configuration of the proposed Patch antenna is shown in Fig. 4.1(a) which shows a conventional patch antenna, Fig. 4.1(b) shows the

metamaterial patch antenna based on a complementary split ring resonators (CSRRs) and Fig. 4.1(c) shows a metamaterial patch antenna based on complementary rose curve resonators (CRCRs). The patch antenna is designed with CSRRs and CRCRs etched on the ground plate under the patch line.

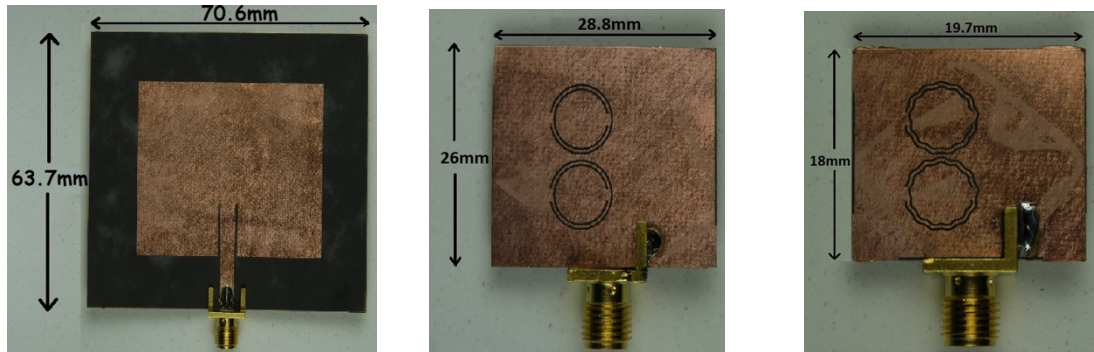


Fig. 4.1 Configurations of patch antennas: (a) Conventional patch antenna, (b) Patch antenna with CSRRs, and (c) Patch antenna with CRCRs

4.1 Analysis and Design of Patch Antenna Conventional

The design of the conventional Patch antenna is shown in Fig. 4.2

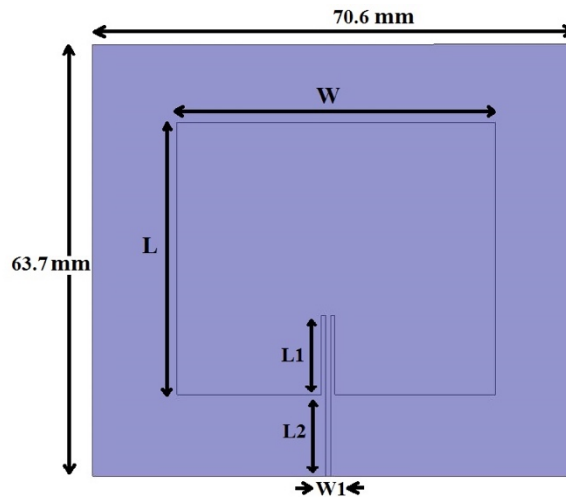


Fig. 4.2 The configuration of a conventional Patch antenna

Table 4.1 Parameters of the conventional Patch antenna

Width of antenna (W)	47mm
Length of antenna (L)	40mm
Insert feeding length	11.7mm
Width of microstrip line (W1)	0.78 mm

The conventional Patch antenna is designed at the operational frequency $f_0 = 2.4$ GHz and with a substrate material made of Duroid Rogers *tm*, with a thickness (h) of 0.25 mm and a relative dielectric constant (ϵ_r) of 2.2. The substrate has dimensions of 63.7 mm x 70.6 mm and is fed by a 50 Ω microstrip transmission line. The top square metal plate has the following parameters: W is the y-length of the patch antenna of 47 mm and L= 40 mm for the x-length of the patch antenna, L1 = 11.7mm, L2 = 12mm, and the width 50 Ω of W1 = 0.78mm. Table 4.1 shows the parameters of the conventional Patch antenna

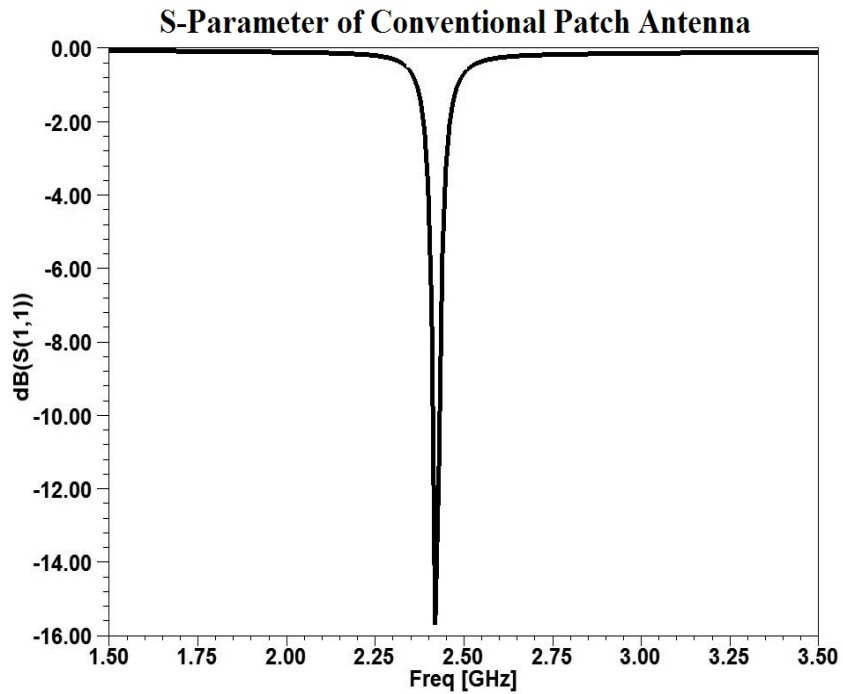


Fig. 4.3 S₁₁ parameter result for conventional Patch antenna

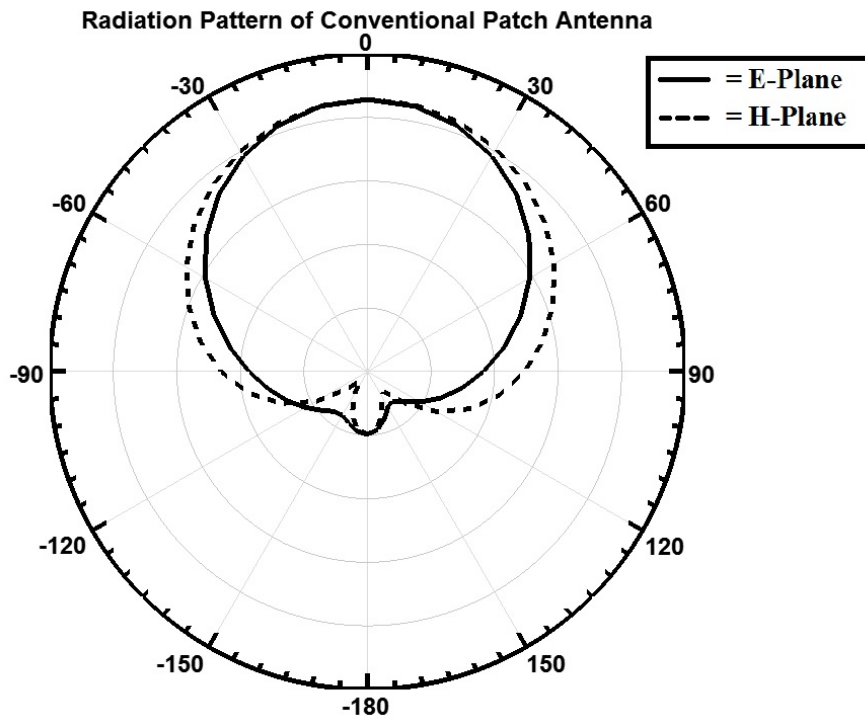


Fig. 4.4 Radiation pattern of the designed conventional patch antenna

The antenna is simulated by using finite-element analysis based on Ansys HFSS version 15. Fig. 4.3 shows the simulation for S_{11} parameter with at conventional patch antenna which resonates at 2.4 GHz with a reflection coefficient of -16 dB. Fig. 4.4 shows the radiation pattern of the designed conventional patch antenna in H_plane and E_plane.

4.2 Analysis and Design of Metamaterial Patch Antenna

The concept of Left-handed material (LHM) was first proposed by Veselago [16]], as well as the electromagnetic dual of SRRs called complementary split ring resonators (CSRRs) proposed by etching of SRRs off a conducting sheet [1, 19].

SRRs have been applied in many applications for design of artificial media. The most interesting feature is the ability to exhibit a quasi-static resonant frequency at wavelengths that are much smaller than its own size. Based on their duality, CSSRs provide a controllable electrical response in applications with a negative permittivity than can be derived from the negative permeability nature of SRRs in a straightforward way. The implementation for their application can be used in designing simple planar filter [23, 24, 63], compact antennas [32, 33], circularly polarized antenna [34, 35] and dual band antenna [36].

Therefore, the application of SRRs for designing an antenna is of great interest. In this section, a novel design of Patch antenna with complementary split ring resonators (CSSRs) and complementary rose curve resonators (CRCRs) is presented. The goal of our design is to shrink the size using both CSRR and CSCR which behave as a left handed material in a narrow band around their resonating frequency [30] [59]. Note that the frequency selectivity properties of CSRR allow their use in applications where miniaturization is a key aspect [30].

The area and perimeter of SRRs are mutually dependent resulting in a limited design capability. However, a primary feature of the rose curve resonators (RCRs) is their geometry perimeter and area independency. Fig. 4.5 shows rose curve of different order while the area is kept constant. It is to be noted that the amplitude of the permeability decreases while the order n increases. Moreover, the resonance frequency decreases when the order of the rose curve increases. In fact, higher order rose curve resonators introduce the higher coupling factor.

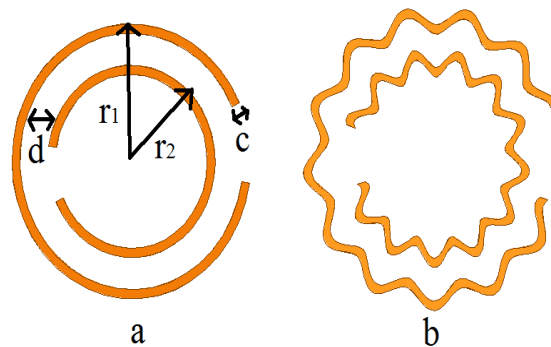


Fig. 4.5 (a) Split Ring Resonator (SRR), and (b) Rose Curve Resonator with order=13

Fig. 4.5(a) shows the parameters of the SRR: the external radius of outer ring $r_1 = 3.9$ mm, the external radius of inner ring $r_2 = 3.4$ mm, the width of the ring $c = 0.2$ mm, and the length between ring $d = 0.5$ mm. Fig. 4.5(b) shows a RCR with the order=13 and amplitude = 0.1.

4.2.1 Patch Antenna based on Complementary Split Ring Resonators (CSSRs)

The design of the Patch antenna based on complementary split ring resonators (CSSRs) is shown in Fig. 4.6. The Patch antenna based on CSSRs is designed at the same operational frequency of $f_0 = 2.4GHz$ and with a substrate material made of Duroid Rogers *tm*, with a thickness (h) of 0.25 mm and relative dielectric constant (ϵ_r) of 2.2 is used. .

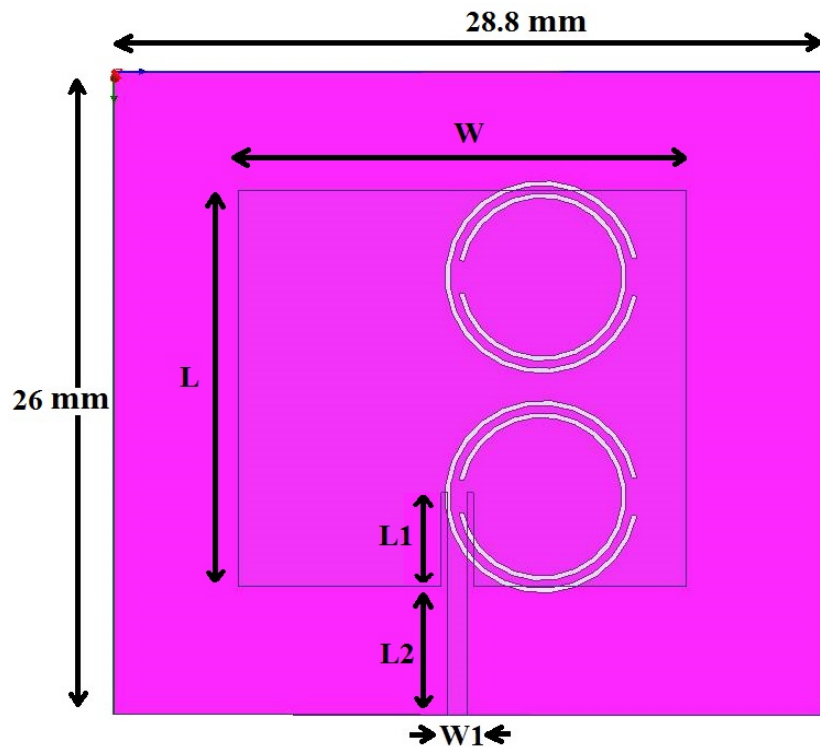


Fig. 4.6 Configuration of Patch antenna based on Complementary Split Ring Resonators (CSSRs)

The substrate has dimensions of 26 mm x 28.8 mm and is fed by a 50 Ω microstrip transmission line. The top square metal plate has the following parameters: W is the y-length of the patch antenna 14.8 mm and L = 13.2 mm for the x-length of the patch antenna, L1 = 2.9 mm, L2 = 4.3mm, and the width 50 Ω of W1 = 0.78mm.

This patch antenna with CSRRs inclusion is simulated by using finite-element analysis based on Ansys HFSS version 15. Fig. 4.7 shows the simulation for the S₁₁ parameter of patch antenna based on CSRRs which resonates at 2.4 GHz with a reflection coefficient of -25 dB. Fig. 4.5 shows the radiation pattern of the designed patch antenna in H_plane and E_plane.

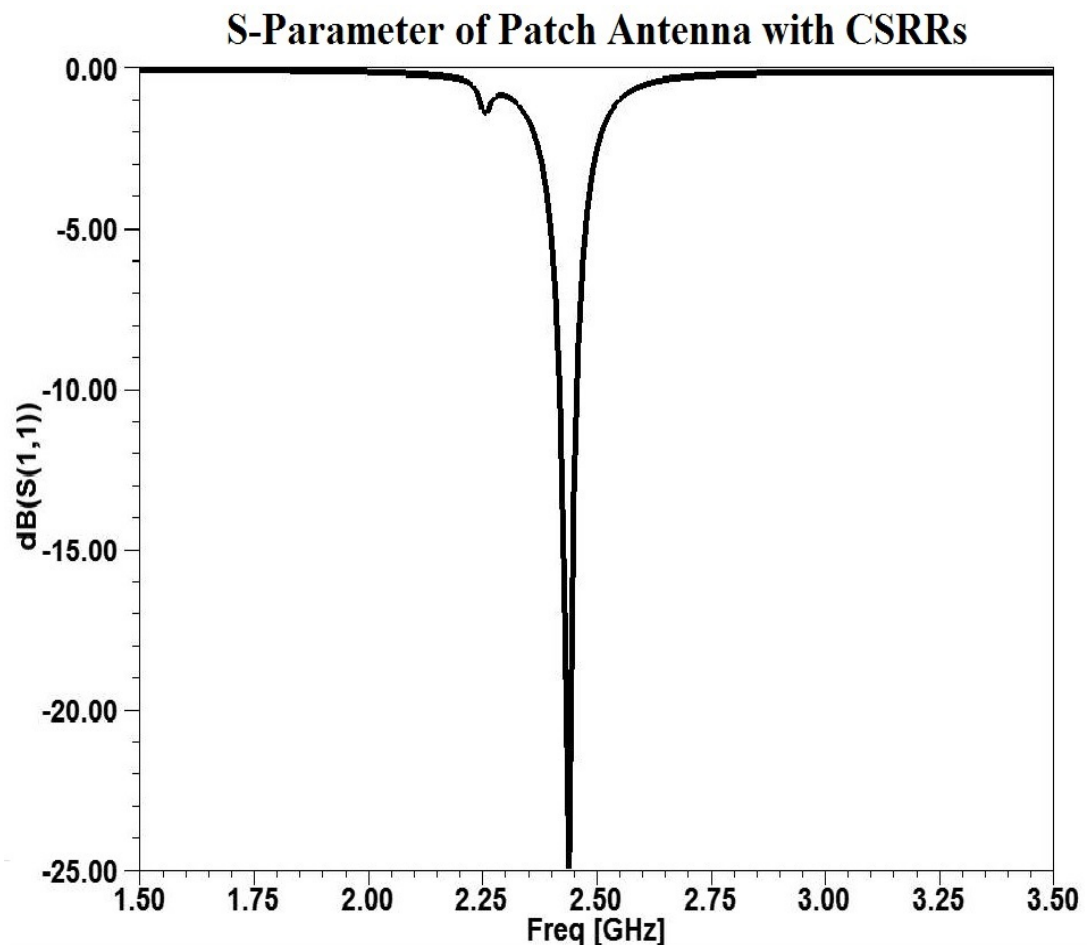


Fig. 4.7 The S₁₁ parameter of Patch antenna based on Complementary Split Ring Resonators (CSSRs)

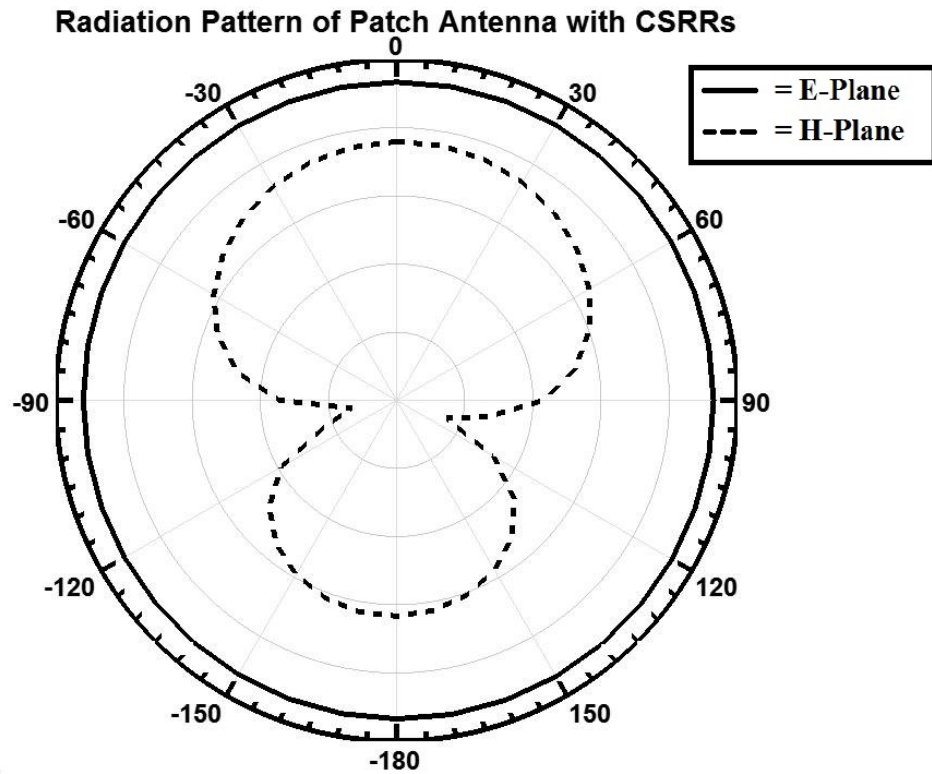


Fig. 4.8 Radiation pattern of Patch antenna based on Complementary Rose Curve Resonators (CRCRs)

4.2.2 Patch Antenna based on Complementary Rose Curve Resonators (CRCRs)

The design of the Patch antenna based on complementary rose curve resonators (CRCRs) is shown in Fig. 4.9. The Patch antenna based on CRCRs is similar with patch antenna based on CSSRs which are designed at the same operational frequency $f_0 = 2.4 \text{ GHz}$ and with a substrate material made of Duroid Roger *tm*. The parameters of Patch antenna with CRCRs are a thickness (h) of 0.25 mm

and relative dielectric constant (ϵ_r) of 2.2, the substrate has dimensions of 18mm x 19.7 mm and is fed by a 50 Ω microstrip transmission line. The top square metal plate has the following parameters: W is the y-length of the patch antenna 12.7 mm and L= 11.3 mm for the x-length of the patch antenna, L1 = 3.7 mm, L2 = 3.7 mm, and the width 50 Ω of W1=0.78mm.

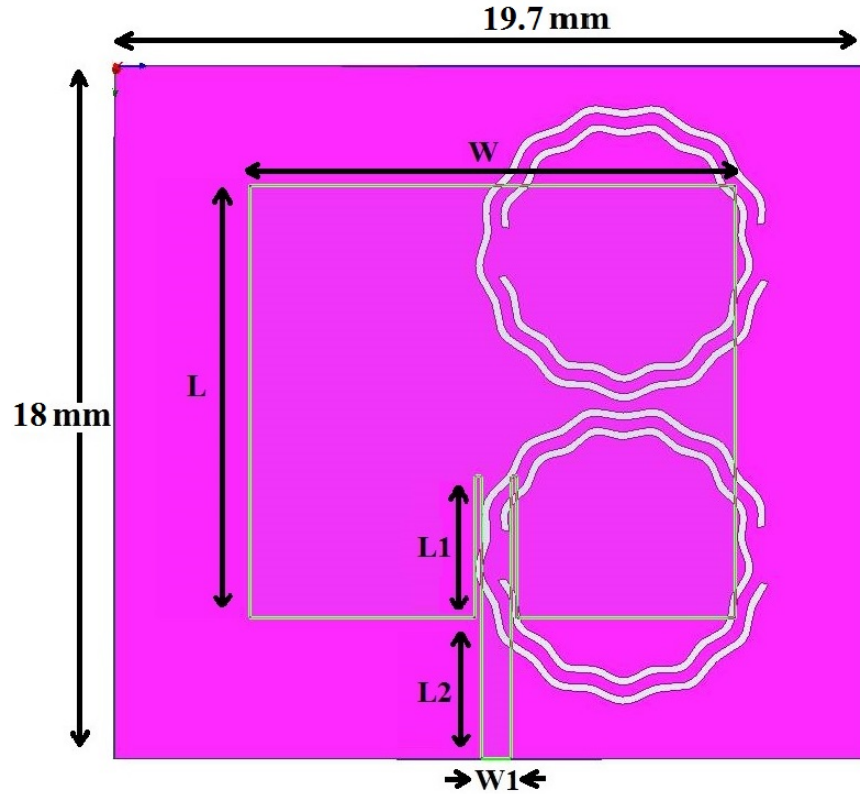


Fig. 4.9 Configuration of Patch antenna based on Complementary Rose Curve Resonators (CSSRs)

According to the simulation result on fig. 4.10, we can determine the patch antenna with CRCRs with a reflection coefficient around -15dB. Fig. 4.11 shows the radiation pattern in H_plane and E_plane for patch antenna based on CRCRs.

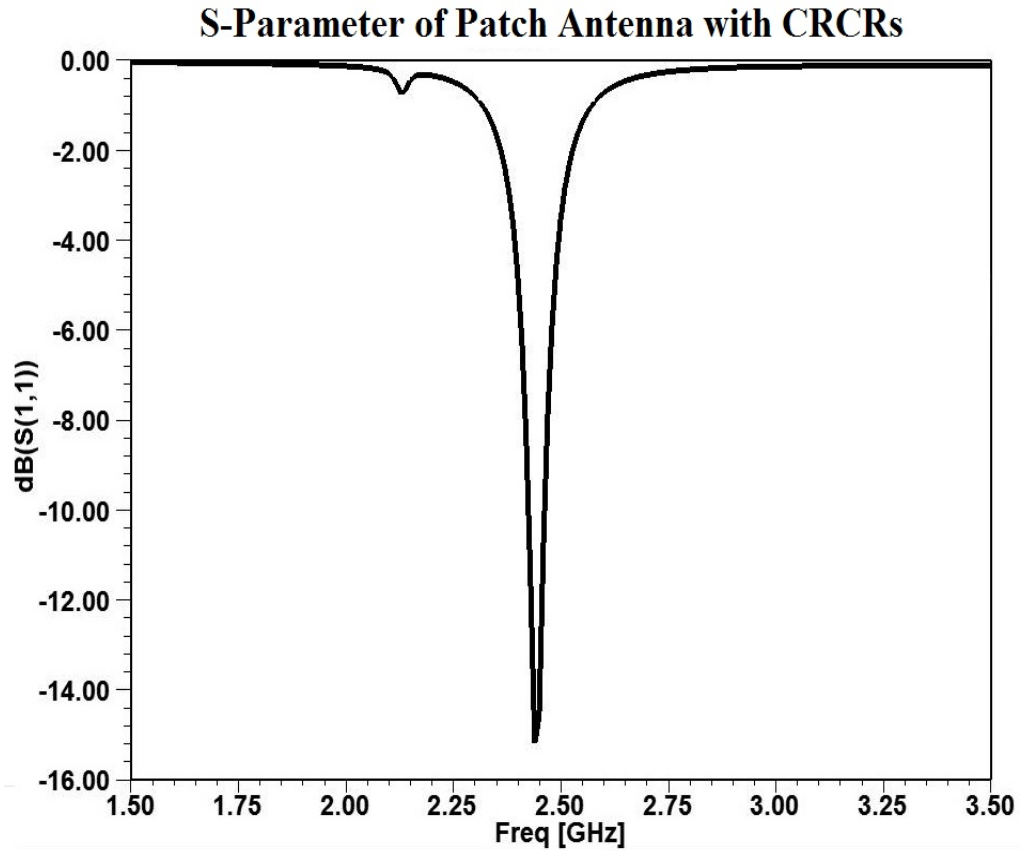


Fig. 4.10 S_{11} Parameter of patch antenna based on CRCRs

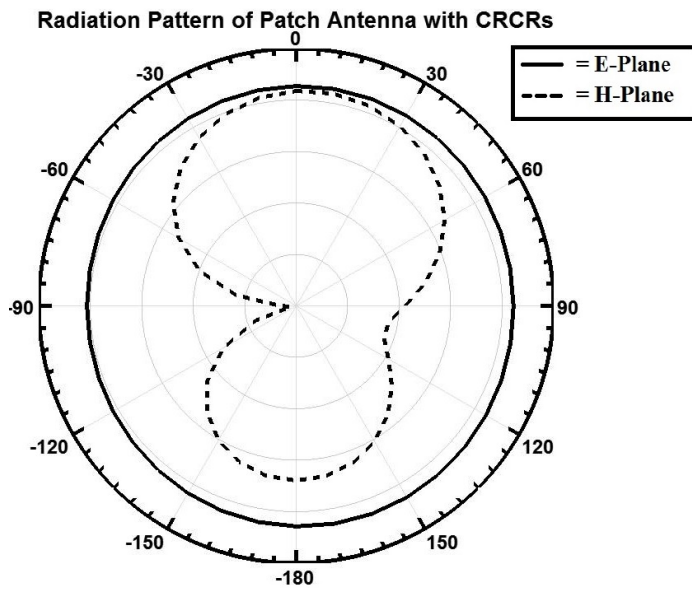


Fig. 4.11 Simulation result of the Radiation pattern of Patch antenna based on CRCRs

4.3 Measurement results

In fig. 4.1, we illustrate the experimental device. We use an Agilent Vectorial Network Analyser to derive the amplitude and phase shifting of S parameter of a patch antenna with CSRR and CRCR. Fig. 4.12 shows the S-parameter for patch antenna with the conventional model, patch antenna with CSRRs and patch antenna with CRCRs.

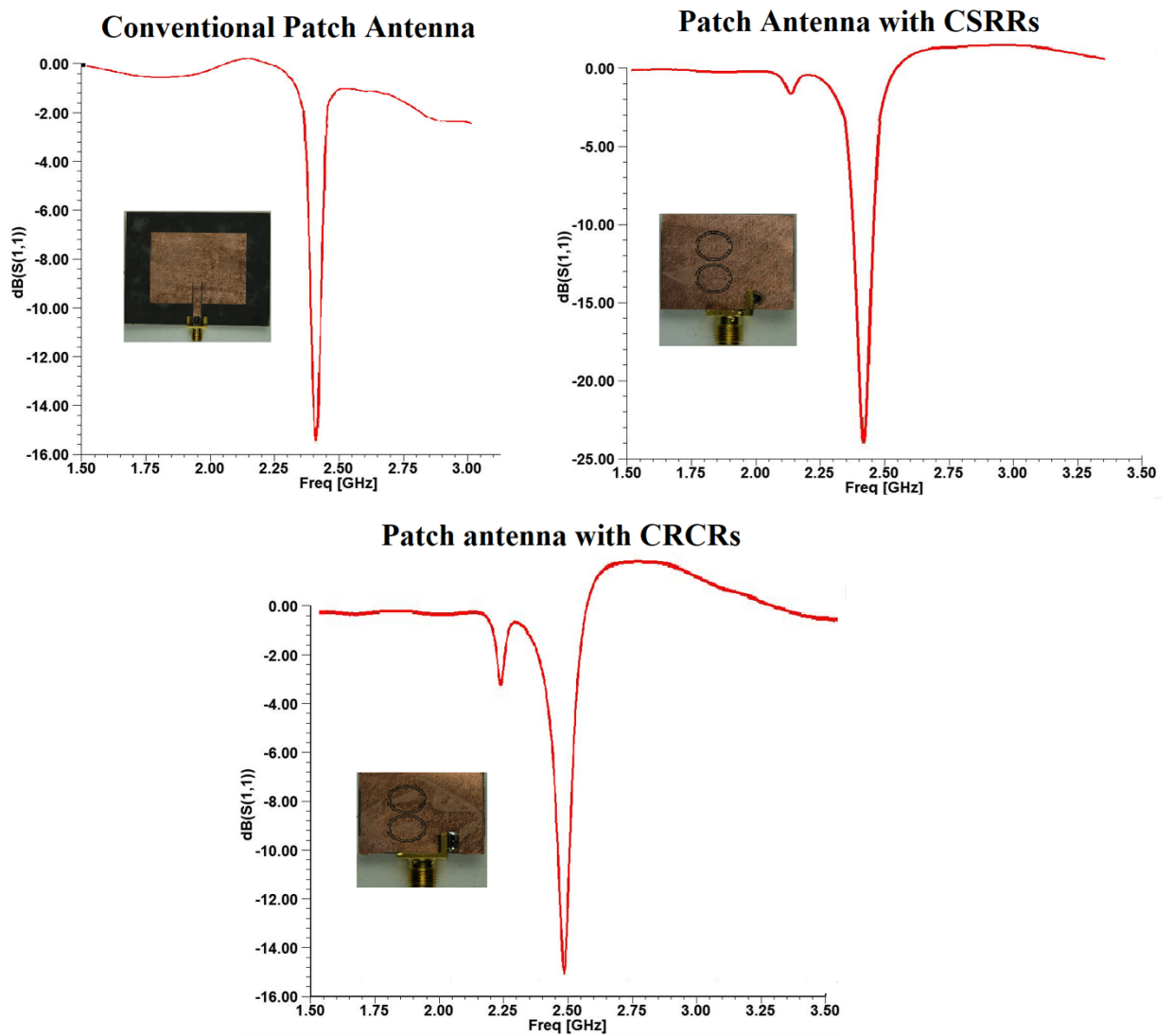


Fig. 4.12 S_{11} Parameter of patch antenna based on conventional and metamaterial model

According to the results of the three patch antenna designs, such as the conventional patch antenna and metamaterial antenna based on CSSRs and CRCRs, we have the different size of each design. Due to the calibration issue when in measurement, there is a result which show the S_{11} over 1 GHz.

Moreover, The area of the patch antenna without inclusion is 4497 mm^2 . M -factor is defined as the miniaturization factor; $(\text{Original patch antenna Area})/(\text{Compact Patch antenna Area})$. The area for a patch antenna based on CSRRs with the M -factor = 8.85 is 508 mm^2 and the area for a patch antenna based on CRCRs with M -factor = 12.66 is 355 mm^2 . The gain of the patch antenna $\approx 5\text{dB}$

Table 4.2 Comparison table of Patch Antenna based on CSRRs and CRCRs

Order (n)	Microstrip Metamaterial Patch Antenna	
	Size (mm^2)	Size Reduction (%)
Conventional	4497	0
0 (CSRRs)	508	88
13 (CRCRs)	355	92

A key feature that make RCRs a perfect candidate in many designs using artificial electromagnetic structures is the independency of the area and perimeter of the shape of the rose curve resonator. A patch antenna has been designed based on the complementary split ring resonator (CSRRs), complementary rose curve resonators (CRCRs) and without using these inclusions. CRCRs are promising with its potential to extend the possibility of design with higher miniaturization factor in comparison with using complementary split ring resonators (CSRRs). The device compactness increases proportionally to the order of

CRCRs. Table 4.2 shows an increase of patch antenna without inclusion to $n=0$ (CSRRs) that result in a 88% miniaturization and without inclusion to $n=13$ (CRCRs) in a 92% miniaturization.

Chapter 5

Beamforming System Based on Butler Matrix

In the broadband wireless point-to point communication system, we use high frequencies in order to provide a digital two-way voice, data, internet and video services. Multibeam antennas are very important to increase channel capacity and to improve transmission quality by decreasing interference and multipath fading. These systems require antenna with high capacities of low-cost beamforming. These are the various type of RF beamforming [39]: Blass matrices [64], Rotman lenses [65], and Butler matrix [40, 41]. The design of a novel ultra-wideband compact 4x4 Butler Matrix is used to provide compact size [42, 43].

The Butler matrix is a microwave network, as a beamformer that feed an antenna array to implement such multibeam antenna systems. The Butler matrix is chosen because it can produce a large number of high- quality orthogonal beams with fewer components and using microstrip technology. This is interesting because its realization are low cost. This feed network typically has N inputs and N outputs. In an $N \times N$ Butler matrix, the input signal is equally divided into N outputs ports that produced a certain constant offset phase between output ports depending on which port is excited [40, 66]. In general, there are some Butler matrix versions such as a 2x2, 4x4, 8x8, and $N \times N$ version. Fig. 5.1 shows a passive reciprocal symmetrical circuit with N inputs ports and N output ports which drive N radiating elements to produce N different orthogonal beams.

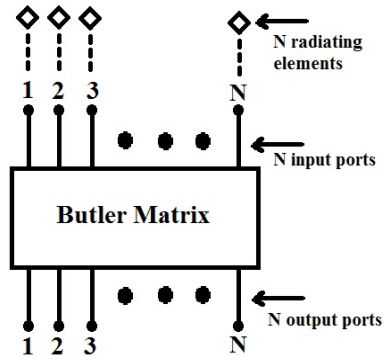


Fig. 5.1 Butler Matrix diagram system

A Butler matrix has been realized by microstrip lines taking a large area with quarter-wavelength transmission lines in the couplers of the Butler matrix. In a beamforming system, the size of a Butler matrix is the main contributor. Furthermore, reducing the size of a Butler matrix is significant to reduce the cost of beam-forming systems. There are some diagrams for Butler matrix model:

- A 2x2 Butler Matrix

Fig. 5.2 is shown a 2x2 Butler matrix. It contains without crossover and phase shifter, only a simple 3-dB coupler.

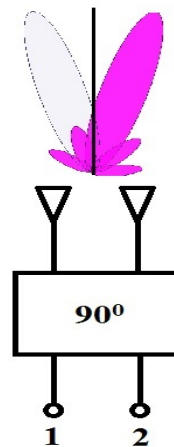


Fig. 5.2 A 2x2 Butler Matrix diagram

- A 4x4 Butler Matrix

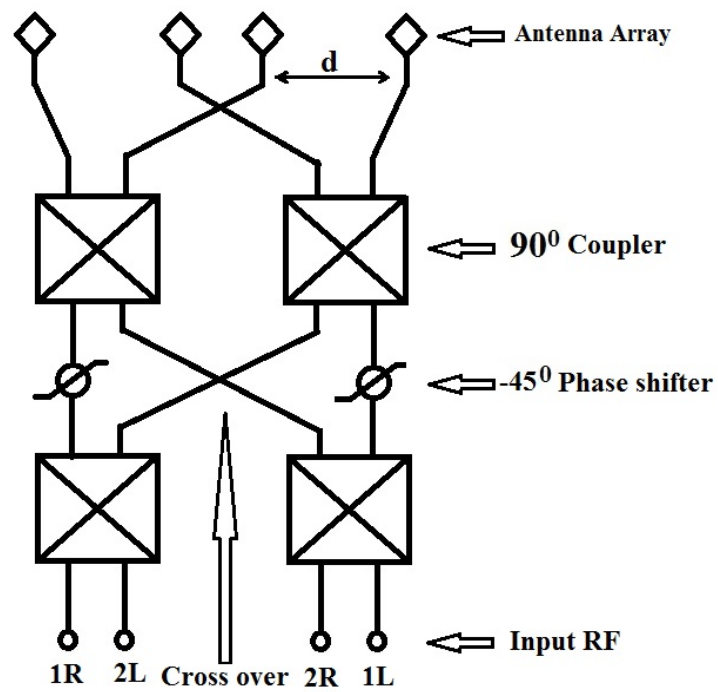


Fig. 5.3 General block diagram of a 4x4 Butler Matrix

- A 8x8 Butler Matrix

Fig. 5.4 shows a block diagram of a 8x8 Butler matrix. It uses four 3-dB coupler, two 45° phase shifters, and a crossover.

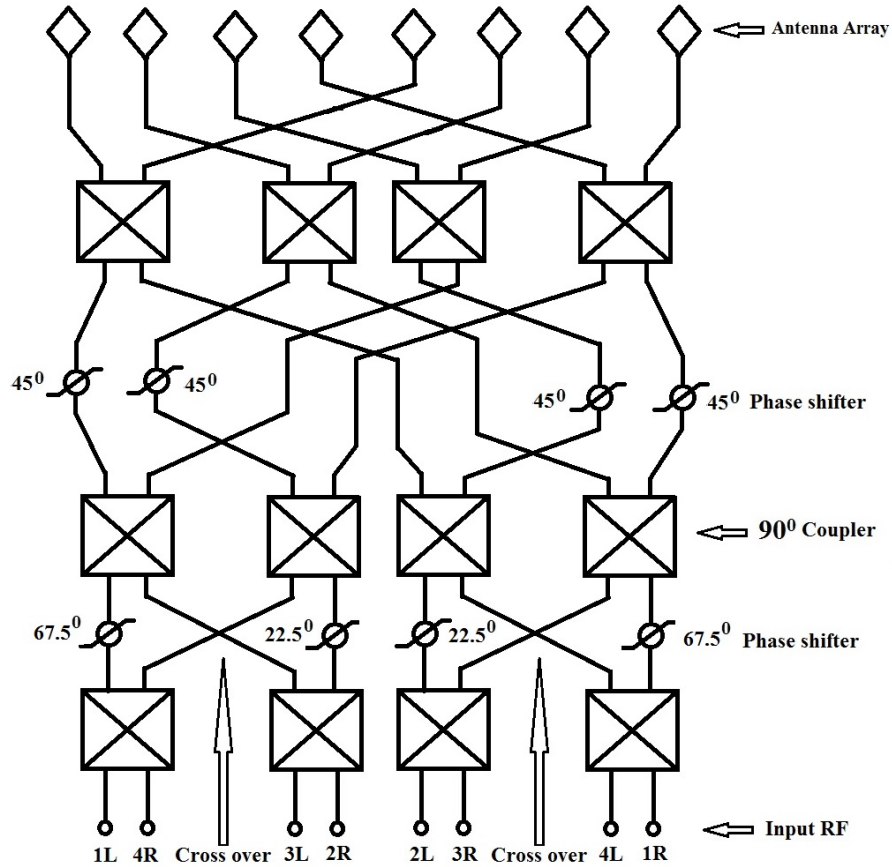


Fig. 5.4 General block diagram of a 8x8 Butler Matrix

5.1 Analysis and Design of a 4x4 Butler Matrix

In switched beam systems, antenna-array systems form multiple-fixed beam with enhanced sensitivity in a specific area [67-69]. This antenna employs a set of radiating elements arranged in the form of an array by adjusting itself to changing traffic condition or signal environments. It works by detecting signal strength, selecting one of the several predetermined fixed beams, switches from one beam to another as the user moves.

In [67-70], they shows the 4x4 planar Butler Matrix array as a key component of switched beam system. In [71-72], These papers present a 4x4 Butler matrix as a beamforming network that is combined with a 4-elements linear aperture coupled antenna

arrays to produce four narrow steerable beams. In [73], it shows a design an 8×8 Butler matrix at 30GHz for 5G application. The era of 5G will dominate mobile network applications sooner or later, supporting the higher data rate communication. This requires much higher frequencies and more complicated system designs over the current 4G LTE system.

The major components of the Butler Matrix are the hybrid coupler, the crossover, the phase shifter and the four rectangular patch microstrip antennas. Another design of a 4x4 Butler Matrix with millimeter microstrip technology at 40 GHz is shown without any crossover circuit [44]. Fig. 5.5 shows the topology of 4x4 Butler Matrix without crossover component

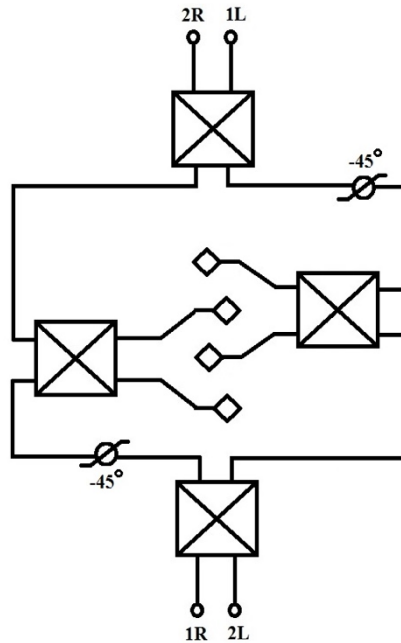


Fig. 5.5 General block diagram of a 4x4 Butler Matrix without crossover

Now, all the individual components (except crossover component) are combined and realized on a single substrate to implement the 4x4 Butler Matrix. The substrate material is made of Duroid Roger *tm* with: the relative permittivity $\epsilon_r = 2.2$, and the thickness $t = 0.25mm$. Furthermore, the implementation of the 4x4 Butler matrix based on

CSRRs and CRCRs are proposed as well. Fig. 5.6, illustrates a schematic design for the conventional 4x4 Butler matrix at 2.4 GHz on Ansys HFSS 15.1 simulation.

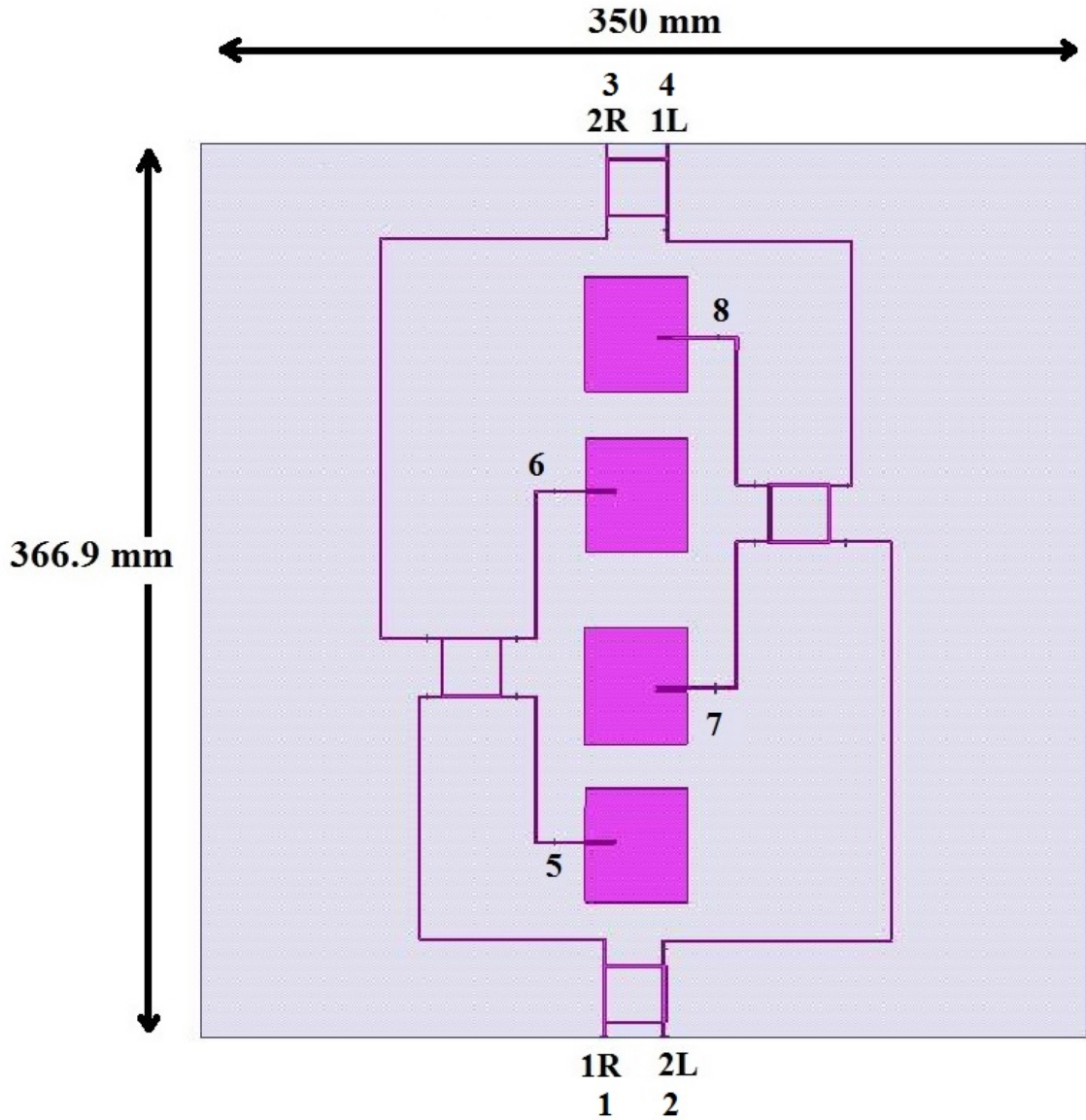


Fig. 5.6 The 4x4 Butler Matrix design on HFSS at 2.4 GHz

The goal of this work is to look at the feasibility of a compact integrated Butler matrix of four beams. This matrix is a reverse symmetric network which consist of four passive four-port hybrid coupler and fixed phase shifters (-45°). The sacrifice of the non-symmetric model is because this Butler matrix designs without crossover circuit.

Simulation Results

- S- Parameters

Fig 5.7 shows the simulated results of the S-Parameters for the 4x4 conventional Butler Matrix at 2.4 GHz and fig. 5.8 shows the phase difference for the antenna port 5, 6, 7 and 8 to the input ports.

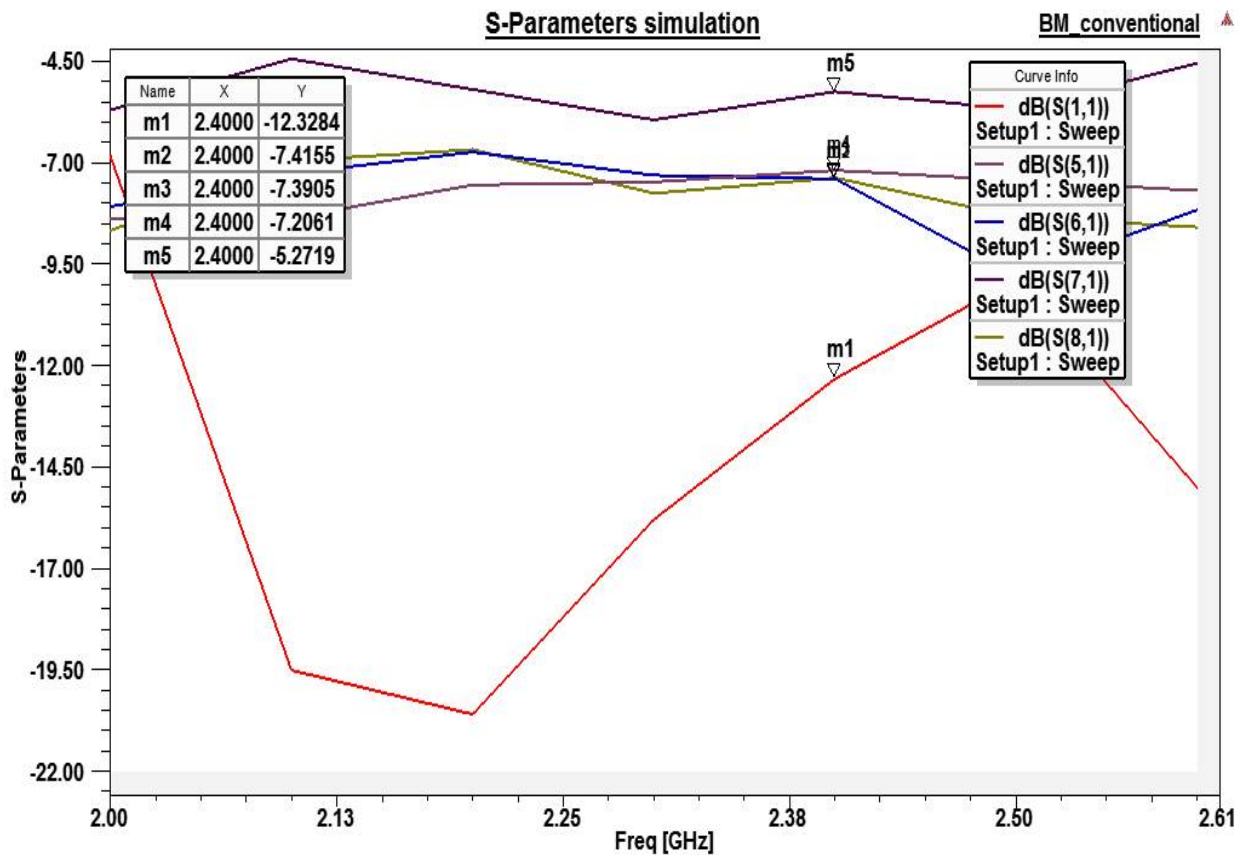


Fig. 5.7 S-Parameters of the 4x4 conventional Butler Matrix

Fig 5.8 shows the simulated results of the S-Parameters for a Coupler which is integrated of the 4x4 conventional Butler Matrix at 2.4 GHz and fig. 5.9 shows the phase difference for the antenna port 5, 6, 7 and 8 to the input ports.

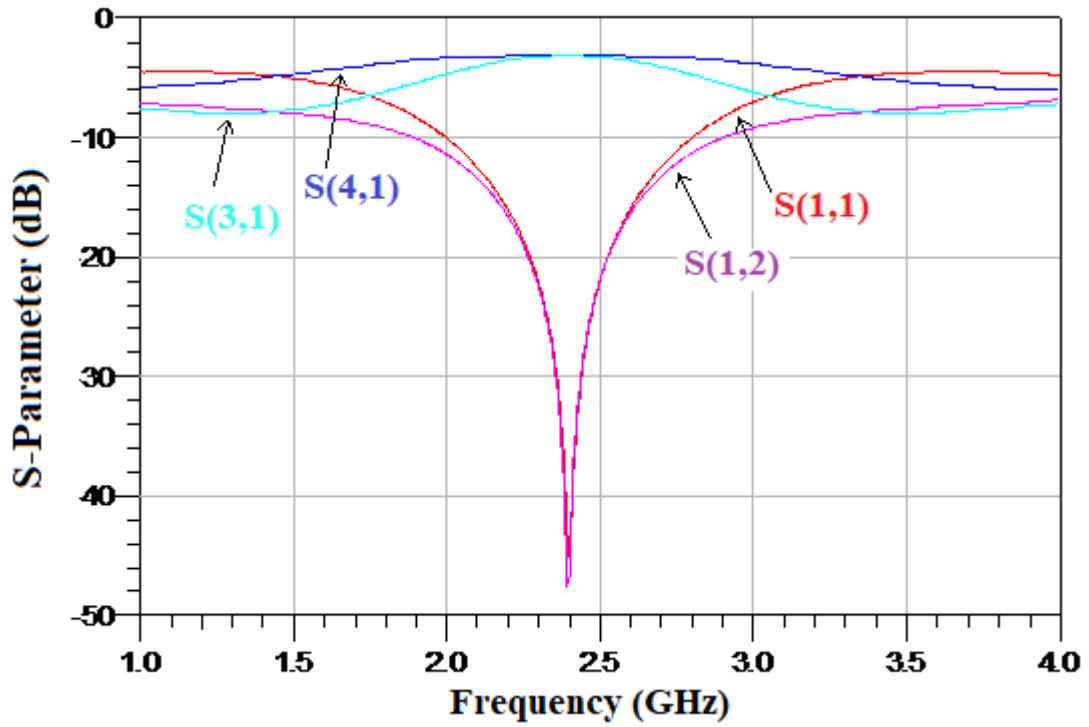


Fig. 5.8 S-Parameters of a coupler on the 4x4 conventional Butler Matrix

- Phase Difference

Table 5.1 Phase difference between input port with the antenna port on the 4x4 Conventional Butler Matrix

Input Port	Antenna Port	5	6	7	8
1	1	0	44.5	89	133.5
2	2	89	133.5	0	44.5
3	3	44.5	0	133.5	89
4	4	133.5	89	44.5	0

5.2 Fut

ure Work

Design of Metamaterial a 4x4 Butler Matrix

It will provide two design of metamaterial a 4x4 Butler Matrix with complementary split ring resonators (CSRRs) and complementary rose curve resonators (CRCRs). The goal of this work is to have the comparison between two models in size reduction working at same frequency of 2.4 GHz. All designs are implemented on Ansys HFSS 15.1 simulation with the substrate material made of Duroid Roger *tm*, with a relative permittivity $\epsilon_r = 2.2$, and a thickness $t = 0.25mm$.

5.2.1 A 4x4 Butler Matrix system based on Complementary Split Ring Resonators (CSSRs)

Fig. 5.9 shows the topology for a 4x4 Butler Matrix based on Complementary Split Ring Resonators (CSRRs) design. Fig. 5.10 and Fig. 5.11 illustrate the simulation results for S-Parameters and phase difference for that design.

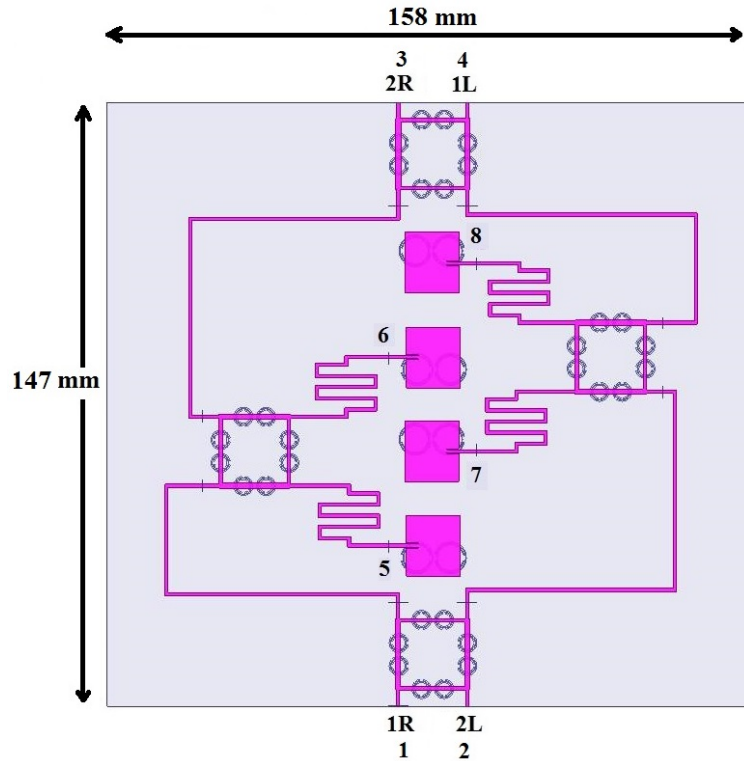


Fig. 5.9 4x4 Butler Matrix design on HFSS at 2.4 GHz

5.2.2 A 4x4 Butler Matrix system based on Complementary Rose Curve Resonators (CRCRs)

Fig. 5.12 shows the topology for the 4x4 Butler Matrix based on Complementary Rose Curve Resonators (CSRRs) design. Fig. 5.13 and Fig. 5.14 are the simulation results for S-Parameters and phase difference for that design.

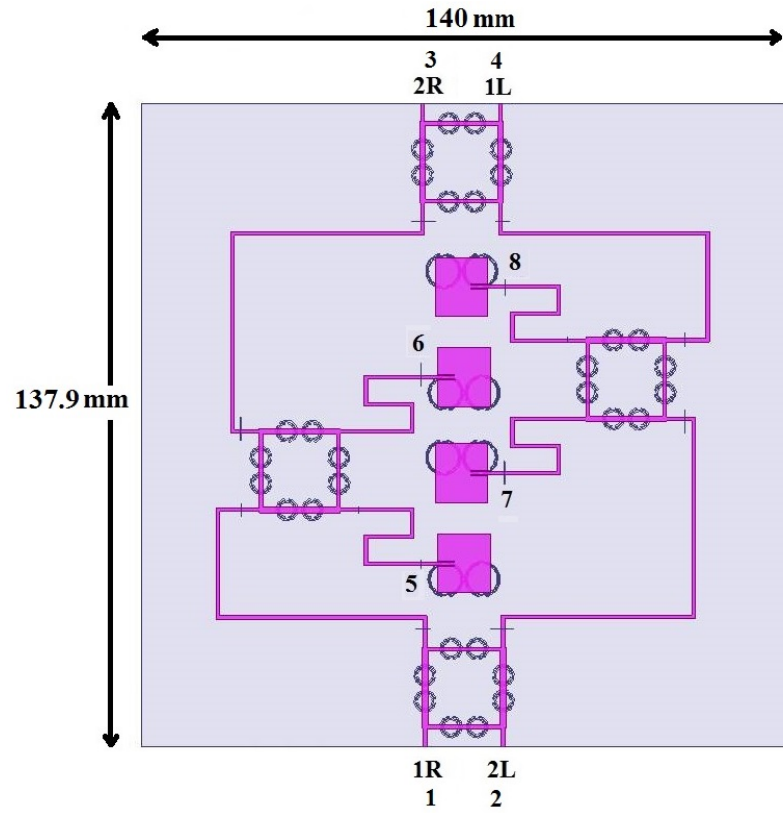


Fig. 5.10 4x4 Butler Matrix design on HFSS at 2.4 GHz

CONCLUSION

Artificial Magnetic Materials (AMMs) are a type of metamaterials which exhibit negative permeability at microwave properties. AMMs composed of split-ring resonators (SRRs) and swiss roll resonators (SR-Rs), as proposed by Pendry et al are produced by an ensemble of small metallic loop inclusions. Using the effective medium theory (EMT) technique, the effective permeability of a medium with looped metallic inclusions such as metal cylinders, Swiss Rolls, and Split Ring Resonators, is calculated. Negative permeability can be obtained in microwave frequencies. An electromagnetic dual of SRRs called complementary split ring resonators (CSRRs) is proposed by etching of SRRs off a conducting sheet. Accordingly, the complementary Rose curve resonators (CRCRs) are defined. The area and perimeter of SRRs are dependent resulting in a limited design capability. However, a primary feature of the Rose curve resonators (RCRs) is their perimeter and area independency. Based on the duality, CRCRs provide a controllable electric response in applications. The CSRRs are widely and effectively used in design of microstrip filters, loading impedances, couplers etc.

The focus of our study is to shrink the size of 90^0 microstrip coupler and the Patch Antenna using CSRRs and CRCRs while maintaining good performance from a conventional model. In the beginning, CSRRs and CRCRs are used in the design of a 90^0 microstrip coupler and a patch antenna. The configurability of the footprint and performance of the design are compared with a coupler and antenna loaded with or without circular shape CSRRs. It is important to mention that the frequency selectivity properties of CSRR allow using them in applications where miniaturization is a key aspect.

The objective of this thesis is to apply the metamaterial in the design and miniaturization of adaptive antennas, multibeam and multi-band. The study and modeling are based on electromagnetic analysis and the theory of transmission lines. The design process and the geometric constraints formulation phase will be carried out based on a number of steps. The first step is to study the feasibility of designing artificial materials unit cells and testing the new formulation to address the fundamental constraints. In the following steps, the various

components of the antenna array will be designed separately, namely Butler matrix and antennas. Finally, the crucial step is to combine all these components in a single device and validate its functionality while achieving the desired miniaturization with sub bands required frequencies. The extend benefit of metamaterial technique is to design antenna array dual band beside of the major goal to reduce the size.

REFERENCES

- [1] J. B. Pendry, A. J. Holden, D. J. Robbins, and W. J. Stewart, "Magnetism from Conductors and Enhanced Nonlinear Phenomena", *IEEE Transaction on Microwave Theory Techniques*, vol. 47, no. 11, pp. 2075-2084, November 1999.
- [2] Anju Pradeep, S. Mridula, and P. Mohanan, "Design of an Edge-Coupled Dual-Ring Split-Ring Resonator", *IEEE Antennas and Propagation Magazine*, Vol. 53, No. 4, August 2011.
- [3] S. Maslovski, P. Ikonen, I. Kolmakov, and S. Tretyakov, "Artificial Magnetic Materials Based on The New Magnetic Particle: Metasolenoid," *Progress In Electromagnetica Research*, PIER, Vol.54, pp. 61-81, 2005.
- [4] Ali Kabiri, Leila Yousefi, and Omar M. Ramahi, "On the Fundamental Limitations of Artificial Magnetic Materials", *IEEE Transaction on Antennas and Propagation*, Vol. 58, No. 7, July 2010.
- [5] Ali Kabiri and Omar M. Ramahi, "A Design Recipe for Artificial Magnetic Materials", *IEEE Antennas and Propagation Society International Symposium (APSURSI)*, 1-5 June 2009.
- [6] A. Kabiri and O.M. Ramahi, "Metamaterial Composed of Rose Curve Inclusions", *IEEE Antennas and Propagation Society International Symposium (APSURSI)*, 11-17 July 2010
- [7] Baena, J. D., Bonache, J., Martin, F., Sillero, R. M., Falcone, F., Lopetegui, T., Laso, M. A., Garcia-Garcia, J., Gil, I. and Portillo, M. F. Equivalent-circuit models for split-ring resonators and complementary split-ring resonators coupled to planar transmission lines. *IEEE transactions on microwave theory and techniques*, Vol.53, No. 4, pp. 1451-1461, 2005.

- [8] Jordi Bonache, Ignacio Gil, Joan García-García, Ferran Martín, “Novel Microstrip Bandpass Filters Based on Complementary Split-Ring Resonators,” *IEEE Transaction on Microwave Theory and Techniques*, Vol.54, No. 1, January 2006.
- [9] Li, C., Liu, K. and Li, F. A microstrip highpass filter with complementary split ring resonators. *PIERS Online*, Vol.3, No.5, pp. 583-586, 2007.
- [10] Marta Gil, Jordi Bonache and Ferran Martin, “Ultra Compact Band pass filters Implemented Through Complementary Spiral Resonators (CSRs),” *IEEE MTT-S Int'l Microwave Symposium Digest Atlanta, USA*, pp. 1119-1122, 2008.
- [11] Narang, S. B. and Hudiera, I. Microwave dielectric properties of M-type barium, calcium and strontium hexaferrite substituted with Co and Ti. *Journal of Ceramic Processing Research*, Vol. 7, No. 2, pp. 113-116, 2006.
- [12] A. Kabiri and O.M Ramahi, “*n*th Order Rose Curve as a Generic Candidate for RF Artificial Magnetic Material”, *Applied Physics A*, Vol. 103, Issue 3, pp. 831-834, 6 January 2011.
- [13] A. Kabiri, L. Talbi, and O. M. Ramahi, “A Super-miniaturized Low Profile Antenna on a Substrate of Rose Curve Resonators”, *PIERS Proceedings*, March 20-23, 2011.
- [14] Callister, W. D. and Rethwisch, D. G. *Fundamentals of materials science and engineering*. Wiley London, 2000.
- [15] Hong, J.-S. G. and Lancaster, M. J. *Microstrip filters for RF/microwave applications*. John Wiley & Sons, 2004.
- [16] V. G. Veselago, “The Electrodynamics of Substances with Simultaneously Negative Values of ϵ and μ ,” *Soviet Physics Uspekhi*, Vol. 10, pp. 509-514, January-February 1968. (Russian version in 1967).
- [17] Marques, R., F. Medina, and R. Rafei-El-Idrissi, “Role of Bianisotropy in Negative Permeability and Left-handed Metamaterials,” *Physical Review B*, Vol. 65, paper 144440, 2002.

- [18] I. Sassi, L. Talbi, K. Hettak, and A. Kabiri, "Magnetic Response of n^{th} Rose curve Resonator in the RF Frequency Regime, " *International Journal of Electrical and Computer Systems*, Vol. 1, 2012.
- [19] R. Marques, F. Mesa, and F. Medina "Near-field Enhanced Imaging by a Metamaterial Magnetized Ferrite Slab." *Appl. Phys. Lett.*, vol. 86, paper 023505, 2005.
- [20] F. Falcone, "Effective Negative- ϵ Stopband Microstrip Lines Based on Complementary Split Ring Resonators", *IEEE microwave and wireless components letters*, VOL. 14, NO. 6, pp. 280-282, June 2004.
- [21] B. Savitri, L. Talbi, K. Hettak and A. Kabiri, "Effect Of Complementary Rose Curve Resonator (CRCRs) On The Effective Negative Permeability," *IEEE Antennas and Propagation Symposium*, July 2012.
- [22] A. Genc. "Metamaterial-Inspired Miniaturized Multi-band Microwave Filters and Power Dividers," Ph.D. dissertation, Elect. and computer Eng. Dept., Utah State Univ., Utah, USA, 2010.
- [23] Martin, F., F. Falcone, J. Bonache, T. Lopetegi, R. Marques, and M. Sorolla, "Miniaturized Coplanar Waveguide Stopband Filters Based on Multiple Tuned Split Ring Resonators," *IEEE Microw. Wireless Compon. Lett.*, Vol.13, No.12, pp. 511-513, Dec 2003.
- [24] . Keshvari and M. Tayarani, " A Novel Miniaturized Bandpass Filter Based on Complementary Split Ring Resonators (CSRRs) and Open Loop Resonators," *Progress In Electromagnetics Research Letter*, Vol.7, 193-201, 2009
- [25] S. Pasakawee. "Left-handed Metamaterials Realized by Complementary Split Ring Resonators for RF and Microwave Circuit Applications ," Ph.D. dissertation, Eng. and Phy. Scien. Fac., Manchester Univ., Manchester, Eng, 2012.

- [26] S A. P. Singh and A. Dubey , “Coupler and Wilkinson Power Divider Design,” Electro and com. Eng., Indian Institute of Technology Roorkee, <https://sites.google.com/site/amitpsingh02/LAB2.pdf>
- [27] Marin V. Nedelchev, Ilia G.Iliev,”Synthesis and Analysis of Reduced-Size Branch-Line Hybrid”, *Mikrotalasna revija*, pp. 16-19, December 2008.
- [28] T. Hirota, A. Minakawa, M. Muraguchi, ”Reduced-Size Branch-Line and Rate-Race Hybrids for Unipolar MMIC’s,” *IEEE Trans on MTT*, pp. 270-275, March 1990
- [29] Sung-Chan Jung, Renato Negra, and Fadhel M. Ghannouchi, ”A Design Methodology for Miniaturized 3-dB Branch-Line Hybrid Couplers Using Distributed Capacitors Printed in the Inner Area”, *IEEE Transaction on Electromagnetics Compatibility*, Vol. 56, No. 12, pp. 2950-2953, December 2008.
- [30] Marqués, R., Martin, F. and Sorolla, M. *Metamaterials with negative parameters: theory, design and microwave applications*. John Wiley & Sons, 2011.
- [31] Savitri, B., Fono, V., Talbi, L. and Hettak, K. Compact 900 Microwave Directional Coupler Based on Complementary Rose Curve Resonator (CRCRs). *Antenna Measurement Techniques Association (AMTA) 2013*, (October 2013).
- [32] Ma, J.J., X. Y. Cao, and T. Liu, “Design the size reduction patch antenna base on complementary split ring resonators,” *Proceedings of International Conference on Microwave and Millimeter Wave Technology (ICMMT)*, pp. 401-402, May 2010.
- [33] R. Karimzadeh Bae, G. Dadashzadeh, and F. Geran Kharakhili, “Using of CSRR and Its Equivalent Circuit Model in Size Reduction of Microstrip Antenna,” *Proceeding of Asia-Pasific Microwave Conference (APMC)*, pp. 1-4, 2007.
- [34] L. Ke, G.-M. Wang, T. Xu, and H.-X. Xu, “A Novel Circularly Polarized Antenna Based on The Single Complementary Split Ring Resonator,” *Proceeding of International Symposium on Signal Systems and Electronics (ISSSE)*, Vol. 2, pp. 1-4, 2010.

- [35] H. Zhang, Y.-Q. Li, X. Chen, Y.-Q. Fu, and N.-C. Yuan, "Design of Circular Polarization Microstrip Patch Antennas with Complementary Split Ring Resonator," *IET Microw. Antennas Propag.*, Vol. 3, No. 8, pp. 1186-1190, Feb. 2009.
- [36] Ortiz, N., F. Falcone, and M. Sorolla, "Dual Band Patch Antenna Based on Complementary Rectangular Split Ring Resonators," *Proceedings of Asia-Pacific Microwave Conference (APMC)*, pp. 2762-2765, 2009.
- [37] Y. Xie, L. Lie, C. Zhu, and C. Liang, "A Novel Dual-Band Patch Antenna with Complementary Split Ring Resonators Embedded in The Ground Plane," *Progress In Electromagnetics Research Letters*, Vol. 25, pp. 117-126, 2011.
- [38] Savitri, B., L.Talbi and Hettak, K. Miniaturization of Patch Antenna Design Based on Complementary Rose Curve Resonators. *Antenna Measurement Techniques Association (AMTA) 2015* (October, 2015).
- [39] P. S. Hall and S. J. Vetterlein, "Review of radio frequency beamforming techniques for scanned and multiple beam antennas," in *IEE Proceedings H - Microwaves, Antennas and Propagation*, vol. 137, no. 5, pp. 293-303, Oct. 1990.
- [40] Butler, J. Beam-forming matrix simplifies design of electronically scanned antennas. *Electronic design*, 12, pp. 170-173, 1961
- [41] D C. Dall'Omo, T. Monediere, B. Jecko, F. Lamour, I. Wolk, and M. Elkael, "Butler Matrices in Millimeter-wave Frequency Band: Two Different Designs," *JINA 2002*, Session 6-16, pp. 407-410, 2002.
- [42] I. Haroun, T.-Y. Lin, D.-C. Chang and C. Plett, " A Compact 24-26 GHz IPD-Based 4x4 Butler Matrix for Beam Forming Antenna Systems," *Proceeding of APMC 2012*, December 2012.

- [43] L. M. Abdelghani, T. A. Denidni and M. Nedil, "Ultra-broadband 4×4 compact Butler matrix using multilayer directional couplers and phase shifters," *2012 IEEE/MTT-S International Microwave Symposium Digest*, pp. 1-3, Montreal, QC, Canada, 2012.
- [44] C. Dall’Omo, T. Monediere, B. Jecko, F. Lamour, I. Wolk, and M. Elkael, “Design and Realization of a 4x4 Microstrip Butler Matrix without any crossing in millimeter waves,” *Microwave and Optical Technology Letters*, Vol. 38, No. 6, September 2003.
- [45] W. Lamb, D. M. Wood, and N. W. Ashcroft, “Long-wavelength electromagnetic propagation in heterogeneous media,” *Physical Review B (Condensed Matter)*, Vol. 21, No. 6, pp. 2248-2266, March 1980.
- [46] D. Rosellas, A. Berthing, O. Ached, J. P. Burchard, and P. G. Gerah, “Effective medium at finite frequency: Theory and experiment,” *Applied Physics*, Vol.74, pp. 475-480, May 1993.
- [47] D. R. Smith, W. J. Padilla, D. C. Vier, R. Shelby, S. C. Nemat-Nasser, N. Kroll, and S. Schultz, “Photonic Crystals and Light Localization in the 21st Century,” chapter Left-handed metamaterials, pages 351-371. *Kluwer Academic Publishers*, 2001..
- [48] J.B. Pendry, “Negative Refraction Makes a Perfect Lens,” *Physical Review Letters*, Vol. 85, No. 18, pp. 3966-3969, 2000.
- [49] N.N. Wan, D. Huang, Q. Cheng, W.X. Jiang, R. Liu, and T.J. Cui, “ Study of Active Superlens and Evanescent Wave Amplification using an Active Metamaterial Model,” *Europe Physics Journal of Applied Physics*, Vol. 48, No. 2, pp. 21101, 1-6 November 2009.
- [50] Bogdan-Ioan Popa and Steven A. Cummer, ”Direct Measurement of Evanescent Wave Enhancement Inside Passive Metamaterials,” *Physical Review E*, Vol. 73, paper 016617, 1-5 January 2006.

- [51] K. B. Tan, C. H. Liang, T. Su, and B. Wu, "Evanescent Wave Amplification in Metamaterials," *Journal of Electromagnetic Waves and Applications*, Vol. 22, No. 10, pp. 1318-1325, 2008.
- [52] Hyesog Lee, Yi Xiong, Nicholas Fang, Werayut Srituravanich, Stephane Durant, Muralidhar Ambati, Cheng Sun, and Xiang Zhang, "Realization of Optical Superlens Imaging below The diffraction Limit," *New Journal of Physics*, Vol. 7, paper 255, 1-16 August 2005.
- [53] Nicholas Fang and Xiang Zhang, "Imaging properties of a metamaterial superlens," *Applied Physics Letters*, Vol. 82, No. 2, pp. 161-182, January 2003.
- [54] D.R. Smith, S. Schultz, P. Markos, C. M. Soukoulis, "Determination of Negative Permittivity and Permeability of Metamaterial from Reflection and Transmission Coefficients," *Physical Review B*, Vol. 65, paper 195104, 1-5 April 2002.
- [55] P. V Parimi, W. T Lu, P. Vodo, and S. Sridhar, "Imaging by Flat Lens using Negative Refraction," *Nature*, Vol. 426, pp. 404, 2003.
- [56] Cheung King Ying, "Multi Band Hybrid for Wifi," Final Year Project Report, BEngECE-2007/08-<WSC>-<WSC06>, City University of Hong Kong.
- [57] A. Kabiri. "Artificial Magnetic Materials: Limitations, Synthesis and Possibilities" Ph.D. dissertation, Elect. and computer Eng. Dept., Waterloo Univ., Waterloo, ON, Canada, 2010.
- [58] Pozar, D. M. *Microwave engineering*. John Wiley & Sons, 2009.
- [59] R. Abhari and G. V. Eleftheriades, "Metallo-dielectric Electromagnetic Bandgap Structures for Suppression and Isolation of the Parallel-plate Noise in High-speed Circuits," *IEEE Transaction on Microwave Theory and Techniques*, Vol. 51, No. 6, pp. 1629-1639, June 2003
- [60] P. Dawar, "Design and Simulation of Magic Tee and Ring Hybrid Coupler using Ansoft HFSS," *International Journal of Computer Science and Technology*, Vol.2, Issue 1, March 2011

- [61] S. Shahparnia, and O. M. Ramahi, "Electromagnetic Interference (EMI) Reduction from Printed Circuit Boards (PCB) using Electromagnetic Bandgap Structures," *IEEE Transaction on Electromagnetics Compatibility*, Vol. 46, No. 4, pp. 580-587, 2004.
- [62] R. C. Johnson, H. A. Ecrer, and J. S. Hollis, "Determination of Far-Field Antenna Patterns From Near-Field Measurements," *Proceeding of The IEEE*, Vol. 61, No. 12, December 1973
- [63] S. S. Karthikeyan and R. S. Kshetrimayum, "Harmonic suppression of parallel coupled microstrip line bandpass filter using CSRR," *Progress In Electromagnetics Research Letters*, Vol. 7, 193-201, 2009.
- [64] J. Blass, " Multi-directional Antenna: New Approach Top Stacked Beam," *IRE Int. Convention record*, Pt 1, pp 48-50, 1960.
- [65] W. Rotman and R. F. Tuner, "Wide-angle Microwave Lens for Line Source Applications," *IEEE Trans Antennas Propagation 11*, pp. 623-632, 1963.
- [66] T. MacNamara, "Simplified Design Procedures for Butler Matrices Incorporating 90° Hybrids or 180° Hybrids," *Microwaves, Antennas and Propagation, IEE Proceedings H*, vol. 134, no. 1, pp. 50-54, Feb 1987.
- [67] Siti Zuraidah Ibrahim and Mohamad Kamal A.Rahim , "Switched Beam Antenna using Omnidirectional Antenna Array" *Asia-Pacific Conference on Applied Electromagnetics Proceedings*, 2007, Malaysia..
- [68] Siti Rohaini Ahmad and Fauziahanim Che Seman, "4-Port Butler Matrix for Switched Multibeam Antenna Array," *IEEE, Asia-Pacific Conference on Applied Electromagnetics Proceedings*, December 20-21.2005.
- [69] D. C. Chang, S. H. Jou. "The study of Butler Matrix BFN for four beams antenna system," *IEEE Antenna and Propagation Society International Symposium*, volume 4, pp. 176-179, 2003.

- [70] W. Bhowmik and S. Srivastava, "Optimum Design of a 4x4 Planar Butler Matrix Array for WLAN application," *Journal of Telecommunication*, Vol. 2, Issue 1, April 2010.
- [71] F. Y. Zulkifli, N. Chasanah, Basari and E. T. Rahardjo, "Design of Butler matrix integrated with antenna array for beam forming," *2015 International Symposium on Antennas and Propagation (ISAP)*, pp 1-4, Hobart, TAS, 2015.
- [72] V.M. Jayakrishnan and S. K. Menon, "Realization of Butlermatrix for Beamforming in Phased Array System," *6th International Conference on Advances in Computing and Communications (ICACC 2016)*, Kochi, India, 6-8 September 2016.
- [73] G. Rosati and J. Munn, "Fast prototyping of an 8x8 butler matrix beamforming network for 5G applications," *2017 International Conference on Electromagnetics in Advanced Applications (ICEAA)*, pp. 1029-1032, Verona, 2017.

Publications

Conferences

1. B. Savitri, L. Talbi, K. Hettak and A. Kabiri, "Effect Of Complementary Rose Curve Resonator (CRCRs) On The Effective Negative Permeability," *IEEE Antennas and Propagation Symposium*, Chicago, USA, July 2012
2. B. Savitri, L. Talbi, and K. Hettak, "Compact 90° Microwave Directional Coupler Based on Complementary Rose Curve Resonators," *Antenna Measurement Techniques Association (AMTA)*, Columbus, USA, October 2013
3. B. Savitri, L. Talbi, and K. Hettak, "Size Reduction of Patch Antenna Based on Complementary Rose Curve Resonators," *Antenna Measurement Techniques Association (AMTA)*, Long Beach, USA, October 2015

Journal

1. B. Savitri, V.A. Fono, L. Talbi, K. Hettak and B. Alavikia, "Novel Approach in Design of Miniaturized Passive Microwave Circuit Components using Metamaterials," *Microwave and Optical Technology Letters*, Vol. 59, No. 6, Pages 1341–134, June 2017.
2. Betty Savitri, Babak Alavikia, Larbi Talbi, and Khelifa Hettak," Parametric Study of the Complementary Rose Curve Resonators (CRCRs) in Miniaturization of the Transmission Lines," *Microwave and Optical Technology Letters*, Vol. 59, No. 3, Pages 538–541, March 2017

Résumé

This thesis focuses on the design and analysis of a novel metamaterial consisting of a 4x4 Butler Matrix system. It will be developed under the following properties and actions: 1) Frequency operation at 2.4 GHz. 2) Parametric studies. 3) Simulations results. 4) Miniaturization compact design. This thesis contains five chapters including preface in chapter 1.

Chapter 1 Preface

Chapter 1 is about background and motivation of this thesis, research contribution, methodology, literature review of previous work and thesis Outline. Background of this thesis is about electromagnetic field and metamaterial and motivation of this thesis is implementation of metamaterial circuit design in antenna application. The purpose of this research is to first develop and analyze a novel design of metamaterial antenna application with a 4x4 Butler Matrix systems with a 2.4 GHz frequency, and secondly to design and compare between the simulations analysis results using HFSS 15. Research contribution of this thesis is design of a 4x4 Butler Matrix to propose the miniaturization of circuit design with metamaterial unit cells. The following works have been completed:

- A 90° Hybrid coupler based on complementary rose curve resonators (CRCRs).
- A Patch Antenna based on complementary rose curve resonators (CRCRs).
- A compact beamforming system based on Butler Matrix design

We designed all circuit with a conventional model, based on CSRRs and CRCRs which behave as left hand material in a narrow band for a specific resonating frequency of 2.4 GHz. As a result, it is shown that CRCRs extend the possibility of design with higher miniaturization factor and relative bandwidth in comparison with using complementary split ring resonators (CSRRs). The device compactness increases proportionally to the order of CRCRs. The methodology of this thesis is that we will initially develop components to design a traditional Butler matrix

system, namely: a directional 90° coupler, a phase shifter and a crossover. In this work, we designed a compact 4x4 Butler matrix for beam forming antenna system without crossover. The literature review of our thesis focused on electromagnetic field, the metamaterial and the parametric study of the behavior of n^{th} order rose curve resonator (n-RCR) and its application on some circuits design. The outline of this thesis shows the main idea of each chapter which is contained of 5 chapters.

Chapter 2 Fundamental Theory of Metamaterial

Chapter 2 is about the fundamental theory of metamaterial. This chapter consists of :

- **Definition of Metamaterial and Left Handed Media**

In electromagnetic wave, electric permittivity and magnetic permeability control the propagation through the materials. Metamaterial belongs to the natural sciences category of physics, to natural materials, which are positive in nature. Metamaterial generates negative permittivity with sub wavelength thin wires and negative permeability with split ring resonators. The metamaterial is a material medium which is aggregated electrically with small inclusion.

In the third quadrant of the effective material parameters represented on a set of Permittivity-permeability ($\epsilon - \mu$), the permittivity and permeability are simultaneously negative. This material is a left-handed materials (LHMs) with a triad (E,H, k) forms, where E corresponds to the electric field and H corresponds to the magnetic field, respectively.

- **Fundamental Formula of Artificial Magnetic Material**

Metamaterials which are designed to enhance the magnetic properties of a medium are known as artificial magnetic materials (AMMs). Artificial Magnetic Material (AMM) consists of metallic broken-loop inclusion which aligned in parallel planes perpendicular to the direction of incident magnetic field. Metamaterials are commonly used to split-ring resonators (SRRs) and swiss roll resonator (SR-Rs). Furthermore, the implementation of SRR-based left-handed metamaterial in one dimension results in microstrip lines. SRRs

provide a negative effective permeability, but, to achieve backward-wave propagation, microstructuring is needed in order to obtain the required negative effective permittivity.

- Determination of Negative Permeability from Reflection and Transmission Coefficient,

In our simulation on HFSS, it has been demonstrated that the reflection and transmission coefficient calculated from transfer matrix simulations on finite lengths of electromagnetic materials, allows us to determine the effective permittivity (ϵ) and permeability (μ). Our approach is shown by the S-parameter, we invert the scattering data to determine n and z to obtain the value of ϵ and μ

- Rose Curve Characteristic

In this section, we propose the n th order Rose Curve. This new innovative inclusion geometry will be analysed and discussed. In fact, the rose curve can minimize the dependency of the inductive and capacitive response of the inclusions. These curves have a principal characteristic, namely the area and the perimeter of these rose curves can be adjusted independently.

- Microwave Application of Metamaterial Concept with Microstrip Line Based on Complementary Rose Curve Resonators (CRCRs).

This work discusses the complementary rose curve resonators (CRCRs) etched on ground plate under the microstrip transmission line. The CRCRs are applied to increase the miniaturizing factor. Using the basic topology of SRRs, the RCRs behave as an LC resonator that can be excited by an external magnetic flux, exhibiting a strong diamagnetism above their first resonance. The miniaturization is defined as the ratio of the wavelength for which the complementary inclusions resonate to the length of the microstrip line in the filter device. a good result of simulation has been obtained with a deep rejection band for design frequency for microstrip lines stopband in 23th order. The rejection frequency with sharp cutoffs is obtained at the maximum of 52 dB at a frequency 2.7 GHz. It should be emphasized that using rose curve resonator improves the miniaturization of the filter. In fact, higher order provides more miniaturization of the bandwidth of the rejection wide. It is shown that

CRCRs extend the possibility of design with higher miniaturization factor, relative bandwidth and rejection depth compare to filters based on split ring resonators. The device compactness increases proportional to the order of CRCRs. An increase from n to $n+1$ of the CRCRs order will result in 2.67% miniaturization. However, the bandwidth and rejection depth decreases.

Chapter 3 Metamaterial Power Divider for Beamforming System Based on Butler Matrix

Chapter 3 is about Metamaterial Power Divider for Beamforming System Based on Butler Matrix. This chapter discusses about theory of compact 90° microwave directional coupler model and design of conventional power divider and metamaterial power divider.

- Theory and circuit model of compact 90° microwave directional coupler
Directional coupler is a four-port circuit with one of ports is isolated from the input ports. Passive reciprocal networks with four ports are ideally matched and lossless. The S-parameters are obtained for -3dB Branch line Hybrid coupler with electrical length of 90° by applying the even-odd mode decomposition techniques. The value of S-parameters relate to the line length and frequency of the 3-dB 90° Hybrid branch line coupler.
- Analysis and design of conventional power divider
A 90° coupler is a special case of four ports directional coupler that is designed for an equal power split. In this research, we propose a conventional coupler size reduction, which behave as left hand material in a narrow band for a specific resonating frequency. The coupler is designed at the operational frequency $f_0 = 2.5GHz$.
- Analysis and design of metamaterial power divider
In this work, we design and make comparison between the conventional 90° microstrip coupler (without ring), 90° microstrip coupler with CSRRs and 90° microstrip coupler with CRCRs. By combining CSRRs with the strip lines in series, compact bandpass filter can be

obtained. With the left hand property of CSRRs due to its negative electromagnetic properties, it behaves as frequency shifting when added to a simple transmission lines. Our approach is to load the ground plane effect of the CSRRs on the microstrip transmission line. We were able to demonstrate an efficient way to shift the resonance frequency of CSRRs by transforming circular circumference to a Rose curve form. It is shown that CRCRs extend the possibility of design with higher miniaturization factor and relative bandwidth in comparison with using complementary split ring resonators (CSRRs). The device compactness increases proportional to the order of CRCRs. An increase from without inclusion to $n=0$ (CSRRs) will result in 44% miniaturization and 53% miniaturization from without inclusion to $n=13$ (CRCRs) for 3 dB branch line microstrip coupler.

Chapter 4 Metamaterial Antenna for Beamforming System Based on Butler Matrix

Chapter 4 is about metamaterial antenna for beamforming system based on butler matrix. In this section, we introduce the properties of arrays antenna for Butler matrix system. Array antennas consist of multiple stationary elements, which are fed by signal of amplitude and phase to have an appropriate beam at different angle in space. They can give the ability to scan in both vertical and horizontal direction. Each antenna of an array radiates a vector directional pattern which has both radial and angle depending on the distance of each antenna. The configuration of the Patch antenna is proposed. Patch antennas have been designed based on the complementary split ring resonator, complementary rose curve resonator and without using these inclusions. The patch antenna is designed with CSRRs and CRCRs etched on the ground plate under the patch line. CRCRs are promising to extend the possibility of design with higher miniaturization factor in comparison with using CSRRs. The device compactness increases proportionally to the order of CRCRs. An increase of standard patch antenna to $n=0$ (CSRRs) will result in 89% miniaturization and to $n=13$ (CRCRs) result in 92% miniaturization.

Chapter 5 Beamforming System Based on Butler Matrix

Chapter 5 is about beamforming system based on butler matrix. The Butler matrix is a microwave network, as a beamformer that feed an antenna array to implement such multibeam antenna systems. The Butler matrix is chosen because it can produce a large number of high-quality orthogonal beams with fewer components and using microstrip technology. In a beamforming system, the size of a Butler matrix is the main contributor. Furthermore, reducing the size of a Butler matrix is significant to reduce the cost of beam-forming systems. . The major components of the Butler Matrix are the hybrid coupler, the crossover, the phase shifter and the four rectangular patch microstrip antennas. This research proposed the topology of 4x4 Butler Matrix without crossover component. In the next Future Works we have an idea to design of metamaterial a 4x4 butler Matrix. It provides two design of metamaterial a 4x4 Butler Matrix with complementary split ring resonators (CSRRs) and complementary rose curve resonators (CRCRs). The goal of this work is to have the comparison between two models in size reduction working at same frequency of 2.4 GHz.

Résumé

Cette thèse porte sur la conception et l'analyse d'un nouveau métamatériau composé d'un système Matrice de Butler 4x4. Il sera développé selon les propriétés et les actions suivantes: 1) Une fréquence d'opération de 2.4 GHz. 2) Des études paramétriques. 3) Des résultats de simulation. 4) une forme compacte miniaturisée. Cette thèse contient cinq chapitres comprenant la préface au chapitre 1.

Chapitre 1 Introduction

Le chapitre 1 traite des antécédents et de la motivation de cette thèse, de la contribution à la recherche, de la méthodologie, de la revue de la littérature sur les travaux antérieurs et du schéma de thèse. Le contexte de cette thèse porte sur l'application des métamatériaux, la motivation de cette thèse est la mise en oeuvre d'un circuit métamatériel destiné à la conception d'antennes. Le but de cette recherche est premièrement de développer et d'analyser une nouvelle conception d'une application d'antenne métamatérielle dans un réseau utilisant la 4x4 matrice de Butler à la fréquence de 2.4 GHz, et deuxièmement de concevoir et de comparer les résultats d'analyses de simulation en utilisant HFSS 15. La contribution à la recherche de cette thèse est la conception d'une matrice 4x4 de Butler la miniaturisée et de la conception de circuits avec des cellules unitaires en métamatériaux. Les travaux suivants ont été réalisés:

- Un coupleur hybride 90^0 basé sur des résonateurs complémentaires avec courbes en forme de rose (CRCRs).
- Une antenne patch basée sur des résonateurs complémentaires avec courbes en forme de rose (CRCRs).
- Une antenna à système de formation de faisceaux compact basé sur le modèle de la matrice de Butler.

Nous avons conçu tous les circuits avec un modèle conventionnel, basé sur des CSRRs et CRCRs qui se comportent comme des matériaux dans une bande étroite pour une fréquence de résonance spécifique de 2.4 GHz. En conséquence, il est démontré que les CRCRs étendent les possibilités de conception avec un facteur de miniaturisation plus élevé et une meilleure bande passante relative par rapport à l'utilisation de résonateurs complémentaires à anneaux séparés (CSRRs). La compacité de l'appareil augmente proportionnellement à l'ordre des CRCRs. La méthodologie de cette thèse est que nous allons d'abord développer des composants pour concevoir un système traditionnel de matrice de Butler, à savoir: un coupleur directionnel à 90°, un déphaseur et un crossover. Dans ce travail, nous avons conçu une matrice compacte 4x4 de Butler pour un système de formation de faisceaux pour antennes sans crossover. La revue littéraire de notre thèse s'est concentrée sur le champ électromagnétique, les métamatériaux et l'étude paramétrique du comportement du résonateur d'ordres n à courbes en forme de rose (n-RCR) et son application sur la conception de certains circuits.

Chapitre 2 Théorie fondamentale sur les métamatériaux.

Le chapitre 2 traite de la théorie fondamentale des métamatériaux. Ce chapitre comprend:

- Définition des métamatériaux et média

En ondes électromagnétiques, la permittivité électrique et la perméabilité magnétique contrôlent la propagation à travers les matériaux. Les métamatériaux appartiennent à la catégorie des sciences naturelles de la physique, aux matériaux naturels, qui sont de nature positive. Le métamatériau génère une permittivité négative avec des fils minces à faible longueur d'onde et une perméabilité négative avec des résonateurs à anneaux fendus. Le métamatériau est un milieu matériel qui est agrégé électriquement avec une petite inclusion.

Dans le troisième quadrant des paramètres matériels effectifs représentés sur un ensemble de perméabilité-perméabilité ($\epsilon-\mu$), la perméabilité et la perméabilité sont simultanément négatives. Ce matériau est un matériau gaucher (LHMs) avec des formes de triade (E, H, k), où E correspond au champ électrique et H correspond au champ magnétique, respectivement.

- Formule fondamentale du matériel magnétique artificiel

Les métamatériaux qui sont conçus pour améliorer les propriétés magnétiques d'un milieu sont connus sous le nom de matériaux magnétiques artificiels (AMMs). Le matériel magnétique artificiel (AMM) consiste en une inclusion métallique en boucle cassée qui s'aligne dans des plans parallèles perpendiculaires à la direction du champ magnétique incident. Les métamatériaux sont couramment utilisés pour les résonateurs à anneaux fendus (SRRs) et le résonateur à rouleaux suisses (SR-Rs). En outre, la mise en œuvre du métamatériau gauche basé sur SRR à une dimension aboutit à des lignes microrubans. Les SRR fournissent une perméabilité efficace négative, mais, pour obtenir une propagation de l'onde inversée, une microstructure est nécessaire pour obtenir la permittivité effective négative requise.

- Détermination de la perméabilité négative depuis les coefficients de réflexion et de transmission

Dans notre simulation sur HFSS, il a été démontré que le coefficient de réflexion et de transmission calculés à partir de simulations de matrice de transfert sur des longueurs finies de matériaux électromagnétiques nous permet de déterminer la permittivité effective (ϵ) et la perméabilité (μ). Notre approche est montrée par le paramètre S, nous inversons les données de diffusion pour déterminer n et z pour obtenir la valeur de ϵ et μ .

- Caractéristiques des courbes en forme de rose

Dans cette section, nous proposons les courbes en forme de rose d'ordre n. Cette nouvelle géométrie d'inclusion innovante sera analysée et discutée. En fait, la courbe en forme de rose peut minimiser la dépendance de la réponse inductive et capacitive des inclusions. Ces courbes ont une caractéristique principale, à savoir la surface et le périmètre de ces courbes en forme de rose peuvent être ajustés indépendamment.

- Application micro-ondes du concept métamatériel avec ligne microruban basée sur des résonateurs complémentaires à courbes en forme de rose (CRCRs).

Ce travail traite des résonateurs complémentaires avec courbes en forme de rose (CRCRs) gravés sur la plaque de terre sous la ligne de transmission microruban. Les CRCRs sont appliqués pour augmenter le facteur de miniaturisation. En utilisant la topologie de base des SRRs, les RCRs se comportent comme un résonateur LC qui peut être excité par un flux magnétique externe, présentant un diamagnétisme fort au-dessus de leur première résonance. La miniaturisation est définie comme le rapport de la longueur d'onde pour laquelle les inclusions complémentaires résonnent à la longueur de la ligne microruban dans le dispositif de filtrage. Un bon résultat de simulation a été obtenu avec une bande de rejet profonde à la fréquence de conception pour les lignes microrubans stopband du 23^{ème} ordre. La fréquence de rejet avec coupure nette est obtenue à un maximum de 52 dB à la fréquence de 2.7 GHz. Il convient de souligner que l'utilisation d'un résonateur à courbes en forme de rose améliore la miniaturisation du filtre. En fait, l'ordre supérieur fournit plus de miniaturisation de la bande passante pour un rejet plus large. Il est démontré que les CRCRs étendent les possibilités de conception avec un facteur de miniaturisation plus élevé, tandis que la bande passante relative et la profondeur de rejet se comparent aux filtres basés sur des résonateurs à anneaux fractionnés.

La compacité de l'appareil augmente proportionnellement à l'ordre des CRCRs. Une augmentation de n à $n + 1$ de l'ordre des CRCRs entraînera une miniaturisation de 2,67%. Cependant, la largeur de bande et la profondeur de rejet diminuent.

Chapitre 3 Diviseur de puissance à base de métamatériaux

Le chapitre 3 concerne le diviseur de puissance métamatériel pour un système de formation de faisceaux basé sur la matrice de Butler. Ce chapitre traite de la théorie du modèle de coupleur directionnel compact micro-ondes à 90^0 et de la conception du diviseur de puissance classique et du diviseur de puissance métamatériel.

- **Modèle théorique et de circuit de coupleur directionnel compact micro-ondes à 90^0**
 Le coupleur directionnel est un circuit à quatre ports avec un des ports isolé des ports d'entrée. Les réseaux passifs réciproques avec quatre ports sont idéalement adaptés et sans perte. Les paramètres S sont obtenus pour un couplage hybride de ligne de dérivation de -3dB avec une longueur électrique de 90^0 en appliquant les techniques de décomposition en mode pair-impair. La valeur des paramètres S correspond à la longueur de ligne et à la fréquence du coupleur de dérivation hybride 90^0 à -3dB.
- **Analyse et conception du diviseur de puissance conventionnel**
 Un coupleur à 90^0 est un boîtier spécial de coupleur directionnel à quatre ports conçu pour une répartition de puissance égale. Dans cette recherche, nous proposons une réduction de taille du coupleur classique, qui se comporte comme un matériau de gauche dans une bande étroite pour une fréquence de résonance spécifique. Le coupleur est conçu à la fréquence de fonctionnement $f_0 = 2,5$ GHz.
- **Analyse et conception du diviseur de puissance métamatériel**
 Dans ce travail, nous concevons et faisons une comparaison entre le coupleur microruban conventionnel à 90^0 (sans anneau), le coupleur microruban à 90^0 avec CSRRs et le coupleur microruban à 90^0 avec CRCRs. En combinant CSRRs avec les lignes ruban en série, on peut obtenir un filtre passe-bande compact. Avec la propriété de gauche des CSRRs en raison de ses propriétés électromagnétiques négatives, il se comporte comme un décalage de fréquence lorsqu'il est ajouté à des lignes de transmission simples. Notre approche consiste à charger l'effet du plan de masse des CSRRs sur la ligne de transmission microruban. Nous avons pu démontrer un moyen efficace de déplacer la fréquence de résonance des CSRRs en transformant la circonférence circulaire en une forme de courbe en forme de rose. Il est démontré que les CRCRs étendent la possibilité de conception avec un facteur de miniaturisation plus élevé et une bande passante relative plus élevée par rapport à l'utilisation de résonateurs à anneaux séparés complémentaires (CSRRs). La compacité de l'appareil augmente proportionnellement à l'ordre des CRCRs. Une augmentation allant de sans

inclusion à $n = 0$ (CSRRs) entraînera une miniaturisation de 44% et une miniaturisation de 53% sans inclusion à $n = 13$ (CRCRs) pour un coupleur microruban de dérivation de 3 dB.

Chapitre 4 Antenne adaptif à base de métamatériaux

Le chapitre 4 concerne l'antenne métamatériel pour le système de formage de faisceau basé sur la matrice de Butler. Dans cette section, nous présentons les propriétés des antennes en tableaux pour le système matriciel de Butler. Les antennes en tableaux se composent de multiples éléments stationnaires, qui sont alimentés par un signal d'amplitude et de phase pour avoir un faisceau approprié à un angle différent dans l'espace. Ils peuvent donner la possibilité de numériser dans les deux directions verticale et horizontale. Chaque antenne d'un tableau rayonne un motif directionnel vectoriel qui présente à la fois un angle radial et un angle en fonction de la distance de chaque antenne. La configuration de l'antenne Patch est proposée. Les antennes patch ont été conçues sur un résonateur à anneau complémentaire fendu, du résonateur complémentaire de courbes en forme de rose et sans utiliser ces inclusions. L'antenne patch est conçue avec CSRRs et CRCRs gravés sur la plaque de masse sous la ligne de raccordement. Les CRCRs promettent d'étendre la possibilité de conception avec un facteur de miniaturisation plus élevé par rapport à l'utilisation de CSRRs. La compacité de l'appareil augmente proportionnellement à l'ordre des CRCRs. Une augmentation de l'antenne patch standard à $n = 0$ (CSRRs) entraînera une miniaturisation de 89% et $n = 13$ (CRCRs) entraînera une miniaturisation de 92%.

Chapitre 5 Système adaptif à base de métamatériaux

Le chapitre 5 présente le système de formage de faisceaux basé sur la matrice de Butler. La matrice de Butler est un réseau micro-onde, comme un formateur de faisceau qui alimente un réseau d'antennes pour implémenter de tels systèmes d'antennes à faisceaux multiples. La matrice de Butler est choisie car elle peut produire un grand nombre de faisceaux orthogonaux de haute qualité avec moins de composants et utilisant la technologie microruban. Dans un système de formation de faisceaux, la taille d'une matrice de Butler est le principal contributeur. En outre, la réduction de la taille d'une matrice de Butler est importante pour réduire le coût des systèmes de

formation de faisceaux. Les principaux composants de la matrice de Butler sont le coupleur hybride, le crossover, le déphaseur et les quatre antennes rectangulaires patch microrubans. Cette recherche a proposé la topologie 4x4 de la matrice de Butler sans composant croisé. Dans les prochains travaux futurs, nous avons une idée de la conception d'une matrice de Butler 4x4 en métamatériau. Il fournit deux modèles de métamatériaux à la matrice de Butler 4x4 avec des résonateurs complémentaires à anneaux fendus (CSRRLs) et des résonateurs complémentaires à courbes en forme de rose (CRRs). Le but de ce travail est d'avoir la comparaison entre deux modèles en réduction de taille fonctionnant à la même fréquence de 2,4 GHz.